

Distribution Agreement

In presenting this thesis or dissertation as a partial fulfillment of the requirements for an advanced degree from Emory University, I hereby grant to Emory University and its agents the non-exclusive license to archive, make accessible, and display my thesis or dissertation in whole or in part in all forms of media, now or hereafter known, including display on the world wide web. I understand that I may select some access restrictions as part of the online submission of this thesis or dissertation. I retain all ownership rights to the copyright of the thesis or dissertation. I also retain the right to use in future works (such as articles or books) all or part of this thesis or dissertation.

Signature:

Anzar Abbas

Date

Understanding brain activity dynamics through the investigation of quasi-periodic patterns

By

Anzar Abbas
Doctor of Philosophy

Neuroscience
Graduate Division of Biological and Biomedical Sciences

Shella D. Keilholz, Ph.D.
Advisor

David Weinschenker, Ph.D.
Committee Member

Eric H. Schumacher, Ph.D.
Committee Member

Helen Mayberg, M.D.
Committee Member

Michael Borich, Ph.D, DPT
Committee Member

Paul Garcia, M.D., Ph.D.
Committee Member

Accepted

Lisa A. Tedesco, Ph.D.
Dean of the James T. Laney School of Graduate Studies

Date

Understanding brain activity dynamics through the investigation of quasi-periodic patterns

By

Anzar Abbas
B.S., Michigan State University

Advisor: Shella D. Keilholz, Ph.D.

An abstract of
A dissertation submitted to the Faculty of the
James T. Laney School of Graduate Studies of Emory University
in partial fulfillment of the requirements for the degree of
Doctor of Philosophy
in Neuroscience
Graduate Division of Biological and Biomedical Sciences
2019

Abstract

Understanding brain activity dynamics through the investigation of quasi-periodic patterns

by

Anzar Abbas

This dissertation explores large-scale brain activity through the investigation of repeating spatiotemporal patterns in the brain. A pattern-finding algorithm applied to brain activity data collected through functional magnetic resonance imaging reveals a reliably recurring quasi-periodic pattern (QPP). The QPP involves propagation of activity in the default mode and task positive networks of the brain. The two networks have been shown to be relevant for task performance and development of neuropsychiatric disorders. Searching for QPPs in resting-state and task-performing individuals reveals that task-performance influences the spatiotemporal pattern of the QPP and the strength and frequency with which it occurs. Differentiating QPPs between healthy individuals and individuals with ADHD, a neuropsychiatric disorder involving disruptions in the default mode and task positive networks, reveals that the spatiotemporal pattern of the QPP is affected in the disrupted regions. Through removal of the QPP from the brain signal, we find that QPPs contribute to functional connectivity within and between the default mode and task positive networks. These findings suggest that QPPs are important for healthy brain function as they contribute to the typical functional architecture of the brain. To understand a neural mechanism behind QPPs, we investigated the role of neuromodulation by deep brain nuclei on the presence of QPPs in brain activity. Pharmacological manipulation of the noradrenergic locus coeruleus in rats led to a disruption in QPP activity compared to healthy controls. This finding advocates for a neural mechanism behind the occurrence of QPPs and subsequently a biological machinery for the maintenance of functional connectivity in the brain. The dissertation provides evidence that studying large-scale brain activity in the form of repeating patterns can assist with understanding healthy brain function and how it is disrupted during disease.

Understanding brain activity dynamics through the investigation of quasi-periodic patterns

By

Anzar Abbas
B.S., Michigan State University, 2014

Advisor: Shella D. Keilholz, Ph.D.

A dissertation submitted to the Faculty of the
James T. Laney School of Graduate Studies of Emory University
in partial fulfillment of the requirements for the degree of
Doctor of Philosophy
in Neuroscience
Graduate Division of Biological and Biomedical Science
2019

Acknowledgements

I am but a result of tangled neurons. Everything I do is inextricably linked to my experiences — be they good or bad. My first acknowledgement belongs to my home, Karachi. Resilience is not innate. Mine was built at an early age. I am forever in debt to the challenges of my upbringing.

Thank you, Dr. Mark Kadrofske, for introducing me to laboratory research. Through you, I learned that a good scientist is always trying to disprove his hypothesis. Thank you, Dr. John Waller, for introducing to me to the joys of academia. Through you, I learned of the need for humility and the important distinction between knowledge and wisdom. Thank you, Dr. Laura Symonds and Dr. James Galligan, for igniting my passion for neuroscience. Through you, I learned that a scientist may be good at asking questions, but he must be good at answering them, too.

The Neuroscience Program at Emory University provided me the opportunity to test these lessons. My greatest acknowledgement belongs to Dr. Shella Keilholz, who trusted me when I certainly didn't deserve to be. The intellectual creativity allowed by her in my training is reflected on every page of this document. After all, my dissertation work could have been accomplished while staring at the back of my desk. Instead, it is the result of early mornings in Viennese cafes, sunny afternoons by the Thames, and rainy evenings in historic Parisian libraries. Shella, I am eternally grateful for your ability to never once let the joy of academia escape the work that lies ahead.

Finally, to my dissertation committee: Naturally, I hope that someday, somewhere, someone else finds reason to read my dissertation. But, I am not writing it for their enjoyment. I am writing it for yours.

Table of Contents

Chapter 1

Introduction to Quasi-periodic patterns	1
1.1 – Brain activity is connected across scales	2
1.2 – Development of fMRI to study brain activity	4
1.3 – Resting-state fMRI and functional connectivity	7
1.4 – Dynamics of functional connectivity	9
1.5 – Quasi-periodic patterns in the brain	12

Chapter 2

Quasi-periodic patterns and functional connectivity in the brain	14
2.1 – Introduction	15
2.2 – Methods	18
2.3 – Results	24
2.4 – Discussion	38
2.5 – Conclusions	49

Chapter 3

Quasi-periodic patterns in individuals with brain disorders	50
Introduction	52
3.1 – Attention-deficit/hyperactivity disorder	54
3.1.1 – Introduction	54
3.1.2 – Methods	57
3.1.3 – Results	65
3.1.4 – Discussion	78
3.1.5 – Conclusions	90
3.2 – Stroke	91
3.2.1 – Introduction	91
3.2.2 – Methods	93
3.2.3 – Results	96

3.2.4 – Discussion	100
3.2.5 – Conclusions	102
Chapter 4	
Predicting neural drivers of quasi-periodic patterns	103
4.1 – Introduction	104
4.2 – Methods	107
4.3 – Results	110
4.4 – Discussion	116
4.5 – Conclusions	119
Chapter 5	
Conclusions on Quasi-periodic patterns	120
Appendix A:	
fMRI Preprocessing Pipeline	128
Appendix B:	
Supplementary Figures	131
Appendix C:	
Supplementary Tables	143
Further Acknowledgements	171
References	173

List of Figures

Figure 2.1: Spatiotemporal pattern of QPPs in RS and TP groups	28
Figure 2.2: Strength and frequency of QPPs in RS and TP groups	30
Figure 2.3: FC in all ROIs in RS and TP groups before/after QPP regression	33
Figure 2.4: FC in DMN and TPN ROIs in RS and TP before/after QPP regression	36
Figure 3.1.1: DMN and TPN maps in the Control and ADHD QPPs	66
Figure 3.1.2: Spatiotemporal differences between the Control and ADHD QPPs	69
Figure 3.1.3: Strength and frequency of QPPs in Control and ADHD groups	73
Figure 3.1.4: FC differences between Control and ADHD groups	76
Figure 3.2.1: FC Differences between Control and Stroke groups	97
Figure 3.2.2: Spatiotemporal pattern of Control and Stroke QPPs	98
Figure 3.2.3: Strength and frequency of Control and Stroke QPPs	99
Figure 4.1: HPLC results in rats from the Control and DSP4 groups	111
Figure 4.2: Spatiotemporal comparison of QPPs in rats	112
Figure 4.3: Examples of QPP sliding correlation vectors in rats	114
Figure 4.4: Histograms of cumulative sliding correlation vectors in rats	115
Supplementary Figure 1: Length of QPPs in RS individuals	133
Supplementary Figure 2: Length of QPPs in TP individuals	135
Supplementary Figure 3: Timecourses of ROIs anti-correlated across QPPs	136
Supplementary Figure 4: Effect of task blocks on QPP strength and frequency	137
Supplementary Figure 5: Strength and frequency of QPPs in Control and ADHD.	139
Supplementary Figure 6: FC changes in Control and ADHD after QPP regression	141

List of Tables

Table 2.1: FC differences between RS and TP group before/after QPP regression	34
Table 2.2: FC differences between RS and TP group before/after QPP regression	37
Table 3.1.1: MRI parameters for ADHD200 Sample datasets	58
Table 3.1.2: DMN and TPN regions anti-correlated across group QPPs	71
Supplementary Table 1: DMN ROIs in the Control and ADHD groups	144
Supplementary Table 2: TPN ROIs in individuals with ADHD	148
Supplementary Table 3: ROIs in DMN and TPN and their correlation across QPPs	154

Chapter 1

Introduction to Quasi-periodic patterns

1.1 – Brain activity is connected across scales	2
1.2 – Development of fMRI to study brain activity	4
1.3 – Resting-state fMRI and functional connectivity	7
1.4 – Dynamics of functional connectivity	9
1.5 – Quasi-periodic patterns in the brain	12

1.1 – Brain activity is connected across scales

The brain is a collaborative effort of molecular interactions, neural activity, and network connectivity — all occurring at their own pace. It is only through integration of knowledge at every level of brain activity that there is any chance of arriving at a complete understanding of consciousness. Indeed, to understand the brain is to understand it across scale and across time.

On the scale of molecules, intricacies of protein interactions give a neuron its identity. Molecular interactions allow neurons to create neurotransmitters and package them for transmission. They build the neuron's electrochemically excitable membrane, enabling action potentials. The distribution of proteins within a cell is a reflection of its state and its relationship with its surroundings. Molecular neuroscience has shown the importance of a perfectly regulated population of proteins to carry out the functions of a neuron (Bickle, 2006; Eyckmans et al., 2011).

On the scale of the neuron, the collaborative actions of billions of proteins come together to form a single unit. A nerve cell consequently has the ability to conduct an action potential to transit information to its surroundings and concurrently receive and react to information from its surroundings (Hodgkin & Huxley, 1952). Its ability to do this is inextricably linked to its molecular makeup. Molecular interactions influence neuronal activity, and neuronal activity influences molecular interactions. Cellular neuroscience has shown how neurons behave as a unit, giving them the capacity to carry information in a network (Ramon, 1976).

On the scale of the network, connectivity between two neurons creates a circuit. Networks of neurons have the capacity to hold and conduct more complex information (Hebb, 1963). As the number of neurons in a network grows to millions, the complexity of the information it can carry grows concurrently. As is the case with molecular and neural activity, the relationship between neural activity and network activity is bidirectional. Network activity is dependent on neuronal activity and neuronal activity is influenced by network activity. Network neuroscience has shown how complex neural circuits can be arranged to perform sophisticated tasks, introducing theories for how organisms with complex neural architectures intelligently respond to their surroundings (Bassett & Sporns, 2017).

Brain activity is connected across scales. Molecular activity, by influencing neural activity, affects network activity. To understand brain dysfunction during neurological and neuropsychiatric disorders, it is important to note that activity at every level of the brain is being disrupted. Hence, to fully understand the etiology of a brain disorder, neuroscientists must establish an understanding of how brain activity is affected at the molecular, neural, and network scale.

However, there is a larger scale of brain activity that remains more elusive than the rest. Large-scale fluctuations in brain activity — much bigger than individual networks — have been reliably observed by the neuroscientific community for years (Buzsáki, 2006). It has been postulated that large-scale activity is also connected to brain behavior at other spatial levels. The exact nature of this relationship is not understood (Varela et al., 2001; Buzsáki, 2006). But, to study large-scale events in brain activity, researchers first needed an imaging technique with the capacity to observe brain activity at this level. The ability to do this came with advancements in functional magnetic resonance imaging technology.

1.2 – Development of fMRI to study brain activity

The development of magnetic resonance imaging (MRI) scanners from nuclear magnetic resonance technology allowed scientists to study the human body non-invasively (Mansfield, 1977). With early work by Peter Mansfield, Paul Lauterbur, and Raymond Damadian, MRI became a popular technique for human imaging (Lauterbur, 1973; Damadian, 1971). The first MRI scans solely served a clinical purpose, allowing physicians to study patient anatomy to assist with diagnosis of diseases such as cancer (Damadian et al., 1973; Damadian et al., 1974). MRI technology grew rapidly in the latter half of the 20th century and its applications grew alongside it.

The use of MRI scanners to observe the brain added to existing brain imaging technologies such as computerized tomography (Natterer, 1986). MRI distinguished itself given it did not require introduction of radioactive material into the patient's body. The first brain scans were purely anatomical (Doyle et al., 1981). They continued to assist researchers in studying human anatomy through observation of brain structure. After all, observing the inside of a living person's head in a harmless and painless way had previously been impossible. However, use of MRI in brain imaging exploded with the realization that MRI scanners could not only study brain anatomy, but brain function.

Functional brain imaging had been a subject matter of interest due to the ability of researchers to study blood flow in the brain through introduction of radioactive water into patients' bloodstreams (Radon, 1986). It was assumed that active regions in the brain will recruit oxygenated blood flow, which has since been confirmed through multi-modal studies (Pan et al,

2013). Hence, researchers were able to map areas of high activity in the brain using CT. It was soon established that MRI could be used to do the same without the exposure to radiation required by CT (Ogawa et al., 1990a; Ogawa et al., 1990b). With the ability to distinguish between oxygenated and deoxygenated blood flow, functional MRI (fMRI) became an exciting new technique to study brain activity.

Initial studies using fMRI mirrored earlier work done using CT and related positron emission topography (PET). Individuals were asked to perform certain tasks while laying in the MRI scanner. Consequently, the brain recruited heavy blood flow to regions that were activated in response to the provided task. The resulting blood flow was recorded in the acquired fMRI images. This allowed scientists to reach conclusions on areas in the brain that were associated with unique tasks (Frahm et al., 1993). Functional MRI continues to provide a window into neural activity through the understanding that oxygenated blood flow to regions — termed the *hemodynamic response* — is a result of neural activation (Friston et al., 1994). The knowledge acquired from such studies provided greater spatiotemporal accuracy compared to older techniques of brain function localization ranging from neurosurgery to PET. However, the general conclusions did not deviate from existing theories of the brain's functional organization.

Task activation studies using fMRI still overlooked the real-time large-scale events in the brain. Brain activity data collected from individuals performing tasks in the MRI scanner was averaged over the course of entire fMRI scans, which last several minutes. The measured signal is an overall representation of how one brain region may behave differently from other brain regions during sustained activity in a task. Functional MRI studies that depended on participants

performing a task in the MRI scanner were still a far ways off from studying large-scale events in the brain in real time.

1.3 – Resting-state fMRI and functional connectivity

In the laboratory of James Hyde in the 1990s, Bharat Biswal studied low-frequency spontaneous brain activity using fMRI in the absence of any specified task (Biswal et al., 1995). The group noticed that the signal originating from the brain's motor regions was highly correlated. This was the first observation that spontaneous activity recorded through fMRI from brain regions that are related in function tend to activate and deactivate simultaneously over time. The finding ushered in the question of why brain regions would exhibit such behavior in the absence of a task and the mechanism behind what was being observed.

Studies in which participants were asked to lay in the scanner in the absence of any particular task — termed resting-state fMRI — exploded after the observation from Hyde's group (Van Den Heuvel & Pol, 2010). Researchers became more interested in the spontaneous behavior of brain regions over time. An inference was made between correlation between timecourses of anatomically distinct brain regions and their *functional connectivity*. Indeed, functional connectivity was observed between brain regions that were already known to be related in function, such as regions in the motor or visual cortices (Power et al., 2011). Functional connectivity was also observed between brain regions that had previously not been associated as strongly, such as regions in entirely separate areas of the brain (Raichle, 2015). Soon, mapping of these functional networks began to take place across the brain.

Functional connectivity being observed between brain regions was conserved across participants and independent studies. This allowed researchers to define reliably observable functional networks, making way for new theories on the functional organization of the brain (Gratton et

al., 2018). It also led to novel topics of study such as the default mode network, a collection of brain regions active during the absence of task (Raichle, 2015), which was a strong shift from task-activation studies. Quickly enough, functional network atlases computed through data-driven approaches to resting-state fMRI (rs-fMRI) studies started appearing in publications (Glasser et al., 2016).

Typical functional connectivity and the resulting organization of functional networks in the brain became a representation of healthy brain function. Studies began to show that functional connectivity — and consequently organization of functional networks — was disrupted in individuals with neurological and neuropsychiatric disorders (Greicius, 2008). This led to a plethora of rs-fMRI studies specifically focusing on the disruption of functional connectivity in brain disorders, with the aim of leading to a more complete understanding of the etiology of those disorders (Konrad & Eickhoff, 2010; Buckner et al., 2010; Cherkassky et al., 2006; Greicius et al., 2007). It turns out, these studies were focusing on large-scale brain activity to understand human brain function and dysfunction.

However, functional connectivity was still a *static* observation of brain activity through a measure of the overall relationship between individual brain regions over time. Brain activity data from several minutes of rs-fMRI scans had to be averaged together to acquire a single number: Pearson correlation between the timecourses of brain regions. Static analyses of rs-fMRI scans still failed to describe large-scale events in the brain as they occur in time, observable by the eye in the spontaneous fluctuations seen in brain activity through fMRI studies. A study of the *dynamics* of large-scale brain activity measured through fMRI remained untapped.

1.4 – Dynamics of functional connectivity

A simple visual observation of the output of an fMRI scan is enough evidence that the brain shows rich, dynamic activity over time. Static functional connectivity analysis consolidates this activity into a number that can be easily understood. However, much more difficult to understand is the time-varying relationship between brain regions (Chang et al., 2018). Researchers needed to progress from traditional static approaches in fMRI to studying the *dynamics* of large-scale brain activity.

Initial work on the dynamics of fMRI using time-frequency through using wavelet transform coherence (Chang & Glover, 2010; Müller et al., 2004) as well as sliding window correlation methods (Allen et al., 2014) allowed studying dynamics of fMRI signal in the initial stages of exploration. These methods reveal that brain regions indeed have measurable time-varying relationships. The statistical robustness of these techniques are weak, not to mention their reliance on arbitrarily defined window lengths. However, they paved the way towards more sophisticated methods for studying brain activity dynamics.

Studying co-activation patterns (CAPs) allows investigation of brain activity dynamics through consideration of individual moments within fMRI scans rather than brain region timecourses (Liu et al., 2018). Analysis of CAPs addresses the issue of fMRI scans having significantly more voxels than they do timepoints. CAPs allow a dissection of functional networks, allowing their dynamics to be better understood (Liu & Duyn, 2013). However, analysis of CAPs is highly dependent on data quality and signal to noise ratio, which makes its applications more difficult (Liu et al., 2018).

A dynamic graph theory approach provides a clear visualization how the functional connectivity strength between brain regions changes over time (Khambhati et al., 2018; Yuan et al., 2017). It is able to reveal that the structure of functional networks — through seemingly robust through static fMRI analyses — is highly flexible. Distinct functional networks show transient moments of inter-connectivity when observed in real time. Dynamic graph theory allows researchers to reconsider the hard spatial boundaries between established functional networks.

The view of the brain as a time-varying network begs the application of modeling approaches to understand large-scale brain activity dynamics. Change point theory has allowed researchers to model state-related fMRI dynamics (Lindquist et al., 2007). Hidden Markov Models have been useful in understanding network activity dynamics (Quinn et al., 2018). Neural Mass Models have allowed researchers to encapsulate the brain's scale free activity (David & Friston, 2003) and its synchronization of activity across scales (Daffertshofer et al., 2018a; Daffertshofer et al., 2018b). Such advances are allowing researchers to learn the true dynamics of brain activity, crucial in understanding large-scale brain activity.

In this dissertation, a unique approach to understanding the dynamics of large-scale brain activity is presented: Searching for patterns. A pattern-finding algorithm is used to look for reliably recurring spatiotemporal sequences of brain activity. The brain regions encapsulated within these patterns and the strength and frequency with which they occur are outlined. Consequently, the functional significance of such a pattern is investigated along with its relationship to brain function and dysfunction. Studying repeating patterns within brain activity is a way to learn

about the dynamics of large-scale activity in the brain and also helps understand how it is related to brain activity in other scales.

1.5 – Quasi-periodic patterns in the brain

Indeed, one of the first papers tackling the dynamics of large-scale brain activity involved searching for patterns: In 2009, Waqas Majeed observed a distinguishable sequence of large-scale events in brain activity recorded from anesthetized rats (Majeed et al., 2009). In 2011, he confirmed that the sequence of events — or spatiotemporal pattern — could be reliably observed through the application of an unbiased pattern-finding algorithm. The spatiotemporal pattern was observed in anesthetized rats but also in awake, resting-state humans (Majeed et al., 2011). Subsequent experiments using electrophysiology demonstrated that the pattern was indeed a representation of neural activity (Pan et al., 2011; Pan et al., 2013; Thompson et al., 2014). Given its distinct spatiotemporal nature and its reliable recurrence at non-periodic intervals, the observable sequence was dubbed a *Quasi-Periodic Pattern* (QPP). This dissertation is an exploration of QPPs.

I argue that searching for inherent patterns is a useful method to understand the dynamics of large-scale activity in the brain. I hypothesize that the QPP, observed upon the application of a pattern-finding algorithm to brain activity data, is a functional component of large-scale brain activity. It contributes to static functional connectivity within and between the default mode and task positive networks, and is disrupted in neuropsychiatric disorders involving those two brain networks. Furthermore, I suggest that QPPs may be the result of neuromodulation originating from the locus coeruleus. I propose that QPPs are a relevant aspect of large-scale brain activity. They can assist in understanding healthy brain function and how it is disrupted during disease.

In Chapter 2, I will be describing the exact nature of QPPs. This includes an illustration of the spatiotemporal pattern itself, the strength and frequency of its occurrence, and the brain regions involved. It describes the involvement of the default mode network (DMN) and task positive network (TPN). It also shows how the spatiotemporal pattern of the QPP changes between resting-state and task-performing individuals. Chapter 2 argues that QPPs are a contributor to functional connectivity in the brain, specifically in the DMN and TPN.

Chapter 3 describes QPPs' contribution to functional connectivity in individuals with neuropsychiatric disorders. Chapter 3 has two sections. The first investigates QPPs in individuals with attention-deficit/hyperactivity disorder, which involves disruption of functional connectivity in the DMN and TPN. The second investigates QPPs in individuals with stroke, which is not linked to functional connectivity disruptions in either of the functional networks. Chapter 3 shows that QPPs contribute to functional connectivity in DMN and TPN regions that show disrupted functional connectivity during neuropsychiatric disorders. Chapter 2 argues for a role of QPPs in the maintenance of healthy brain function.

Chapter 4 describes an experiment in rodents, which probes the locus coeruleus as a possible driver of the brain activity captured in QPPs. In doing so, it investigates the ability of deep brain nuclei to influence QPPs and large-scale brain activity dynamics through neuromodulation. The experiment reveals that QPPs are disrupted when locus coeruleus activity is pharmacologically manipulated. Chapter 4 argues for a neural driver of QPPs.

Finally, Chapter 5 closes the argument from all chapters, presenting and discussing the conclusions from all experimental observations in the dissertation.

Chapter 2

Quasi-periodic patterns and functional connectivity in the brain

2.1 – Introduction	15
2.2 – Methods	18
2.2.1 – Data acquisition and preprocessing	18
2.2.2 – Pattern acquisition	19
2.2.3 – Blocks in the task-performing scans	21
2.2.4 – QPP regression	22
2.2.5 – Analysis of functional connectivity	22
2.3 – Results	24
2.3.1 – Default mode and task positive networks	24
2.3.2 – Quasi-periodic patterns	25
2.3.3 – QPP regression	29
2.3.4 – Overall functional connectivity differences	31
2.3.5 – Functional connectivity changes in the DMN and TPN	35
2.4 – Discussion	38
2.4.1 – DMN and TPN differences across groups	38
2.4.2 – Spatiotemporal pattern of QPPs	39
2.4.3 – Strength and frequency of QPPs	41
2.4.4 – Functional connectivity changes	42
2.4.5 – Implications for fMRI	45
2.4.6 – Limitations	46
2.5 – Conclusions	49

2.1 – Introduction

Functional connectivity (FC) is a defining feature of rs-fMRI. Correlation of the blood oxygenation level dependent (BOLD) signal fluctuations across brain regions is assumed to indicate functional relevance between them (Biswal et al. 1995). FC has proven to be a useful tool in studying the brain, particularly when brain organization is disrupted during neurological disorders (Gillebert & Mantini 2013; Mohan et al. 2016; Pievani et al. 2014).

Despite the wide use of rs-fMRI and its clinical potential, the mechanisms that give rise to FC are not fully understood. In other words: We do not know what drives the coordination of neural activity in large-scale networks. It has been postulated that the functional architecture of the brain derives from large-scale, low-frequency fluctuations of neural activity (Buzsáki 2006; Canolty & Knight 2010; He et al. 2008; Nir et al. 2008). Infra-slow activity (< 1 Hz) has a similar frequency to BOLD fluctuations and appears highly relevant to FC between distant brain regions (Grooms et al. 2017; Hiltunen et al. 2014; Palva & Palva 2012; Pan et al. 2013). Phase-amplitude coupling between different frequencies of brain activity demonstrates the strong relationship between the large-scale infra-slow brain activity observable through BOLD and activity in higher frequency bands (Monto et al. 2008; Raichle et al. 2011; Thompson et al. 2014a). This suggests that large-scale brain activity in lower frequencies could provide a framework for the organization of functional systems (Foster et al. 2016).

Studies on FC typically focus on the average correlation between areas over the course of the scan. Several studies have shown that this approach ignores complex spatiotemporal patterns of activity such as global signal changes to propagating waves or time-lagged patterns of activation

(Cole et al. 2016; Matsui et al. 2016; Mitra et al. 2016). Techniques for analysis of the dynamics of the BOLD signal allow for a more insightful understanding of real-time brain activity in rs-fMRI (Chang & Glover, 2010; Hutchison et al. 2013).

Quasi-periodic patterns (QPP) are large-scale network activity that dominate BOLD fluctuations (Belloy et al. 2018; Majeed et al. 2011; Thompson et al. 2014b; Yousefi et al. 2018). They involve propagation of activity across several cortical and subcortical regions. Brain regions initially involved in the QPP are those within the default mode network. Activity then follows in regions pertaining to executive control, or the task positive network, alongside deactivation in the DMN. QPPs appear to reflect spatial patterns of infra-slow electrical activity (Pan et al. 2013; Thompson et al. 2014b; Grooms et al. 2017). The wide spatial extent of the coordinated changes in the QPP is likely to contribute strongly to the BOLD correlation observed in the involved brain networks.

Task performance drastically alters the functional architecture of the brain, shifting focus towards task-positive regions (Elton et al. 2015; Goparaju et al. 2014; Thompson et al. 2013). So far, a detailed analysis of QPPs has only been conducted in anesthetized animals and resting-state humans (Belloy et al. 2018; Majeed et al. 2009; Majeed et al. 2011; Thompson et al. 2014b; Yousefi et al. 2018). Task performance tends to increase anti-correlation between the DMN and TPN (Thompson et al. 2013), suggesting that QPP strength or frequency may be increased, altering measured FC as a result. The involvement of specific brain areas in any given task could also influence the spatiotemporal pattern of the observed QPPs.

In this Chapter, we identify QPPs in humans during rest and while performing a working memory task. We look for differences in the spatiotemporal pattern, strength, and frequency of the QPPs acquired from each group. We then minimize the QPP's contribution to the BOLD signal through a linear regression of the QPP from the functional scans. By doing so, we measure the impact of the QPP on FC by calculating FC before and after the regression. We look at FC changes throughout the brain and specifically within and between the DMN and TPN. We hypothesize that removal of the QPPs from the functional scans through linear regression leads to a reduction in FC strength within the DMN as well as a decrease in anti-correlation between the DMN and TPN. Our findings suggest that QPPs play an important role in maintaining the normal functional architecture of the two functional networks and that low-frequency activity in the form of QPPs contribute substantially to the organization of FC in the brain.

2.2 – Methods

2.2.1 – Data acquisition and preprocessing

MRI data from 100 randomly-selected unrelated individuals (ages 22-36, 54 female) was downloaded from the Human Connectome Project (Van Essen et al. 2012). One anatomical scan was used for each individual (T1-weighted three-dimensional magnetization-prepared rapid gradient echo (T1w 3D MPRAGE) sequence; TR = 2400 ms, TE = 2.14 ms, TI = 1000 ms, FA = 8°, FOV = 224 mm x 224 mm, voxel size 0.7 mm isotropic) (Milchenko & Marcus 2012).

Two resting-state (RS) functional scans approximately 15 minutes in length were used (Gradient-echo Echo Planar Imaging; TR = 720 ms, TE = 33.1 ms, FA = 52°, FOV = 208 mm x 180 mm (RO x PE), matrix = 104 x 90 (RO x PE), slice thickness = 2.0 mm; 72 slices; 2.0 mm isotropic voxels, multi-band factor = 8, echo spacing 0.58 ms) with right-to-left (RL) phase encode direction in one scan and left-to-right (LR) phase encode direction in the other (Chen et al. 2015; Feinberg et al. 2010; Setsompop et al. 2011). Two working memory task functional scans (TP) were also used (RL and LR phase encode direction) with the same scan parameters as RS scans, except that the duration was approximately 5 minutes in length. Though any cognitively demanding task could have been chosen for this study, working memory was chosen for its high demand for controlled processing and its relatively long duration compared to other HCP task fMRI scans. To adjust for the difference in the lengths of RS and TP scans, the RS scans were truncated to the same length as the TP scans. The task, described in Barch et al. (2013), involved a version of the N-back task assessing working memory and cognitive control in block format. In each functional scan, there are 8 task blocks, each lasting 25 seconds, and 4 fixation blocks, each

lasting 15 seconds. Half the alternating task blocks use a 2-back working memory task whereas the other half use a 0-back memory task (Owen et al., 2005). The blocks were divided into four categories: Faces, places, tools, and body parts. For all preprocessing steps, the preprocessing pipeline outlined in Appendix A of this dissertation was applied.

2.2.2 – Pattern acquisition

A spatiotemporal pattern-finding algorithm was used to search for repeating patterns of BOLD activation in the functional scans from RS and TP individuals separately. A detailed description of the algorithm used and the parameters inputted are outlined in Majeed et al. (2011). The pattern-finding algorithm selects a user-defined starting segment from within a functional scan and conducts a sliding correlation of the segment with the same functional scan. If the activity in the segment repeats at other instances in the functional scan, the resulting sliding correlation vector contains peaks indicating those occurrences. Additional segments are extracted at each of these instances and averaged together into an updated segment. Subsequent sliding correlations are then conducted between the continually updated segment and the functional scan. This process is repeated until the updated segment no longer shows variation and represents a reliably repeating pattern of activity within the functional scan. The result of the algorithm is a repeating spatiotemporal pattern from within the functional scan and a sliding correlation vector of the pattern with the functional scan itself.

There are two user-defined parameters that can influence the output of the algorithm: The length and location of the starting segment. Previous work in resting-state fMRI has shown that a reliably observable QPP lasts approximately 20 seconds. Based on previous literature (Majeed et

al., 2011; Yousefi et al., 2018) and preliminary analysis (Supplementary Figure 1; Supplementary Figure 2), a length of 20 seconds was used when selecting a starting segment for the pattern-finding algorithm. The location of the starting segment can affect the spatiotemporal pattern that is outputted by the algorithm. According to initial observations, QPPs involve an initial increase in BOLD signal in regions within the DMN and a decrease in BOLD signal in regions within the TPN. The activity propagates along the cortex to a decrease in BOLD signal in the DMN and an increase in BOLD signal in the TPN. Simply put, the QPP consists of a propagation of BOLD activity between the DMN, or a DMN/TPN switch (Majeed et al. 2011; Yousefi et al. 2018). Though the pattern-finding algorithm has been shown to reliably output this pattern, the DMN/TPN switch can occur in varying phases depending on the location of the starting segment (Yousefi et al. 2018). To ensure the DMN/TPN switch occurs in the same phase in both groups, the algorithm is run multiple times for each group with starting segments selected at random locations in the functional scan.

For the RS and TP groups separately, 25 randomly-selected functional scans from unique individuals were concatenated. DMN and TPN maps for each group were acquired by selecting 10% of brain voxels most correlated and most anti-correlated with the posterior cingulate cortex respectively. This was primarily based on the observation by Fox et al. (2005), which demonstrated that the DMN and TPN are reliably observable anti-correlated functional networks in the brain and a review on the DMN by Raichle (2015), which describes the PCC as a central node of the DMN. For each group, the pattern-finding algorithm was applied to the concatenated functional scans 100 times with unique randomly-selected starting segments. All 100 patterns acquired for each group from the pattern-finding algorithm were analyzed for a DMN-to-TPN

switch. The pattern most closely matching a DMN-to-TPN transition was selected and designated as a representative QPP for that group. By doing so, one representative QPP was chosen for the RS group and another for the TP group. The spatiotemporal pattern of the two QPPs was later compared.

Next, sliding correlation vectors were calculated between the two observed QPPs and functional scans from both RS and TP groups. Peaks, or local maxima, in the sliding correlation vectors signify occurrences of the QPP during the functional scan. This helps quantify the strength and frequency of QPP occurrence over time. The strength refers to correlation strength of the QPP with the functional scan, measured by the height of the peaks in the sliding correlation vectors. Frequency refers to how often these peaks occur. The sliding correlation vectors from all scans in each group were concatenated for the RS and TP QPPs separately. First, the mean height of peaks greater than 0.1 was calculated for the RS and TP QPPs in both the RS and TP scans. Second, the mean time interval between the peaks was also calculated for both QPPs in both groups. Third, the sliding correlation vectors were represented as histograms for comparison across groups without the need of the arbitrary 0.1 correlation threshold.

2.2.3 – Blocks in the task-performing scans

As described earlier, the working memory task involved four 15-second fixation blocks, four 25-second 0-back memory task blocks, and four 25-second 2-back memory task blocks. To investigate the effects of the individual blocks on the QPPs, the sliding correlation vectors of the RS and TP QPPs were separated by block. The mean peak height for all peaks > 0.1 was calculated and the sliding correlation vectors were represented as histograms to be compared.

2.2.4 – QPP regression

The RS and TP QPPs were regressed separately from the RS and TP scans to study their contributions to FC. For each functional scan, a unique regressor was calculated per brain voxel. This was done by convolving the QPP's sliding correlation vector with the timecourse of each brain voxel during the QPP. The obtained regressor was z-scored to match the signal in the functional scan. Then, linear regression was carried out using standardized/beta coefficients and the regressors calculated for each brain voxel. This method produced a functional scan with attenuated presence of the QPP in the BOLD signal. The RS QPP was regressed from both RS and TP scans and the TP QPP was regressed from both RS and TP scans.

The efficacy of this regression method was demonstrated by conducting a subsequent sliding correlation of the QPPs with the QPP-regressed functional scans. Like the analysis of the concatenated sliding correlation vectors before QPP regression, the mean peak height and time interval between QPPs was calculated and the sliding correlation vectors were represented as histograms. The mean values and the histograms were compared to the ones created before QPP regression quantify the efficacy of the QPP regression in removing the presence of the QPPs in the functional scans.

2.2.5 – Analysis of functional connectivity

A region of interest (ROI) atlas was used to summarize FC between all brain regions. Each functional scan was parceled into 273 ROIs from the Brainnetome Atlas (Fan et al. 2016). The mean signal over time, or timecourse, of each ROI was calculated. The ROI timecourses were

used to acquire the strength of FC between brain regions through Pearson correlation. FC strengths between all ROIs over the course of a functional scan were compiled into one FC matrix per scan. All FC matrices from each group underwent a Fischer's z-transformation and were averaged into a mean FC matrix for that group. FC matrices were also calculated for the functional scans after the QPPs had been regressed. Two-sample t-tests were performed for each ROI connection to check for significant differences in FC between groups. Multiple comparisons correction was performed by means of false discovery rate correction using the Benjamini and Yekutieli method (2001).

2.3 – Results

2.3.1 – Default mode and task positive networks

Maps for the DMN and TPN were acquired by locating areas strongly correlated or anti-correlated with the posterior cingulate cortex respectively (Figure 2.1a, Figure 2.1b, *bottom-right*). The mean anti-correlation between the DMN and TPN in RS individuals was -0.78 with a standard deviation of 0.11 . The mean anti-correlation between the DMN and TPN in TP individuals was -0.84 with a standard deviation of 0.10 . The anti-correlation strength was significantly stronger in TP individuals with a p value of 4.78×10^{-10} calculated using a two-sample t-test.

The DMN map contained similar regions in both RS and TP individuals. For both the RS and TP groups, the DMN included parts of the superior and middle frontal gyri, orbital gyrus, paracentral lobule, middle and inferior temporal gyri, inferior parietal lobule, precuneus, cingulate gyrus, and cuneus. In the RS group, the DMN included parts of the cerebellum, which was not seen in the TP group. In the TP group, the DMN included parts of the precentral and postcentral gyri, superior temporal gyrus, superior parietal lobule, and striatum, which was not seen in the RS group.

The TPN map also contained some variabilities between the RS and TP groups. For both groups, the TPN included parts of the superior and inferior frontal gyri, precentral and postcentral gyri, inferior temporal gyrus, fusiform gyrus, superior and inferior parietal lobules, insula, cuneus,

occipital gyrus, and cerebellum. Unique to the RS group, the TPN included areas in the superior temporal gyrus. Unique to the TP group, the TPN included areas in the middle frontal gyrus.

2.3.2 – Quasi-periodic patterns

2.3.2.1 – *Comparison of spatiotemporal pattern*

Application of the spatiotemporal pattern-finding algorithm resulted in the observation of a quasi-periodic pattern spanning 20 seconds in both RS and TP individuals (Figure 2.1a, Figure 2.1b; Supplementary Figure 1; Supplementary Figure 2). For both groups, the QPP involved an initial increase in BOLD signal in the DMN with decrease in BOLD signal in the TPN. This was followed by decrease in BOLD signal in the DMN and increase in BOLD signal in the TPN. Though DMN and TPN behavior was similar in both groups, there were differences in the specific brain regions involved.

A comparison of the spatiotemporal pattern between the two QPPs was conducted by comparing the mean activity of all ROIs during the course of the 20-second QPP. For each of the 273 ROIs, a Pearson correlation was conducted between its timecourse in the RS QPP and its timecourse in the TP QPP. Strong correlation signifies that the ROI behaved similarly in both groups, whereas a strong anti-correlation signifies the ROI behaved in the opposite manner. All ROIs within the DMN and TPN that were either strongly correlated (> 0.6 Pearson correlation) or strongly anti-correlated (< -0.6 Pearson correlation) are shown in Figure 2.1c. For the most part, DMN and TPN ROI timecourses were similar between the two groups, with differences dominated by task-relevant areas. Correlation strength of all 273 ROIs between the two groups' QPPs can be found

in Abbas et al. (2019a). Timecourses of example ROIs that were significantly different between the RS and TP QPPs are plotted in Supplementary Figure 3.

2.3.2.2 – Comparison of strength and frequency

Sliding correlation of both the RS and TP QPPs with all functional scans showed reliably recurring quasi-periodic peaks (Figure 2.2a, Figure 2.2b), though at varying strengths and frequencies. By concatenating all sliding correlation vectors for each group, three comparisons of the temporal aspect of the QPPs were made:

First, the mean correlation strengths at all peaks > 0.1 in the sliding correlation vectors were calculated and compared for the RS and TP QPPs in both groups (Fig 2.1c). The mean correlation strength of the RS QPP in RS scans was significantly higher than the TP QPP ($p = 1.14 \times 10^{-8}$). The mean correlation strength of the TP QPP in TP scans was significantly higher than the RS QPP ($p = 1.7 \times 10^{-110}$). Also, the mean correlation strength of the TP QPP in TP scans was significantly higher than the RS QPP in RS scans ($p = 5 \times 10^{-46}$).

Second, the mean time intervals between all peaks > 0.1 in the sliding correlation vectors was calculated and compared for the RS and TP QPPs in both the RS and TP scans (Fig 2.1d). The mean time interval between RS QPP occurrences in the RS scans was significantly shorter than the TP QPP ($p = 2.9 \times 10^{-9}$). The mean time interval between TP QPP occurrences in the TP scans was shorter than the RS QPP, though with a relatively smaller significance ($p = 0.0237$). The mean time interval between TP QPP occurrences in the TP scans was significantly longer than the mean time interval between RS QPP occurrences in the RS scans ($p = 9.8 \times 10^{-17}$).

Third, the sliding correlation vectors of the RS and TP QPPs with all scans were represented as histograms for comparison between groups without the use of an arbitrary 0.1 correlation threshold (Fig 2.2e, 2.2f). A wide, short histogram indicates higher frequency of correlation values in the sliding correlation vector that are far from zero. This suggests a stronger presence of the QPP in the functional scan. A narrow, tall histogram indicates higher frequency of correlation values in the sliding correlation vector that are closer to zero. This suggests a weaker presence of the QPP in the functional scan. The histograms were compared using a Kolmogorov-Smirnov (KS) test and only significant differences with an alpha value of 1×10^{-6} are discussed. The RS QPP showed a stronger presence in the RS group compared to the TP group. Similarly, the TP QPP showed a stronger presence in the TP group compared to the RS group. Finally, the TP QPP showed a stronger presence in the TP group than the RS QPP showed in the RS group.

Additionally, the sliding correlation vectors of the RS and TP QPPs were compared for the fixation, 0-back, and 2-back task blocks in the working memory task scans. Comparison showed that the blocks did not have a significant effect on the strength and/or frequency of the QPPs (Supplementary Figure 4).

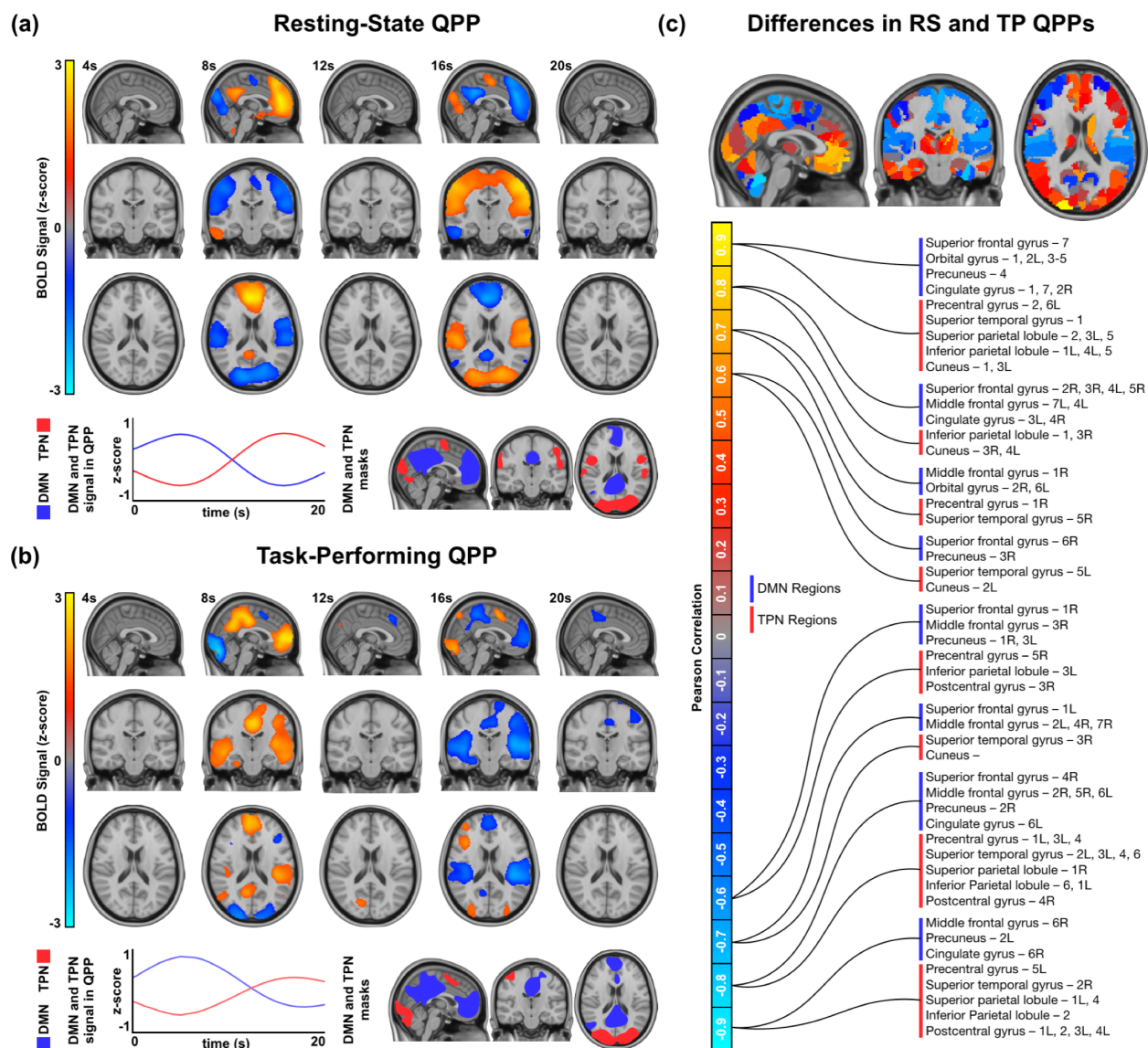


Figure 2.1: Spatiotemporal pattern of QPPs in RS and TP groups

(a) Top: Spatiotemporal pattern seen in the RS QPP. Only BOLD signal changes 1.5x the standard deviation from the mean are shown. **Bottom-left:** DMN and TPN timecourse during the RS QPP. **Bottom-right:** Maps of DMN and TPN acquired from RS individuals. **(b) Top:** Spatiotemporal pattern seen in the TP QPP. Only BOLD signal changes 1.5x the standard deviation from the mean are shown. **Bottom-left:** DMN and TPN timecourses during the TP QPP. **Bottom-right:** Maps of DMN and TPN acquired

from TP individuals. **(c) Top:** Spatiotemporal differences between the RS and TP QPPs. *Bottom:* Regions in the DMN and TPN that showed strong similarity between groups (> 0.6 Pearson correlation, shown in red/yellow) and strong dissimilarity between groups (< -0.6 Pearson correlation, shown in blue/turquoise). A full list of these regions can be found in Abbas et al., (2019a).

2.3.3 – QPP regression

Linear regression was effective in attenuating the presence of QPPs in the functional scans. The sliding correlation vectors of the QPPs with QPP-regressed functional scans showed a diminished presence of the QPPs in the functional scans (Figure 2.2). For peaks in the sliding correlation vectors > 0.1 , the mean correlation strength of the RS and TP QPPs with QPP-regressed RS and TP scans was significantly reduced ($p = 1.3 \times 10^{-88}$, $p = 1.2 \times 10^{-58}$, $p = 1.2 \times 10^{-48}$, $p = 2.6 \times 10^{-92}$ respectively). The mean time interval between occurrences of the RS and TP QPPs with QPP-regressed RS and TP scans significantly increased ($p = 1 \times 10^{-33}$, $p = 3 \times 10^{-21}$, $p = 5.2 \times 10^{-26}$, $p = 1.4 \times 10^{-7}$ respectively). The histograms representing the sliding correlation of the RS and TP QPPs with QPP-regressed RS and TP scans also showed a significantly weaker presence of the QPPs.

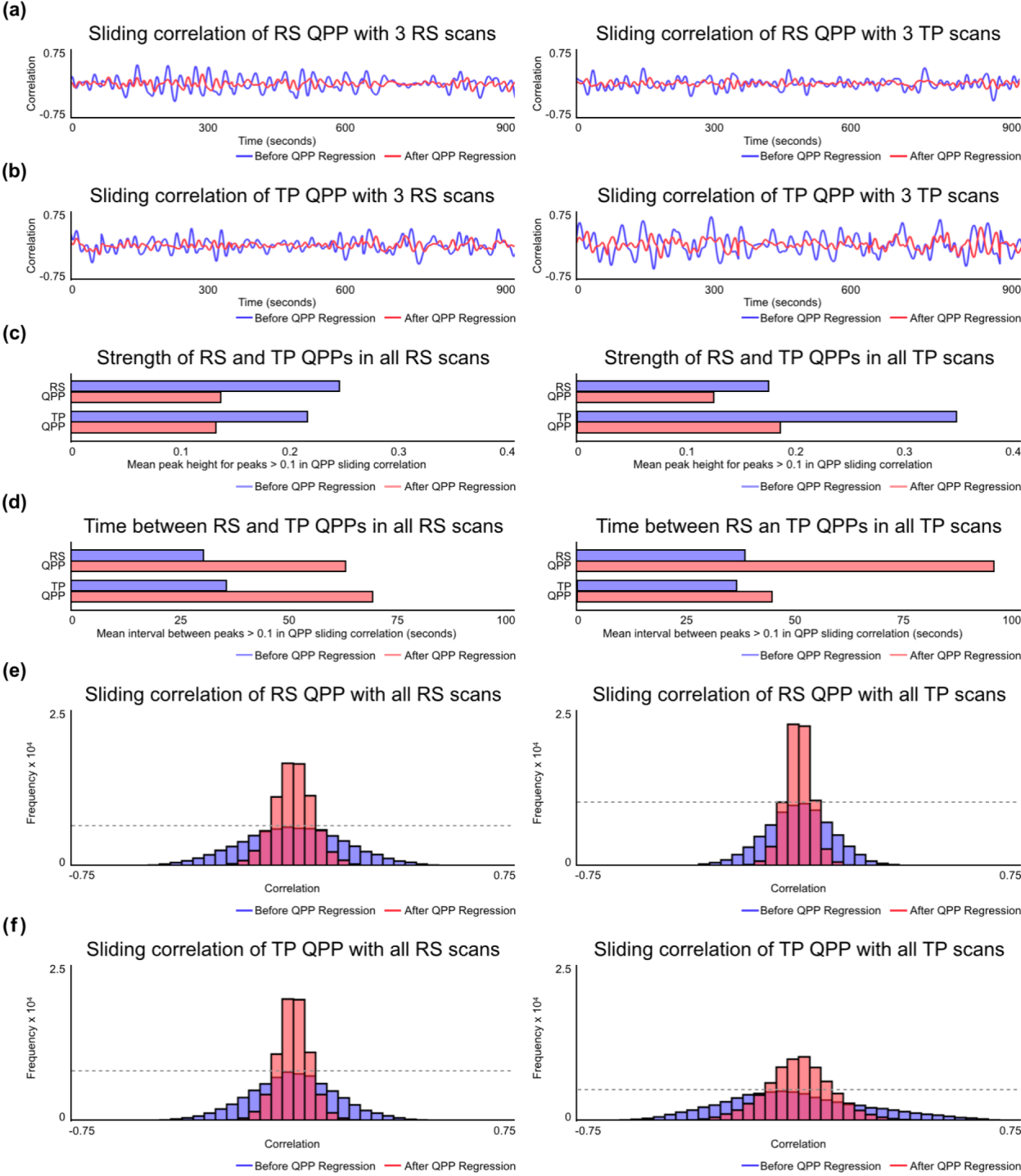


Figure 2.2: Strength and frequency of QPPs in RS and TP groups

(a) Example sliding correlation of the RS QPP with three concatenated scans from unique individuals during rest (*left*) and the same scans during task (*right*) before QPP

regression (*blue*) and after QPP regression (*red*). **(b)** Example sliding correlation of the TP QPP with three concatenated scans from unique individuals during rest (*left*) and the same scans during task (*right*) before QPP regression (*blue*) and after QPP regression (*red*). **(c)** Mean correlation strength of peaks > 0.1 in the cumulative sliding correlation of the RS and TP QPPs with all RS scans (*left*) and all TP scans (*right*) before QPP regression (*blue*) and after QPP regression (*red*). **(d)** Mean time interval between peaks with correlation strength > 0.1 in the cumulative sliding correlation of the RS and TP QPPs with all RS scans (*left*) and all TP scans (*right*) before QPP regression (*blue*) and after QPP regression (*red*). **(e)** Histogram of the cumulative sliding correlation of the RS QPP with all RS scans (*left*) and all TP scans (*right*) before QPP regression (*blue*) and after QPP regression (*red*). **(f)** Histogram of the cumulative sliding correlation of the TP QPP with all RS scans (*left*) and all TP scans (*right*) before QPP regression (*blue*) and after QPP regression (*red*).

2.3.4 – Overall functional connectivity differences

The FC matrices display the strength of FC in all 37,128 connections between the 273 ROIs in one image representing the static functional architecture of the brain. Data points closer to the central diagonal show FC strength in local connections while data points further away from the central diagonal show FC strength in long-range connections between brain regions.

An average FC matrix was calculated for RS and working memory TP individuals (Figure 2.3a). Significant FC differences between RS and TP individuals were widespread (Figure 2.3b, *bottom-left*), with 17,156 connections seeing a difference in FC strength. Native QPPs are those

acquired from the same group; for example, the RS QPP is native to RS functional scans. Once native QPPs were regressed from all functional scans in each group, the number of FC differences between RS and TP individuals decreased by 40% to 10,259 (Figure 2.3b, *top-right*; Table 2.1).

Regression of the RS QPP from RS functional scans led to 8,662 significant changes in FC (Figure 2.3c, *bottom-left*). When the TP QPP was regressed from the RS scans, only 188 connections were significantly altered (Figure 2.3c, *top-right*; Table 2.2). Regression of the TP QPP from TP functional scans led to 5,756 significant changes in FC (Figure 2.3d, *top right*). When the RS QPP was regressed from the TP scans, the number of significant changes decreased to 1,062 (Figure 2.3d, *bottom-left*; Table 2.2).

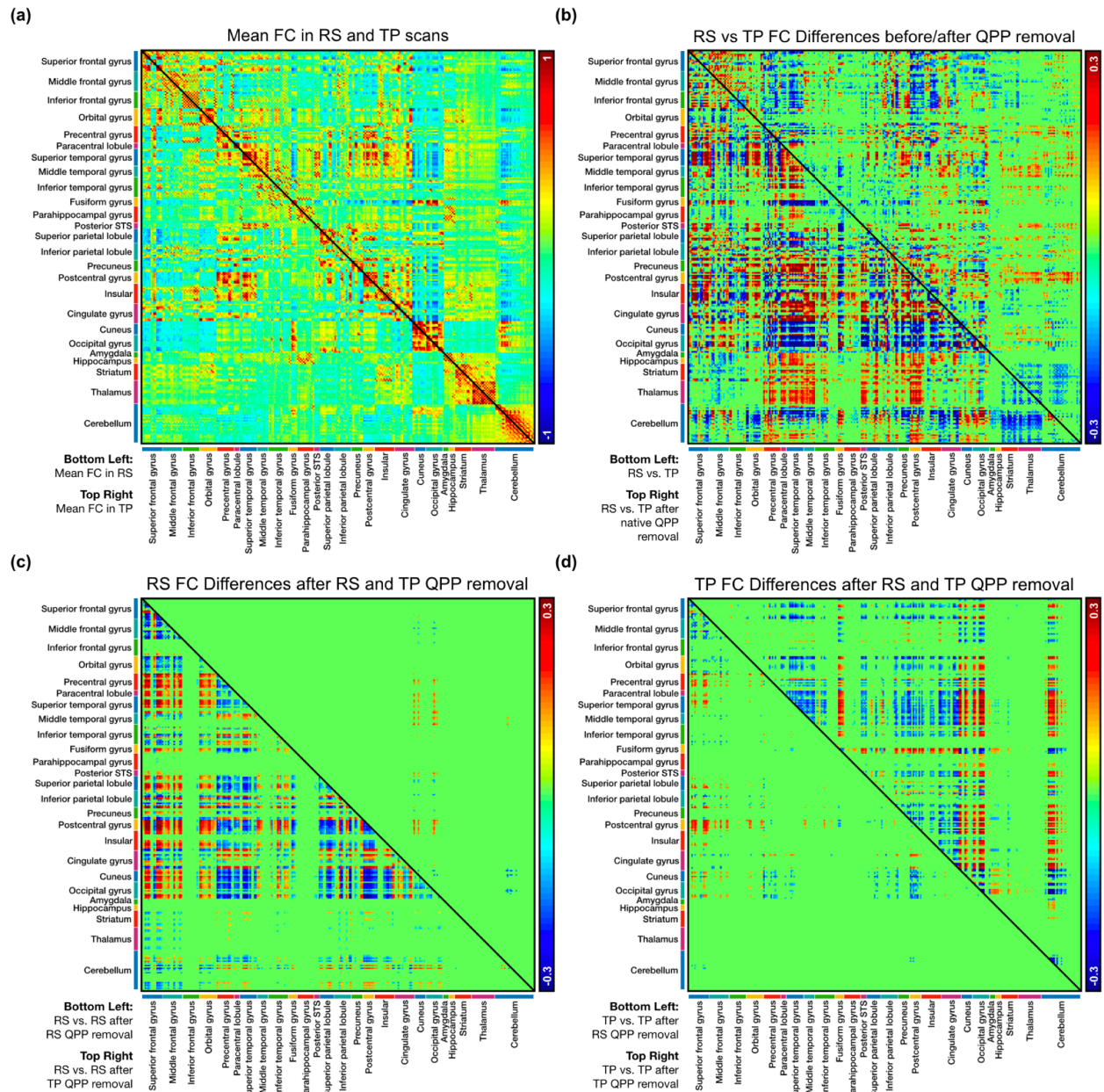


Figure 2.3: FC in all ROIs in RS and TP groups before/after QPP regression

Functional connectivity in 273 regions of interest. (a) *Bottom-left*: Mean FC in the RS group. *Top-right*: Mean FC in the TP group. (b) *Bottom-left*: Significant differences in FC between the RS and TP group ($n = 17,156$). *Top-right*: Significant differences in FC between the RS and TP group after regression of their native QPPs ($n = 10,259$). (c)

Bottom-left: Significant differences in FC in the RS group after regression of the RS QPP ($n = 8,662$). *Top-right:* Significant differences in FC in the RS group after regression of the TP QPP ($n = 188$). **(d)** *Bottom-left:* Significant differences in FC in the TP group after regression of the RS QPP ($n = 1,062$). *Top-right:* Significant differences in FC in the TP group after regression of the TP QPP ($n = 5,756$).

		FC changes	Original functional scans			After regression of native QPPs		
RS vs. TP	Increases	- → +	44%	↑ 0.24	9,133	34%	↑ 0.17	5,138
		+ → +	27%	↑ 0.19		28%	↑ 0.17	
		- → -	29%	↑ 0.17		38%	↑ 0.14	
	Decreases	+ → -	33%	↓ 0.23	8,023	31%	↓ 0.17	5,121
		- → -	42%	↓ 0.20		41%	↓ 0.15	
		+ → +	25%	↓ 0.18		28%	↓ 0.16	

Table 2.1: FC differences between RS and TP group before/after QPP regression

When comparing significant FC differences between the original functional scans and after the QPPs had been regressed, the first column shows the percent distribution of the different directions the FC changes occurred in, the second column shows the mean magnitude shift in strength of Pearson correlation for each of the directions, and the third column shows the total number of ROI connections with a significant change in FC between groups. The total number of significant changes in FC decreased by 40% after regression of native QPPs.

2.3.5 – Functional connectivity changes in the DMN and TPN

QPP regression particularly affected connections within the DMN and TPN as well as between the two networks. After regression of the RS QPP from RS scans, there was a strong decrease in local FC in the anterior regions of the DMN, namely the superior frontal, middle frontal, and orbital gyri. There was also a sharp decrease in connectivity between the anterior and posterior regions of the DMN. Additionally, the anti-correlation between the DMN and TPN diminished significantly. The TPN itself showed a decrease in FC, both locally and across regions (Figure 2.4a, *bottom-left*). Alternatively, regression of the TP QPP from RS scans did not result in as widespread changes in the DMN and TPN (Figure 2.4a, *top-right*).

Regression of the TP QPP from TP scans also affected areas in the DMN and TPN (Figure 2.4b, *top-right*). Similar to the RS group, there was a decrease in FC between anterior and posterior regions of the DMN. However, the local decreases in FC were seen in the posterior regions, namely the precuneus and cingulate gyrus. There were both decreases and increases in anti-correlation between the DMN and TPN, and a mixture of decreases and increases in FC between regions within the TPN. The FC changes when the RS QPP was regressed from the TP group showed similarity with RS individuals, though were significantly smaller in number.

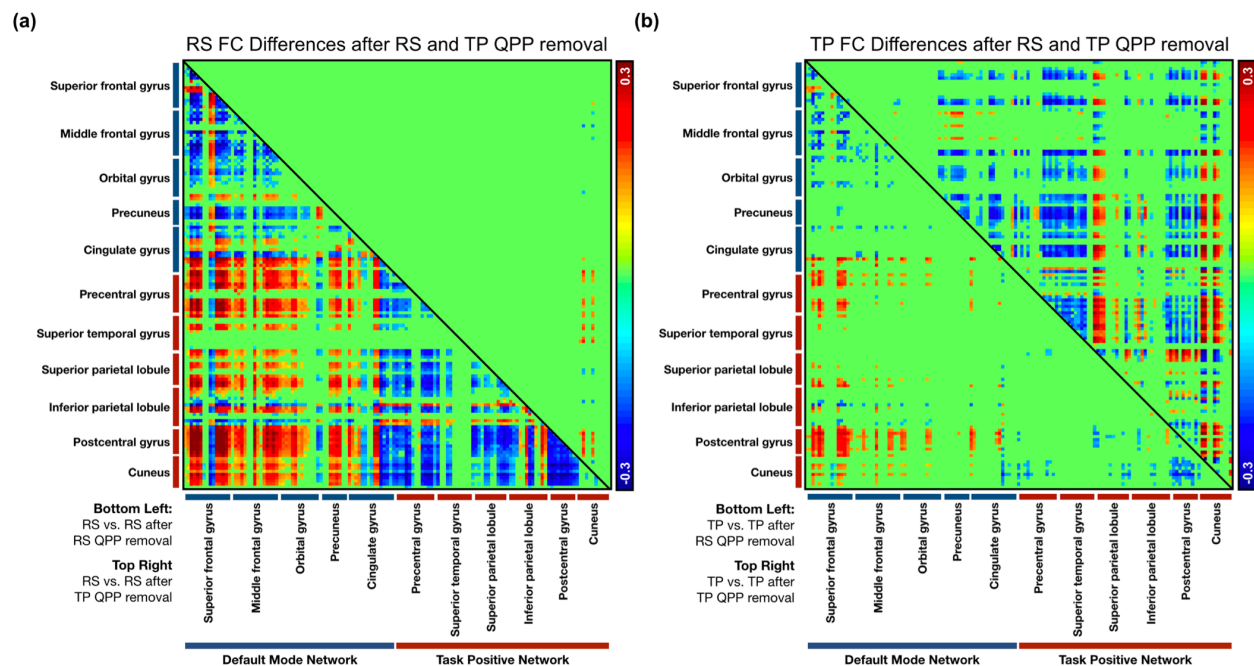


Figure 2.4: FC in DMN and TPN ROIs in RS and TP before/after QPP regression

(a) *Bottom-left*: Significant differences in FC in the RS group after regression of the RS QPP. *Top-right*: Significant differences in FC in the RS group after regression of the TP QPP. (b) *Bottom-left*: Significant differences in FC in the TP group after regression of the RS QPP. *Top-right*: Significant differences in FC in the TP group after regression of the TP QPP.

		FC changes	Regression of RS QPP			Regression of TP QPP		
RS	Increases	- → +	22%	↑ 0.18	4,271	60%	↑ 0.15	139
		+ → +	7%	↑ 0.14		27%	↑ 0.15	
		- → -	71%	↑ 0.16		13%	↑ 0.13	
	Decreases	+ → -	35%	↓ 0.18	4,391	26%	↓ 0.14	49
		- → -	21%	↓ 0.15		33%	↓ 0.14	
		+ → +	44%	↓ 0.16		41%	↓ 0.16	
TP	Increases	- → +	26%	↑ 0.16	553	8%	↑ 0.15	2,481
		+ → +	27%	↑ 0.16		2%	↑ 0.13	
		- → -	47%	↑ 0.14		90%	↑ 0.19	
	Decreases	+ → -	18%	↓ 0.15	508	29%	↓ 0.16	3,275
		- → -	61%	↓ 0.15		6%	↓ 0.13	
		+ → +	21%	↓ 0.15		65%	↓ 0.17	

Table 2.2: FC differences between RS and TP group before/after QPP regression

For the RS and TP groups separately, when comparing significant changes in FC after regression of the RS QPP and after regression of the TP QPP, the 1st column shows the percent distribution of the different directions the FC changes occurred in, the 2nd column shows the mean magnitude shift in strength of Pearson correlation for each of the directions, and the 3rd column shows the total number of ROI connections with a significant change in FC between groups. Regression of the TP QPP from the RS scans showed a 98% decrease in significant FC changes when compared to regression of the RS QPP from RS scans. Regression of the RS QPP from the TP scans showed a 82% decrease in significant FC changes when compared to regression of the TP QPP from TP scans.

2.4 – Discussion

This experiment adds to similar reports on the presence of reliably recurring quasi-periodic patterns in the brain (Belloy et al. 2018; Majeed et al. 2011; Thompson et al. 2014; Yousefi et al. 2018). This was the first time QPPs were examined in whole-brain data from TP individuals. Comparison of the QPPs acquired from RS and TP individuals show distinct spatiotemporal differences. These differences are specific to brain regions involved in the working memory task, suggesting that variability in the QPPs may be task-specific. Regression of the QPPs from the functional scans showed that QPPs have a strong effect on connectivity strength between brain regions. This effect is concentrated towards DMN and TPN FC, two networks central to the pattern.

2.4.1 – DMN and TPN differences across groups

Details on the working memory task used in this study can be found in Barch et al. (2013), along with the brain regions activated and deactivated during the 0-back and 2-back tasks respectively. Overall, presence of a task led to strong activations in TPN regions and deactivations in DMN regions. Since the DMN and TPN maps for RS and TP scans were created using all time points irrespective of task blocks, the differences in brain regions that were involved in either task block are not considered when comparing DMN and TPN maps between the groups.

Regions mapped as DMN areas in this study largely agreed with previous findings (Fox et al. 2005). However, there were some differences in DMN maps created from the RS group and the TP group. The inclusion of certain cerebellar regions in the DMN was unique to the RS group.

These same regions were activated during task (Barch et al. 2013), reducing their co-activation with other DMN regions in the TP group. Inclusion of parts of the precentral and postcentral gyri, superior temporal gyrus, superior parietal lobule, and striatum in the DMN was unique to the TP group. The precentral and postcentral gyri as well as the superior temporal gyrus were deactivated during task. This increase in anti-correlation with TPN areas is likely why these regions were included in the DMN map in the TP group. The superior parietal lobule and striatum did not follow this pattern as they were activated during task.

The TPN map also agreed with previous findings (Fox et al. 2005) and was similar across groups, with exceptions. A small area in the middle frontal gyrus was included in the TPN map for TP individuals. The middle frontal gyrus is one of the regions strongly activated during task, when the DMN is being deactivated. Its categorization as a TPN area unique to TP individuals is likely due to this anti-correlation with the DMN during the task. Similarly, inclusion of the superior temporal gyrus in the TPN was unique to the RS group. This region showed a strong deactivation during task. This lack of anti-correlation with DMN regions is likely why the superior temporal gyrus was not part of the TPN in the TP group.

2.4.2 – Spatiotemporal pattern of QPPs

A spatiotemporal comparison of the DMN portion of the QPPs acquired from both groups demonstrates differences similar to those noted in the DMN maps. Both groups' QPPs show a strong increase in BOLD signal in the DMN in the first half of the pattern followed by a decrease in BOLD signal in DMN regions in the second half. As a result, DMN regions are highly correlated between the two groups' QPPs. However, there are exceptions. This includes regions

in the superior and middle frontal gyri, the cingulate gyrus, precuneus, inferior parietal lobule, paracentral lobule, precentral gyrus, and superior parietal lobule. These regions follow the opposite trend in the TP QPP when compared to the RS QPP. This is consistent with the observation that some of these regions are only seen in the DMN map from the TP group, and not the RS group. Both groups' QPPs also show a strong decrease in BOLD signal in the TPN in the first half of the pattern followed by an increase in BOLD signal in TPN regions in the second half. As was seen with the DMN, there are exceptions. This includes regions in the superior and middle frontal gyri, the superior and middle temporal gyri, the pre- and post-central gyri, superior and inferior parietal lobule, fusiform gyrus, insula, and cerebellum. These regions follow the opposite trend in the TP QPP when compared to the RS QPP. Interestingly, Barch et al. (2013) shows that many of the regions that behave differently across the two QPPs are also relevant to the task being performed.

The robust spatiotemporal differences in the QPPs during task performance compared to RS are intriguing and suggest that the QPP is not a fixed pattern of coordinated activity but rather a flexible framework that organizes the brain into large-scale networks to optimize task performance. Thus, variabilities in the QPP's spatial pattern may be task-specific, and other tasks involving different brain regions may alter the spatial pattern of the QPP in a different way.

Since application of the pattern-finding algorithm requires a few minutes of continuous data at the very least, spatiotemporal comparison of the QPPs across the fixation, 0-back, and 2-back blocks during the TP scan is not feasible. Given that all time points in the scans were used to acquire QPPs, the differences highlighted between the RS and TP QPPs are meant to reflect

changes as an overall product of task performance rather than changes specifically due to 0-back or 2-back tasks.

2.4.3 – Strength and frequency of QPPs

The QPPs acquired from both the RS and TP groups showed quasi-periodic peaks in their sliding correlation vectors with all functional scans. Unsurprisingly, the RS and TP QPPs showed stronger presence in their native scans compared to the opposing scans. Additionally, the TP QPP showed greater correlation strength in the TP scans than the RS QPP did in RS scans, which may account for the significantly stronger anti-correlation between the DMN and TPN in the TP group observed here and in prior studies (Hampson et al. 2010; Kelly et al. 2008).

Though a spatiotemporal comparison of the QPPs between fixation, 0-back, and 2-back blocks was not possible, a comparison of the strength and frequency of the QPPs in each task block was conducted. The sliding correlation vectors of both RS and TP QPPs did not show any differences across the three blocks in the TP scans. Hence, the differences in the strength and frequency of QPPs highlighted between RS and TP individuals are meant to highlight changes as an overall result of task performance, rather than an effect of 0-back or 2-back tasks specifically.

A cognitively demanding task such as the one used in this study leads to an inherently higher state of vigilance compared to rest. Given the QPP's involvement of both DMN and TPN activity, its possible origin in neuromodulatory input, and the relationship between infra-slow electrical activity and vigilance levels, it seems plausible that the greater strength of the QPP in the TP group might arise from the increased alertness needed for task performance. A

preliminary analysis conducted in data from rhesus macaques showed that QPPs occur with greater strength and frequency in awake macaques compared to anesthetized macaques (Abbas et al. 2016), suggesting that vigilance may be playing a role. Another study showed that when performing a psychomotor vigilance task, greater anti-correlation between the DMN and TPN was tied to faster performance on the task (Thompson et al. 2013), which may be tied to the strength of the QPP. The effect of neuromodulatory inputs on QPPs is further investigated in Chapter 4.

The observation of the RS QPP in TP scans and the TP QPP in RS scans is likely due to the similarity in the spatial patterns of the QPPs. As described above, though there are distinct differences in the QPPs acquired from both groups, there are strong similarities as well. When a sliding correlation is being calculated, any similarities between the RS and TP QPPs may lead to higher correlation values than if the spatial pattern of the QPPs had been entirely different. If this is true, then the sliding correlation vectors of the RS and TP QPPs should align for the same scan. To investigate this, a cross-correlation of the sliding correlation vectors of the RS QPP and TP QPP in both groups was conducted. At the lag showing maximum correlation strength, the correlation between the two QPPs' sliding correlation vectors was 0.55. This suggests that the sliding correlation vectors of the two QPPs could indeed be aligned, which would explain the 'presence' of the RS QPP in TP scans and vice versa.

2.4.4 – Functional connectivity changes

With regression of the RS QPP from RS scans, there were strong local FC decreases in the anterior regions of the DMN and in the longer-range connections between anterior and posterior

DMN nodes. A general decrease in connectivity within the TPN also occurred. As would be expected, there was an attenuation of anti-correlation between the DMN and TPN. Loss of FC in these regions is significant in that many neurological and psychiatric patients exhibit similar connectivity disruptions during RS scans. Previous studies have shown that local connectivity changes in the anterior regions of the DMN are associated with schizophrenia (Holt et al. 2011), while reduced FC between anterior and posterior regions of the DMN is associated with ADHD (Choi et al. 2013), Alzheimer's Disease (Sheline et al. 2010a; Zhang et al. 2009), as well as aging (Andrews-Hanna et al. 2007). The relationship between DMN and TPN activity and the strength of their anti-correlation is important for normal brain function and task performance (Fox et al. 2005; Thompson et al. 2013). Decreased anti-correlation between the DMN and TPN is even seen in individuals with ADHD (Hoekzema et al. 2013; Posner et al. 2014) and is restored after treatment with atomoxetine and methylphenidate (Liddle et al. 2010; Lin et al. 2015). The next chapter will show that QPPs are disrupted in individuals with ADHD (Abbas et al. 2018a). Given that regression of the QPP leads to altered FC in those same connections, a disruption of the QPP may be one of the factors in the development of such disorders.

Regression of the TP QPP from RS scans did not result in many significant changes in FC. This suggests that the TP QPP may be particular to the task or TP states in general, and may occur only rarely while the individual is at rest.

In TP scans, FC differences were seen after regression of both the RS and TP QPPs. Once more, the differences seen pertained to DMN and TPN regions and their interconnectivity. Similar to regression of the RS QPP from RS scans, regression of the TP QPP from TP scans led to an overall decrease in FC strength between anterior and posterior regions of the DMN. Unlike the

RS group, the major short-range FC decreases in the DMN were seen in its posterior node. Additionally, regression of the TP QPP in TP scans led to a decrease in FC between DMN and TPN areas. Since the DMN and TPN are already anti-correlated, this meant a stronger anti-correlation between the two networks. This suggests that though the RS QPP may be playing a constructive role in distinguishing DMN and TPN regions from each other, the TP QPP in TP scans is doing the opposite. Hyper-connectivity between anterior and posterior regions of the DMN is seen during Major Depressive Disorder particularly during task performance as a potential result of the inability to shut off DMN activity during tasks (Grimm et al. 2008; Sheline et al. 2009; Sheline et al. 2010b). There were two regions that showed the similar changes to FC as the RS group, namely the superior parietal lobule and the cuneus. However, even for these regions, the middle frontal gyrus showed an increase in anti-correlation rather than a decrease.

Regression of the RS QPP from TP scans did result in some significant differences in FC. These changes followed the same trend as when the RS QPP was regressed from RS scans, albeit at a much smaller scale. These findings suggest that the RS QPP may still be occurring at a weaker frequency in the TP state. If so, it would be serving a similar purpose in maintaining strong FC within the DMN and TPN whilst contributing towards their overall anti-correlation.

There were wide-ranging significant differences in FC between RS and TP individuals. This was expected due to the significantly altered functional architecture of the brain during TP states compared to RSs (Elton et al. 2015; Goparaju et al. 2014; Thompson et al. 2013). The significance of these FC differences is beyond the scope of this study. However, they confirm work done by previous studies highlighting FC differences between RS and TP individuals. Noteworthy for this paper is the decrease in the number of FC differences between RS and TP

scans after regression of the QPP. Many of the FC differences seen between RS and TP individuals were diminished significantly once the QPP was regressed. This suggests that the different brain states could partially be a result of QPP activity.

2.4.5 – Implications for fMRI

Resting-state fMRI is popular for patient groups as it does not require the performance of a task, reducing the need for active patient cooperation. Alterations in FC have been observed in numerous neurological and psychiatric disorders, especially in the DMN. The differences in FC tend to be interpreted in terms of network interactions (i.e., a brain region is hypo-connected, or modularity is decreased (Mohan et al. 2016)). However, the presence of QPPs suggests a complementary interpretation where activity within and between networks is coordinated by a non-localized mechanism that simultaneously modulates activity in large swaths of the brain. Thus, the disruption of FC could at least in part reflect dysfunction of the process that produces QPPs. A recent paper shows that different brainstem nuclei are linked to activity in the DMN and TPN (Bär et al. 2016). The QPP could arise from coordinated input from these neuromodulatory regions, a hypothesis supported by findings reported in Chapter 4 that QPPs are weaker in rats with diminished locus coeruleus activity (Abbas et al. 2018b). Several neurological disorders such as Alzheimer's disease and Parkinson's disease exhibit early degeneration of neuromodulatory nuclei, which could then account for the disrupted FC that is observed in those individuals.

Besides implications for clinical FC studies, the strong contribution of QPPs to FC also affects the interpretation of more basic neuroscience studies. If QPPs are related to neuromodulatory

input and arousal, changes in FC observed during task performance may be tied to increased arousal during difficult tasks and lower levels of arousal during less difficult tasks. This complicates the use of FC to understand how the large-scale networks of the brain are reorganized for optimal task performance.

2.4.6 – Limitations

While the pattern-finding algorithm depends on a few parameters that must be chosen by a user, a substantial body of work has shown that QPPs can be reliably detected in multiple species, under different physiological conditions, and by using several variations of the basic pattern-finding algorithm. Hence, QPP detection appears quite robust. This study builds upon previous work to examine the contribution of the QPPs to FC using regression.

The use of regression to minimize the contribution of QPPs fundamentally assumes that QPPs are additive to the remaining BOLD signal. Multi-modal experiments in rodents support this assumption: QPPs are more closely linked to infra-slow activity while dynamic measures of BOLD correlation are more reflective of higher frequency activity (Thompson et al. 2014a), and no phase-amplitude coupling was consistently observed between the infra-slow activity and higher frequencies (Thompson et al. 2014b). The lack of phase-amplitude coupling does not rule out other types of interactions such as phase-phase coupling or amplification, but it suggests that treating QPPs as an additive signal is a reasonable first approximation. Further work using animal models is needed where neural recordings can provide a ‘ground truth’ comparison.

Furthermore, while the QPP can be generally described as involving the DMN and TPN, it is clear from this study that the precise brain areas involved can vary across cognitive conditions. The spatiotemporal differences seen between the QPPs during rest and task performance in this study may be specifically reflective of a working memory task, or they may reflect a general shift between task performance and rest. Participants were requested to keep their eyes fixated and stay awake for both rest and task conditions, so the differences in QPPs should not be related to state differences associated with eye closure. However, it is well-established that participants do tend to fall asleep during RS scans. In our study, only the first 5 minutes of 15-minute RS scans were used, which hopefully reduces the effect sleepiness or drowsiness could have had on our results and conclusions. Further work will be necessary to determine if different tasks involving different brain regions may affect the QPP in a unique way.

Finally, it is important to mention our decision to implement global signal regression during preprocessing. Yousefi et al. (2018) demonstrated that global signal regression reduces variability in QPPs acquired from different subjects. In the study, subjects were divided into two groups; those with low levels of global signal fluctuation and those with high levels of global signal fluctuation. Subjects with low levels of global signal fluctuation showed a QPP demonstrating anti-correlated network activity, as has been described in this paper. Subjects with high levels of global signal fluctuation showed that the global signal had an additive effect on the QPP: Though the observed spatial distribution of the pattern and its frequency of occurrence was relatively unchanged, the whole-brain global changes in BOLD signal obscured the underlying pattern. When global signal regression was conducted on individuals with high levels of global signal

fluctuation, their QPPs aligned with the QPPs of individuals with low levels of global signal fluctuation.

For this paper, the aim was to understand the effects of QPP regression on FC in the brain. If global signal had not been regressed from the functional scans, it could have served as a confounding factor in the subsequent analysis. Depending on the levels of global signal fluctuation in each subject, the spatiotemporal pattern observed in QPPs would have varied and their regression would have affected static FC differently across subjects. Hence, for a study investigating the effect of QPP regression on FC, we believe global signal regression in all functional scans was the appropriate decision, especially given that there are existing studies that demonstrate the effects of global signal regression on FC (Murphy & Fox 2017).

2.5 – Conclusions

Quasi-periodic patterns can be detected in both RS and TP individuals, with the task influencing the spatiotemporal pattern seen within the QPP as well as the strength and frequency of its occurrence. Removal of QPPs from functional scans through linear regression leads to significant changes in FC, especially within the DMN and TPN. This suggests that QPPs are relevant to healthy brain function and may account for changes in connectivity in certain patient groups. The findings also suggest that infra-slow electrical activity reflected by QPPs may play a role in the organization of network activity within the brain.

Chapter 3

Quasi-periodic patterns in individuals with brain disorders

Introduction	52
3.1 – Attention-deficit/hyperactivity disorder	54
3.1.1 – Introduction	54
3.1.2 – Methods	57
3.1.2.1 –Data acquisition and preprocessing	57
3.1.2.2 – Acquisition of default mode and task positive networks	59
3.1.2.3 – Acquisition of quasi-periodic patterns	60
3.1.2.4 – Removal of QPPs from functional scans	62
3.1.2.5 – Analysis of functional connectivity	62
3.1.3 – Results	65
3.1.3.1 – Differences in DMN and TPN masks between groups	65
3.1.3.2 – Differences in QPPs between groups	68
3.1.3.3 – Functional connectivity differences	74
3.1.4 – Discussion	78
3.1.4.1 – Default mode and task positive networks	78
3.1.4.2 – Quasi-periodic patterns	79
3.1.4.3 – Functional connectivity	81
3.1.4.4 – Implications for ADHD	84
3.1.4.5 – Limitations	87
3.1.5 – Conclusions	90

3.2 – Stroke	91
3.2.1 – Introduction	91
3.2.2 – Methods	93
3.2.2.1 – Participants	93
3.2.2.2 – Data acquisition	93
3.2.2.3 – Functional connectivity	94
3.2.2.4 – Standardization of lesioned hemispheres	94
3.2.2.5 – Quasi-periodic patterns	95
3.2.3 – Results	96
3.2.3.1 – Functional connectivity	96
3.2.3.2 – Quasi-periodic patterns	97
3.2.4 – Discussion	100
3.2.5 – Conclusions	102

Introduction

Chapter 2 demonstrated that quasi-periodic patterns contribute to FC in the default mode and task positive networks. FC in the DMN and TPN has been shown to be disrupted during several neuropsychiatric disorders (Whitfield-Gabrieli & Ford, 2012). This raises the question of the relationship between QPPs and the disruption of FC seen during disease.

If QPPs are disrupted in individuals with neuropsychiatric disorders, it further supports the hypothesis that QPPs play a role in maintaining healthy brain function. The hypothesis would predict that QPPs are disrupted in individuals with neuropsychiatric disorders that show disruption of FC within brain regions that are involved in the QPPs; i.e., the DMN and TPN. The hypothesis would then also predict that this should *not* be the case in brain diseases that are unrelated to the DMN and TPN.

The first section of Chapter 3 investigates QPPs in individuals with attention-deficit/hyperactivity disorder (ADHD). Previous literature demonstrating static FC differences between healthy individuals and those diagnosed with ADHD has clearly shown the involvement of the DMN and TPN (Konrad & Eickhoff, 2010): FC within the DMN and TPN and the strength of their anti-correlation is decreased. In the first section, I hypothesize that the spatiotemporal pattern of QPPs in individuals with ADHD will be disrupted in a way that will lead them not contribute to FC as strongly as they do in healthy individuals.

The second section of Chapter 3 investigates QPPs in individuals with stroke affecting motor ability. Though previous literature has demonstrated that cortical reorganization post-stroke

affects FC measures, these are not expected to overlap with the DMN in the individuals participating in this study. For this section, I hypothesize that the QPPs in individuals with stroke will be unchanged and will contribute to FC to the same extent as they do in healthy individuals.

The two experiments described in Chapter 3 provide further evidence that QPPs contribute to FC in the DMN and TPN. They further suggest that the ability of QPPs to maintain a healthy architecture of the brain is relevant in the development of neurological disorders. Lastly, they show how large-scale brain activity can be disrupted following disease and how such disruption is related to brain activity at smaller scales.

3.1 – Attention-deficit/hyperactivity disorder

3.1.1 – Introduction

Attention-deficit/hyperactivity disorder (ADHD) is the most commonly diagnosed neurodevelopmental disorder among children and adolescents in the United States (Subcommittee on Attention-Deficit/Hyperactivity Disorder, 2011). Changing attitudes towards the diagnosis of ADHD are leading to a further increase in its prevalence worldwide (Davidovich et al., 2017). ADHD is characterized by pervasive levels of inattention, hyperactivity, and impulsivity (American Psychiatric Association, 2013). It can lead to difficulties in personal and academic endeavors (Bagwell et al., 2001; Barkley et al., 1991) and cause significant burden on families and society (Matza et al., 2005). Understanding the pathophysiology behind ADHD is crucial for the development of effective treatments.

Etiological models of brain disorders such as ADHD are shifting from focusing on individual brain regions to prioritizing the investigation of large-scale network interactions across the brain (Raj et al., 2018; Konrad & Eickhoff, 2010). As a consequence, non-invasive whole-brain imaging methods are playing an important role in understanding the etiology of brain disorders (Wintermark et al., 2018; Weyandt et al. 2013). Notably, fMRI has been critical in studying network interactions in the brain and how they can be disrupted (Stam et al., 2014). Individuals with brain disorders, such as ADHD, often show altered FC in the brain (Konrad & Eickhoff et al., 2010; Cortese et al., 2012; Hart et al., 2012).

Such disruptions in FC have been a central focus of a number of studies on brain disorders (Du et al., 2018), including ADHD (Konrad & Eickhoff, 2010). Findings from these studies have assisted in identifying brain regions and functional networks relevant to understanding the etiology of brain disorders. However, most of these studies have relied on traditional static analyses of FC (Chang & Glover, 2010; Du et al., 2018). Hence, more recent fMRI studies have focused on dynamic analysis of the BOLD signal to better understand network interactions over time. This can help uncover the cause of FC disruptions seen in individuals with brain disorders (Hutchinson et al., 2013).

ADHD is associated with dysfunction in the DMN (Castellanos et al., 2008; Uddin et al., 2008) and its relationship with the TPN (Tian et al., 2006; Wang et al., 2008; Wolf et al., 2009; Rubia et al., 2009a; Konrad & Eickhoff, 2010; Cortese et al., 2012; Hart et al., 2012). Though there remains uncertainty on the directionality of some observed differences, evidence has predominantly converged on the relevance of the DMN and TPN when studying FC in individuals with ADHD. This also aligns with the prevailing understanding that DMN-TPN interactions are relevant for attentional control and vigilance (Fox et al., 2005; Raichle, 2015; Thompson et al., 2013). An investigation of the dynamics of these functional networks may help further the understanding of FC differences seen in individuals with ADHD.

Chapter 2 demonstrated that QPPs contribute to FC in the brain. It may be that QPPs are contributing to FC differences in the connections typically disrupted during ADHD. Such a conclusion would further the understanding of the dynamic processes involved in the etiology of the disorder. In this experiment, we first create masks of the DMN and TPN in healthy controls and adolescents with ADHD. Next, we search for FC differences between the Control and

ADHD groups. We then apply a pattern-finding algorithm to search for QPPs in both groups, and differentiate between the spatiotemporal patterns that are observed. Finally, we use regression to remove the QPPs from the functional scans in each group and measure their contribution to FC in the DMN and TPN. Our findings confirm FC differences previously observed in individuals with ADHD. Notably, we show that QPPs contribute to FC in the brain in regions relevant to ADHD. This is the first investigation of QPPs in any individuals with a brain disorder and suggest a role of QPPs in maintaining a healthy functional architecture of the brain.

3.1.2 – Methods

3.1.2.1 –Data acquisition and preprocessing

All resting-state data was downloaded from the ADHD-200 Sample, accessible through the 1000 Functional Connectomes Project (ADHD-200 Consortium, 2012; Biswal et al. 2010). Within the ADHD-200 Sample, the New York University, Peking University, and NeuroImage datasets were used. These datasets were selected based on the similarity of their scan parameters and availability of diagnostic information and data quality control assessments. An overview of scan acquisition parameters for each dataset is provided in Table 3.1.1.

Scan	Parameter	NeuroImage	New York University	Peking University
Anatomical (MPRAGE)	TR (ms)	2730	2530	2530
	TE (ms)	2.95	3.25	3.39
	TI (ms)	1000	1100	1100
	FA (deg)	7°	7°	7°
	FOV (mm)	256	256	256
	Slice (mm)	1.00	1.33	1.33
Functional (EPI)	TR (ms)	1960	2000	2000
	TE (ms)	40	15	30
	FA (deg)	80°	90°	90°
	FOV (mm)	224	240	200
	No. Slices	37	33	33
	Slice (mm)	3.0	4.0	3.5
	Voxel (mm)	3.5 x 3.5 x 3.0	3.0 x 3.0 x 4.0	3.1 x 3.1 x 3.5

Table 3.1.1: MRI parameters for ADHD200 Sample datasets

Anatomical and functional scan parameters for the ADHD 200 Sample datasets used in the study. In all cases, the anatomical scans were acquired through a T1-weighted 3D magnetization-prepared rapid gradient echo (MPRAGE) sequence and the functional scans were acquired through a gradient echo-planar imaging (EPI) sequence.

Each dataset contained MRI scans from healthy children, adolescents, and some adults and individuals diagnosed with ADHD. Of the three main sub-types of ADHD (Inattentive, Hyperactive-Impulsive, and Combined), only individuals diagnosed with the Combined ADHD sub-type were used in this study. The selection of one sub-type was intended to reduce variability in the results and the Combined sub-type provided the largest dataset among the three. Though the ADHD group had a combination of treated and medically naive individuals, all participants had been removed from any psycho-stimulant medication 24-48 hours prior to collection of functional data. For all individuals, only scans that had passed the ADHD 200 Sample quality control assessment were used. For individuals that had more than one functional scan, only the first scan was used in the study. In the end, the Control group contained 106 healthy individuals (age range 7–26, $\mu = 14.6$ years ± 3.8 ; 56 females) and the ADHD group contained 106 individuals with the Combined sub-type of ADHD (age range 7–21, $\mu = 12.6 \pm 3.3$; 10 females). Of the 106 individuals in each group, 22 were from the NeuroImage Sample, 57 were from the New York University dataset, and 33 were from the Peking University dataset.

For all preprocessing steps, the preprocessing pipeline outlined in Appendix A of this dissertation was applied.

3.1.2.2 – Acquisition of default mode and task positive networks

A data-driven method was used to acquire masks of the DMN and TPN from the Control and ADHD groups. For each group, 30 functional scans were concatenated in time. The 30 scans selected had 10 scans each from the three datasets (NeuroImage, New York University, and Peking University) to ensure results were not biased by any one dataset. The average BOLD timecourse of the posterior cingulate cortex (PCC) was calculated from the concatenated scans. Pearson correlations were then conducted between the mean timecourse of the PCC and the timecourse of every voxel in the brain. The 10% of voxels that were most correlated with the PCC were labeled as the DMN. The 10% of voxels that were most anti-correlated with the PCC were labeled as the TPN (Fox et al., 2005).

The functional scans were segmented into 273 regions of interest (ROIs) from the Brainnetome ROI atlas (Fan et al., 2016). For each ROI, the binary mask of the ROI was multiplied by the binary masks of the DMN and TPN to check for any spatial overlap between the ROI and either network. If the ROI contained voxels that were also part of either the DMN or TPN, the number of such voxels were counted and their mean correlation with the PCC was recorded. By doing so, a list of ROIs in the DMN and TPN was constructed, which contained information on how much the ROI overlapped with the DMN or TPN and how strongly it was correlated or anti-correlated with the PCC (Supplementary Table 1 for the DMN and Supplementary Table 2 for the TPN). The list was used to compare the ROIs included in the DMN and TPN masks acquired from the Control and ADHD groups. It was also used to compare the correlation strength of the ROIs with the PCC across the Control and ADHD groups. Finally, the DMN and TPN masks were used to acquire mean timecourses of the DMN and TPN from every scan in each group. The overall anti-

correlation between the mean timecourse of the DMN and the mean timecourse of the TPN across all scans was compared between the Control and ADHD groups using a Mann–Whitney U test.

3.1.2.3 – Acquisition of quasi-periodic patterns

The spatiotemporal pattern-finding algorithm, described in Majeed et al. (2011), was used to search for repeating patterns in the functional scans. The method through which the algorithm was applied and all parameters used are outlined in Chapter 2.

For the Control and ADHD groups separately, 30 functional scans were again concatenated (10 scans from each dataset). The pattern-finding algorithm was applied to the concatenated timeseries 100 times with unique, randomly-selected starting segments. The resulting 100 patterns outputted by the algorithm for each group were analyzed for a DMN-to-TPN transition in BOLD activation. The pattern most closely matching a DMN-to-TPN switch was selected and designated as a representative QPP for its respective group. By doing so, one representative QPP was established for the Control group and another representative QPP was established for the ADHD group. It is unlikely that the 30 scans concatenated before application of the algorithm biased the spatiotemporal pattern captured in the QPP. Chapter 2 showed that 25 concatenated scans (of similar length) were sufficient in removing variability in the pattern outputted by the algorithm. It has also been shown that QPPs acquired from concatenated data are the same as averaged QPPs from individual scans (Yousefi et al., 2018).

The spatiotemporal pattern captured in the QPP was compared between the Control and ADHD groups. The QPPs were segmented into the 273 ROIs in the Brainnetome ROI atlas. The mean timecourse of each ROI was calculated for both QPPs. For each ROI, a Pearson correlation was conducted between its mean timecourse in the Control QPP and its mean timecourse in the ADHD QPP. The resulting values for all 273 ROIs were compiled into Supplementary Table 3. Strong correlation of an ROI's timecourse in the two QPPs indicates that the ROI behaved similarly in both groups' QPPs. Anti-correlation of an ROI's timecourse in the two QPPs indicates that the ROI behaved differently in the QPP acquired from individuals with ADHD.

Next, the strength and frequency of the QPPs was compared between groups. Sliding correlations of the Control and ADHD QPPs were conducted with all functional scans in their respective groups. The resulting sliding correlation vectors contained local maxima, or peaks, in correlation, which signified the occurrence of QPPs at those instances in the functional scans. The strength of the QPP was defined as the mean height of those peaks. The frequency of the QPP was defined as the rate of occurrence of those peaks over time. In this study, frequency was measured in peaks per minute. To compare the strength and frequency of the QPPs across groups, an arbitrary peak height threshold of 0.1 was chosen. First, the mean height of all peaks greater than the threshold was compared between the Control and ADHD groups. Second, the overall frequency of all peaks greater than the threshold was compared between the Control and ADHD groups. Finally, the arbitrary 0.1 threshold was discarded and the cumulative sliding correlations of the Control and ADHD QPPs with their respective functional scans were plotted as histograms. The distribution of values observed in these histograms were compared between the Control and ADHD groups using a Kolmogorov-Smirnov test.

3.1.2.4 – Removal of QPPs from functional scans

To study the contributions of the Control and ADHD QPPs to FC in the DMN and TPN, they were removed from the BOLD signal using the regression method described in Chapter 2. The native QPP from all functional scans from each group was regressed from the BOLD signal. Native QPPs are defined as the QPPs acquired from that group. For example, the Control QPP is native to all the functional scans in the Control group. For each functional scan, a unique regressor was calculated for every brain voxel: The sliding correlation of the QPP was convolved with the timecourse of each brain voxel during the QPP. The obtained regressor was z-scored to match the signal in the functional scan. Next, linear regression was carried out using standardized/beta coefficients and the regressors calculated for each brain voxel. By doing so, a functional scan with attenuated presence of the QPP in the BOLD signal was produced. The efficacy of this regression method was demonstrated by conducting subsequent sliding correlations of the QPPs with all QPP-regressed functional scans. The same comparison of strength and frequency of QPPs described in the last paragraph of Section 3.1.2.3 was conducted in the QPP-removed functional scans. Differences in the strength and frequency of QPPs after their removal were compared.

3.1.2.5 – Analysis of functional connectivity

Before analysis of FC, a new set of ROIs focused only on regions in the DMN and TPN were created. First, the 273 ROIs from the Brainnetome atlas were consolidated into 26 ROIs based on the structural hierarchy of the atlas. For example, the 14 ROIs within the superior frontal gyrus were consolidated into a single ROI depicting the entire superior frontal gyrus. Next, the binary

mask of each consolidated ROI was multiplied by the binary masks of the DMN and TPN to check for any spatial overlap between the consolidated ROI and either network. Only ROIs that had spatial overlap with either network were included in the new atlas. Within these ROIs, only the voxels that overlapped with the DMN or TPN were included. For example, the superior frontal gyrus has a total of 11341 voxels. Of these, 3093 voxels overlapped with the DMN mask. Only those 3093 voxels were included in the DMN's superior frontal gyrus ROI. However, 1253 separate voxels in the superior frontal gyrus overlapped with the TPN mask. Those 1253 voxels were included in the TPN's superior frontal gyrus ROI. In the end, the new set of ROIs contained a total of 36 ROIs, half of which were DMN ROIs and half of which were TPN ROIs. Since there were differences in the DMN and TPN masks acquired from the Control and ADHD groups, a union of the DMN and TPN masks from the two groups was used during the construction of the new set of ROIs.

FC matrices were created to visualize the strength of connectivity within and across the DMN and TPN in both groups. For each functional scan, one FC matrix was created before QPP regression, and one FC matrix was created after its native QPP had been regressed. To create each of these matrices, the Pearson correlation between the mean timecourse of each ROI in the functional scan and the mean timecourse of all other ROIs in the functional scan was calculated. The values from each of the correlations were Fischer z-transformed and arranged into a 36 ROI x 36 ROI matrix. The FC matrices from all scans were averaged to obtain the mean FC for that group. In the end, each group had a mean FC matrix both before and after regression of its native QPP.

The newly created FC matrices were used to compare the strength of FC between ROIs in the DMN and TPN. First, FC strength was compared between the Control and ADHD groups. This was done once before regression of any QPPs, and again after regression of native QPPs from the functional scans. The FC differences observed between the two groups before and after regression of native QPPs were compared. Second, FC strength was compared within the Control and ADHD groups after removal of their native QPP. The effect of the regression of the native QPPs on FC strength was then compared between the Control and ADHD groups. To conduct all comparisons, a two-sample t-test was performed for each ROI connection to check for a significant change in FC strength. Given that there were 648 connections to compare, multiple comparisons correction was performed using the false detection rate correction method presented in Benjamini and Hochberg (1995). For all connections that were significantly different in FC strength, the mean difference in connectivity was displayed in the same style as the FC matrices.

3.1.3 – Results

3.1.3.1 – Differences in DMN and TPN masks between groups

Masks of the DMN and TPN acquired from the Control and ADHD groups were largely similar (Figure 3.1.1a; Figure 3.1.1b). A full list of ROIs in the Brainnetome atlas that overlapped with either the DMN or TPN is shown in Supplementary Table 1 and Supplementary Table 2. The tables also list the number of voxels in each ROI that overlapped with the DMN or TPN, and the mean correlation strength between the overlapping voxels in each ROI and the PCC.

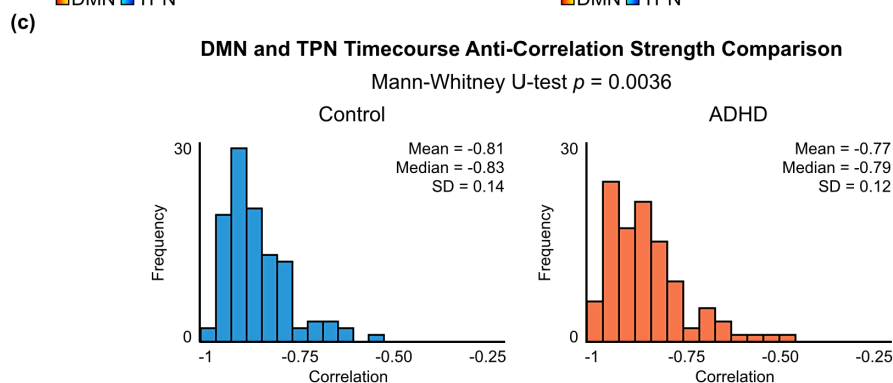
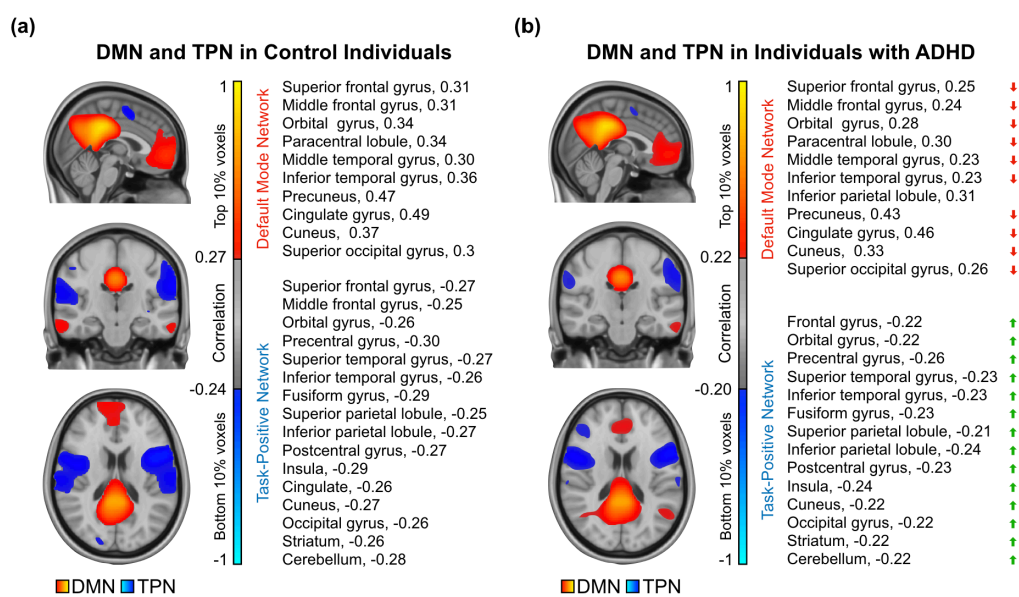


Figure 3.1.1: DMN and TPN maps in the Control and ADHD QPPs

Correlation between the mean timecourse of the PCC and every voxel in the brain was calculated. The 10% of voxels most and least correlated with the PCC were defined as the DMN and TPN respectively. **(a) Left:** The DMN and TPN in the Control group. The DMN comprises all voxels that had correlation with the PCC > 0.27 . The TPN comprises all voxels that had correlation with the PCC < -0.24 . *Right:* Names of regions in the DMN and TPN in the Control group. **(b) Left:** The DMN and TPN in the ADHD group. The DMN comprises all voxels that had correlation with the PCC > 0.22 . The TPN comprises all voxels that had correlation with the PCC < -0.20 . *Right:* Names of regions in the DMN and TPN in the ADHD group. A full list of ROIs in the DMN and TPN, including subdivisions, number of voxels, and strength of correlation with PCC is provided in Supplementary Table 1 and Supplementary Table 2. Compared to the Control group, areas in the DMN had overall lower correlation with the PCC, while areas in the TPN had overall weaker anti-correlation with the PCC. **(c)** Distributions of anti-correlation strength between DMN and TPN timecourses in all Control (left) and ADHD (right) scans. Given the non-parametric distributions, a Mann-Whitney U-test was performed to compare the strength of anti-correlation, which showed weaker anti-correlation in the ADHD group compared to the Control group ($p = 0.0036$).

For both the Control and ADHD groups, the DMN included regions in the superior and middle frontal gyri, orbital gyrus, paracentral lobule, middle and inferior temporal gyri, inferior parietal lobule, precuneus, cingulate, cuneus, superior occipital gyrus, hippocampus, and cerebellum. In the ADHD group, the DMN also included regions in the superior temporal gyrus, superior parietal lobule, striatum, and thalamus. Though DMN ROIs unique to the ADHD group are

considered in all analyses, the number of voxels in those ROIs that overlapped with the DMN mask was relatively low (< 10 voxels for each ROI, as opposed to a mean of 1461 ± 1464 voxels for the other ROIs in the ADHD DMN), with possible exception of the thalamus (33 voxels in the ADHD DMN as opposed to 0 voxels in the Control DMN). Additionally, though the hippocampus and part of the cerebellum were in the DMN mask from both groups, the number of voxels in those ROIs that overlapped with the DMN were also relatively low (< 10 voxels).

For both the Control and ADHD groups, the TPN included regions in the superior, middle, and inferior frontal gyri, orbital gyrus, precentral gyrus, superior temporal gyrus, inferior temporal gyrus, fusiform gyrus, superior and inferior parietal lobules, postcentral gyrus, insula, cuneus, occipital gyrus, striatum, and cerebellum. In the Control group, the TPN also included the cingulate. In the ADHD group, the TPN also included the middle temporal gyrus. Though TPN ROIs unique to either the Control or ADHD groups are considered in all analyses, the number of voxels in those ROIs that overlapped with the TPN mask was relatively low (< 25 for each ROI, as opposed to a mean of 1238 ± 750 voxels and 1163 ± 787 voxels for the other ROIs in the Control and ADHD TPNs respectively). Additionally, the middle frontal and middle temporal gyri had far greater overlap with the ADHD TPN mask (361 and 393 voxels respectively) than they did with the Control TPN mask (24 voxels each).

As described in the Methods, ROIs in the DMN and TPN masks were selected based off their correlation with the PCC. The strength of correlation of the DMN ROIs and the strength of anti-correlation of the TPN ROIs with the PCC was compared between the Control and ADHD groups. For ROIs in the DMN, the mean correlation with the PCC was greater in the Control group ($\mu = 0.37 \pm 0.11$) than the ADHD group ($\mu = 0.31 \pm 0.12$; $p = 0.0066$). For ROIs in the

TPN, the mean anti-correlation with the PCC was greater in the Control group ($\mu = -0.28 \pm 0.02$) than the ADHD group ($\mu = -0.23 \pm 0.02$; $p = 4.6995e-33$).

The strength of anti-correlation between the DMN and TPN timecourses for all scans were also compared between the Control and ADHD groups (Figure 3.1.1c). Given anti-correlation values had a skewed distribution, a Mann–Whitney U-test was used to compare the strength of DMN and TPN anti-correlation across groups. The ADHD group had significantly weaker anti-correlation between the DMN and TPN ($\mu = -0.77 \pm 0.12$, median = -0.79) compared to the Control group ($\mu = -0.81 \pm 0.13$, median = -0.83; $p = 0.0036$).

3.1.3.2 – Differences in QPPs between groups

Application of the pattern-finding algorithm resulted in the observation of a quasi-periodic pattern lasting approximately 20 seconds in both the Control and ADHD groups (Figure 3.1.2a; Figure 3.1.2b). The spatiotemporal pattern involved an initial increase in BOLD signal in the DMN accompanied by a decrease in BOLD signal in the TPN. This was followed by a decrease in BOLD signal in the DMN accompanied by an increase in BOLD signal in the TPN. The spatiotemporal pattern and its strength and frequency in functional scans was compared between the Control and ADHD groups.

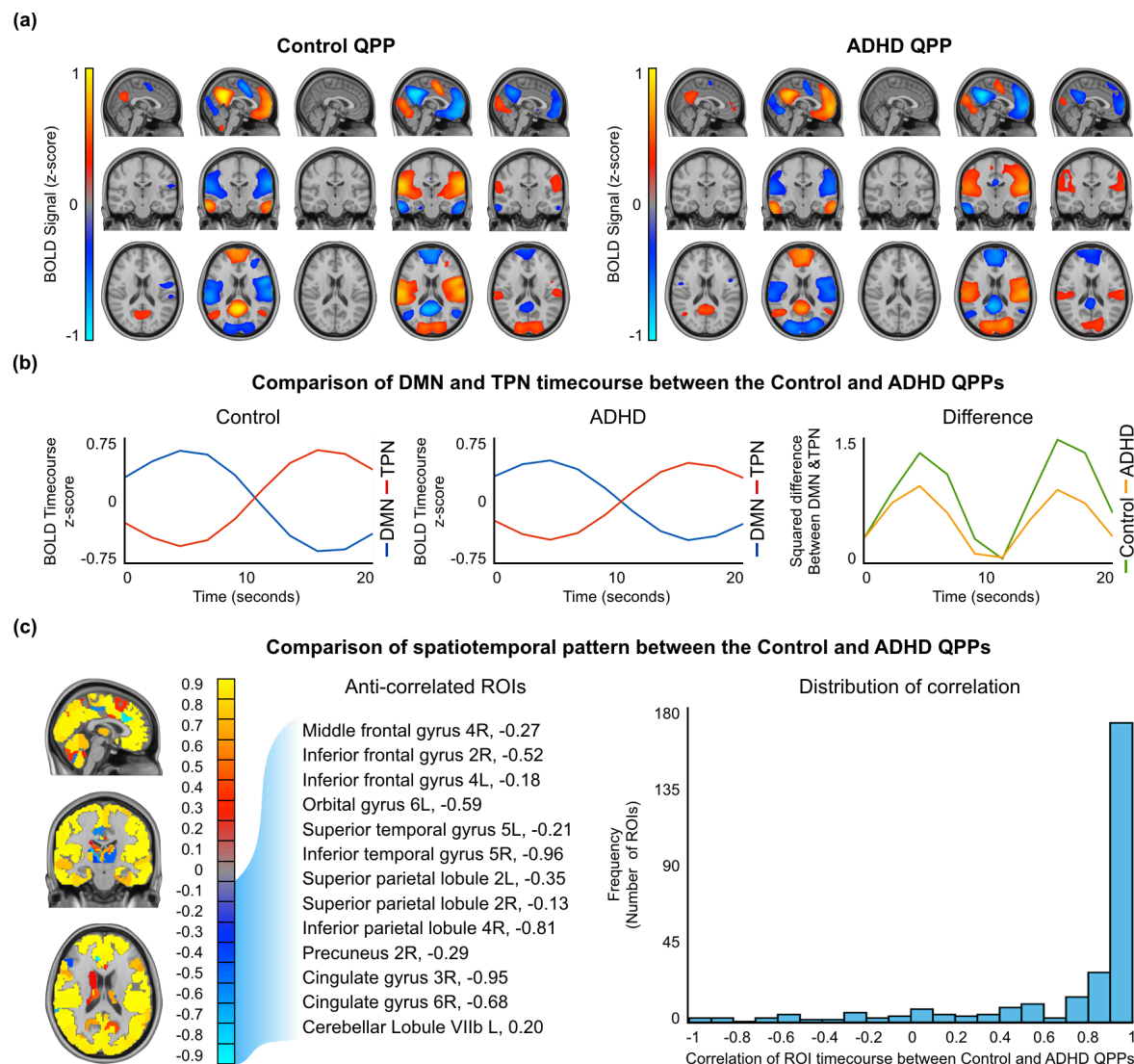


Figure 3.1.2: Spatiotemporal differences between the Control and ADHD QPPs

(a) Areas with large increases or decrease in the BOLD signal during the Control (left) and ADHD (right) QPPs. Only top and bottom 10% values are shown. (b) *Left*: Timecourse of the DMN and TPN during the Control (left) and ADHD (right) QPPs. *Right*: The square of the difference between the Control and DMN timecourse at each timepoint in the Control and ADHD QPPs. (c) *Left*: Map of similarities and differences between the Control and ADHD QPPs. Areas of positive correlation are shown in red/

yellow. Areas of negative correlation are shown in blue/turquoise. All anti-correlated regions that were also in the DMN and TPN masks in either the Control or ADHD groups are listed. *Right*: Distribution of correlation values for all 273 ROIs shows that most ROI timecourses had > 0.9 correlation between the the two QPPs.

3.1.3.2.1 – Differences in the spatiotemporal pattern

For each of the 273 ROIs in the Brainnetome ROI atlas, a correlation was performed between the timecourse of the ROI in the Control QPP and its timecourse in the ADHD QPP. The results of all 273 correlations are listed in Supplementary Table 3 and displayed using a colormap in Figure 3.1.2c on the left. Overall, the spatiotemporal pattern captured in both QPPs was similar. The distribution of correlation values, shown on the right in Figure 3.1.2c, demonstrates that most ROI timecourses were strongly correlated between the Control and ADHD QPPs. A few ROIs had anti-correlated timecourses between the two QPPs. Among them, the ROIs that overlapped with either the DMN or TPN are listed in Table 3.1.2 and further explored in the discussion.

Region	DMN	TPN	Correlation
Middle frontal gyrus, part 4 (ventral area 9/46), right		✓	-0.27
Inferior frontal gyrus, part 2 (inferior frontal sulcus), right		✓	-0.52
Inferior frontal gyrus, part 4 (rostral area 45), left	✓	✓	-0.18
Orbital gyrus, part 6 (lateral area 12/47), left	✓	✓	-0.59
Superior temporal gyrus, part 5 (lateral area 38), left	✓	✓	-0.21
Inferior temporal gyrus, part 5 (ventrolateral area 37), right	✓	✓	-0.96
Superior parietal lobule, part 2 (caudal area 7), left		✓	-0.35
Superior parietal lobule, part 2 (caudal area 7), right		✓	-0.13
Inferior parietal lobule, part 4 (caudal area 40), right		✓	-0.81
Precuneus, part 2 (medial area 5), right	✓	✓	-0.29
Cingulate gyrus, part 3 (pregenual area 32), right	✓	✓	-0.95
Cingulate gyrus, part 6 (caudal area 24), right	✓	✓	-0.68
Cerebellar lobule VIIb, left		✓	-0.20

Table 3.1.2: DMN and TPN regions anti-correlated across group QPPs

List of regions of interest in the DMN and TPN which showed anti-correlated timecourses when comparing quasi-periodic patterns from the Control and ADHD groups. Blue tick marks indicate the overlap of the ROI with the DMN or TPN from the Control group. Red tick marks indicate the overlap of the ROI with the DMN or TPN from the ADHD group. The correlation column shows the strength of anti-correlation between the timecourse of the ROI in the Control and ADHD QPPs.

3.1.3.2.2 – Difference in the DMN and TPN timecourses

Both groups' QPPs clearly showed a DMN/TPN switch in the spatiotemporal pattern. However, calculating the square of the difference between the DMN and TPN timecourses in each of the

QPPs revealed a clear difference in the magnitude of that difference (Figure 3.1.2b, *right*). At the two points where DMN and TPN signal was most separated, the mean square difference was 1.4 in the Control group and 0.9 for the ADHD group.

3.1.3.2.3 – Differences in the strength and frequency

Sliding correlations of the Control and ADHD QPPs were conducted with all functional scans in their respective groups. Examples of the sliding correlation vectors are shown in Figure 3.1.3a. The strength of a QPP in a functional scan is defined by the height of the peaks in the sliding correlation vectors. The frequency of a QPP in a functional scan is defined by how often the peaks occur over time. For the purposes of this study, the frequency of a QPP is measured in peaks per minute.

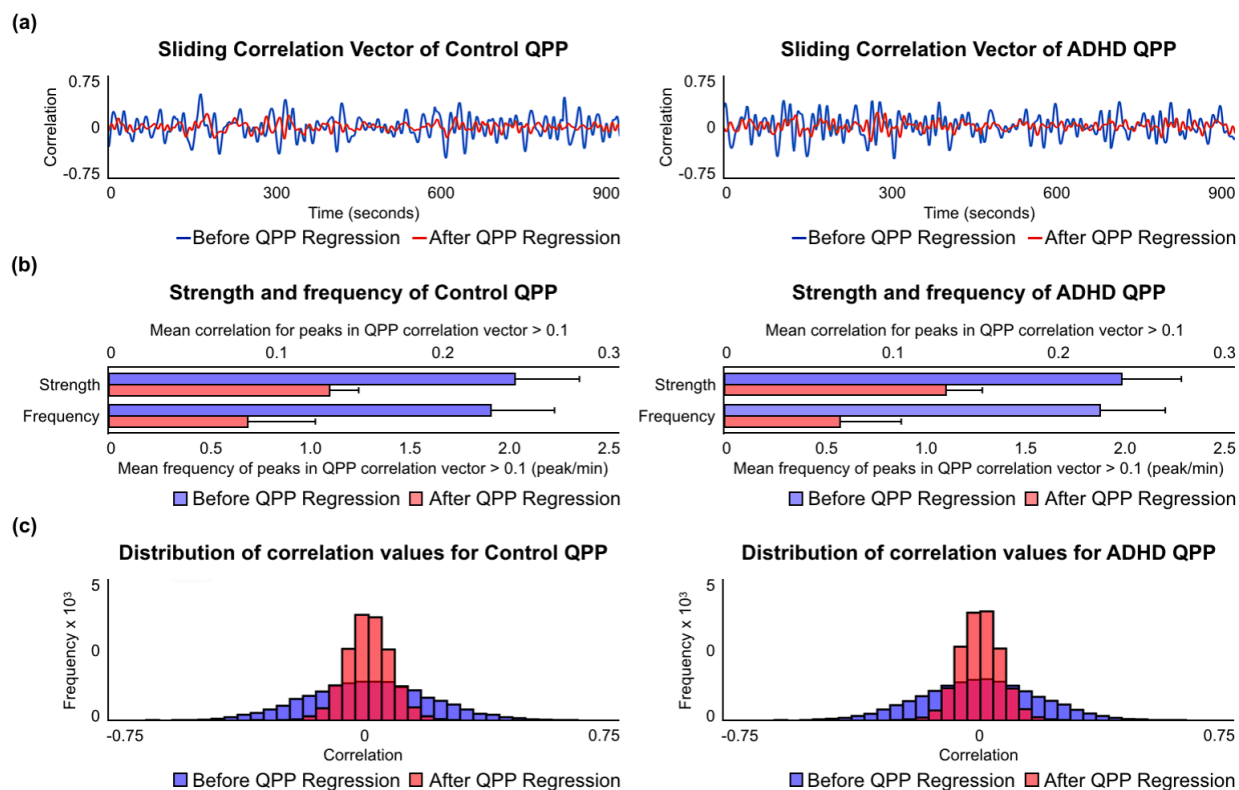


Figure 3.1.3: Strength and frequency of QPPs in Control and ADHD groups

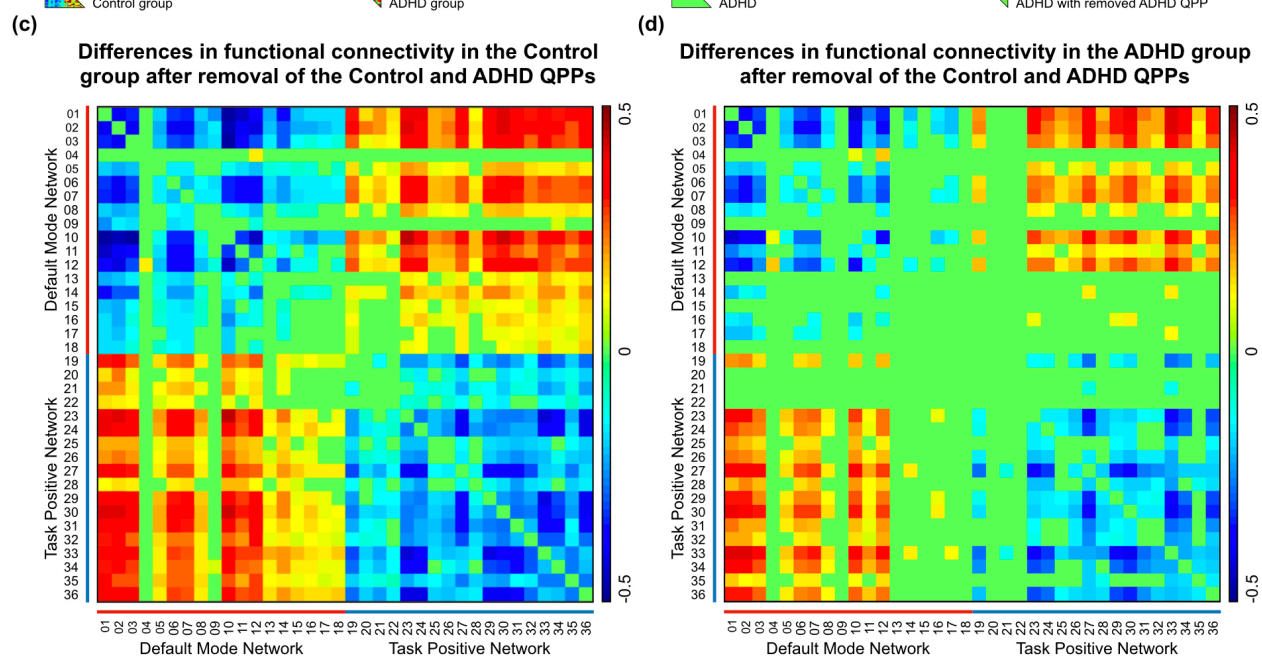
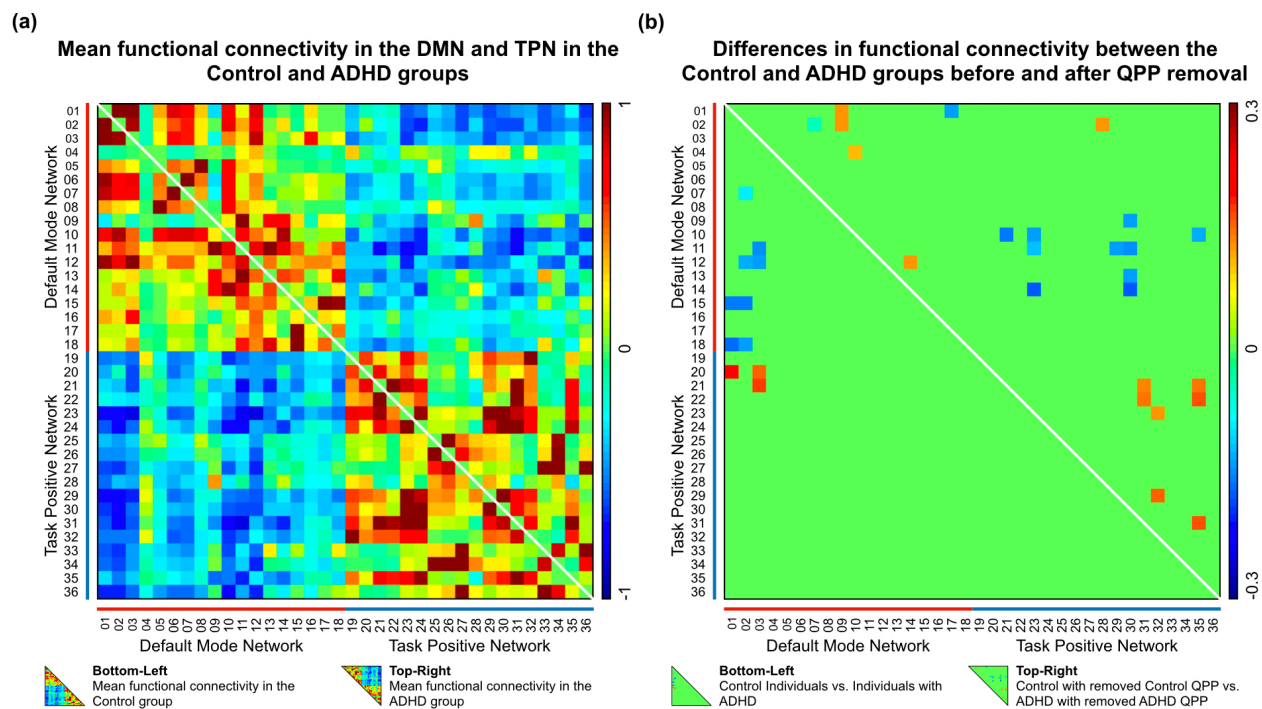
(a) Example of sliding correlation vector acquired through sliding correlation of the Control (*left*) and ADHD (*right*) QPPs with three (randomly selected) concatenated functional scans from their respective groups before (*blue*) and after (*red*) native QPP regression (b) Strength and frequency of of the Control (*left*) and ADHD (*right*) QPPs compared by setting an arbitrary 0.1 correlation threshold for identifying peaks in the correlation vectors. Top axis shows the strength in correlation and bottom axis shows frequency in peaks per minute before (*blue*) and after (*red*) native QPP regression. (c) Strength and frequency of the Control (*left*) and ADHD (*right*) QPPs compared by representing all correlation values in a histogram before (*blue*) and after (*red*) native QPP regression.

For all peaks > 0.1 in correlation, the strength and frequency of the Control QPP in its cumulative sliding correlation with the Control scans (strength $\mu = 0.24 \pm 0.04$; frequency $\mu = 1.87 \pm 0.31$ peaks/minute) was similar to the ADHD QPP in its cumulative sliding correlation with the ADHD scans (strength $\mu = 0.23 \pm 0.04$; frequency $\mu = 1.84 \pm 0.32$ peaks/minute). The cumulative sliding correlation vectors of the QPPs with each group was also compared without the use of an arbitrary 0.1 threshold by plotting them as histograms (Figure 3.1.3e; Figure 3.1.3f). Wide, short histograms indicate higher strength and frequency of the QPP, while narrow, tall histograms indicate lower strength and frequency of the QPP. Kolmogorov-Smirnov (KS) tests confirmed that the strength and frequency of the Control and ADHD QPPs in their native scans did not differ. Comparison of the strength of frequency of the QPPs in their non-native scans also did not show any differences (Supplementary Figure 5).

3.1.3.3 – Functional connectivity differences

An FC matrix displays the strength of FC in all 648 connections between the 36 brain regions compared in one image, which represents the functional architecture of the DMN and TPN. The matrix has been arranged so that data points closer to the central diagonal show FC in local connections. Data points further from the central diagonal show FC in long-range connections. The top-left and bottom-right quadrants show the local FC in the DMN and TPN respectively. The strength of these connections was expected to be positive as they are depicting functional networks. Alternatively, the top-right and bottom-left quadrants show the FC between the DMN and TPN. The strength of these connections was expected to be negative, given they are depicting connectivity between anti-correlated networks.

Figure 3.1.4a shows the mean FC in the DMN and TPN in the Control (*bottom-left*) and ADHD (*top-right*) groups. Individuals with ADHD showed weaker overall connectivity with the DMN and TPN and weaker anti-correlation across the DMN and TPN. FC within DMN ROIs in the ADHD group ($\mu = 0.23 \pm 0.40$) was weaker than the Control group ($\mu = 0.25 \pm 0.45$; $p = 3.72e-39$). FC within TPN ROIs in the ADHD group ($\mu = 0.26 \pm 0.45$) was weaker than the Control group ($\mu = 0.31 \pm 0.42$; $p = 6.41e-53$). Anti-correlation between the DMN and TPN was also weaker in individuals with ADHD ($\mu = -0.21 \pm 0.32$) compared to the Control group ($\mu = -0.26 \pm 0.30$; $p = 3.80e-73$).



Default Mode Network

01 Superior frontal gyrus	10 Inferior parietal lobule
02 Middle frontal gyrus	11 Precuneus
03 Orbital gyrus	12 Cingulate gyrus
04 Paracentral lobule	13 Cuneus
05 Superior temporal gyrus	14 Superior occipital gyrus
06 Middle temporal gyrus	15 Hippocampus
07 Inferior temporal gyrus	16 Striatum
08 Pos. superior temporal sulcus	17 Thalamus
09 Superior parietal lobule	18 Cerebellum

Task Positive Network

19 Superior frontal gyrus	28 Superior parietal lobule
20 Middle frontal gyrus	29 Inferior parietal lobule
21 Inferior frontal gyrus	30 Postcentral gyrus
22 Orbital gyrus	31 Insula
23 Precentral gyrus	32 Cingulate gyrus
24 Superior temporal gyrus	33 Cuneus
25 Middle temporal gyrus	34 Occipital gyrus
26 Inferior temporal gyrus	35 Striatum
27 Fusiform gyrus	36 Cerebellum

Figure 3.1.4: FC differences between Control and ADHD groups

(a) *Bottom-left*: Mean FC in the Control group. *Top-right*: Mean FC in the ADHD group. **(b)** *Bottom-left*: Significant differences in FC between the Control and ADHD groups ($n = 11$). *Top-right*: Significant differences in FC between the Control and ADHD group after regression of their native QPPs ($n = 24$). **(c)** Significant differences in FC in the Control group after removal of its native QPP ($n = 494$). **(d)** Significant differences in FC in the ADHD group after removal of its native QPP ($n = 280$).

Figure 3.1.4b shows significant differences in FC between the Control and ADHD groups. The bottom-left part of the matrix shows differences in FC before the QPPs were regressed from the functional scans ($n = 11$). Individuals with ADHD showed decreased local FC in the DMN and decreased anti-correlation between DMN and TPN ROIs. The top-right part of the matrix shows differences in FC after native QPPs had been regressed from both groups ($n = 24$). The differences were more widespread in this case, but largely comprised on increases in local FC in the DMN and TPN and increased anti-correlation between the DMN and TPN in individuals with ADHD. These differences are further explored in the discussion.

Figure 3.1.4c and Figure 3.1.4d show significant differences in FC in the Control and ADHD groups after regression of their native QPPs. In both groups, QPP regression led to an overall decrease in local connectivity in the DMN and TPN and a decrease in anti-correlation between the DMN and TPN. However, regression of the Control QPP from Control scans led a greater number of FC differences ($n = 494$; 76% of all connections within and across the DMN and TPN) than regression of the ADHD QPP from ADHD scans ($n = 280$; 43% of all connections within and across the DMN and TPN). Though the overall direction of FC differences was the

same, removal of the ADHD QPP from ADHD scans resulted in far fewer significant changes in FC compared to removal of the Control QPP from Control scans. A comparison of FC differences that includes the regression of the ADHD QPP from Control scans and regression of the Control QPP from ADHD scans is shown in Supplementary Figure 6.

3.1.4 – Discussion

We studied the dynamics of BOLD fluctuations in individuals with ADHD through the investigation of quasi-periodic patterns in the brain. As Chapter 2 demonstrated, QPPs contribute to FC in key functional networks and their activity could be relevant for healthy brain function. However, until this study, there had not been an investigation of QPPs in individuals with a brain disorder. ADHD is associated with atypical FC in the DMN and TPN. Given the strong involvement of the two networks in the spatiotemporal pattern captured within QPPs, we hypothesized a relationship between QPPs and the atypical FC associated with ADHD. We find that QPPs contribute to FC in the very connections that are disrupted during ADHD. Individuals with ADHD showed differences in the spatiotemporal pattern captured within the QPP, which resulted in the QPP contributing less to FC in the DMN and TPN. Our observations provide insight into the possible mechanisms behind FC differences seen in individuals with ADHD, allowing a better understanding of the etiology of the disorder.

3.1.4.1 – Default mode and task positive networks

The brain regions in the DMN and TPN that were common to both the Control and ADHD groups largely agreed with previous literature (Raichle, 2015; Fox et al., 2005). The ROIs unique to the DMN or TPN masks acquired from the ADHD group were difficult to interpret as only a relatively small number of their voxels overlapped with the DMN or TPN masks. The differences observed could be within the margins of error associated with functional MRI or the ROI boundaries in a brain atlas such as the one used in this study. One exception to this was the inclusion of the thalamus in DMN mask from individuals with ADHD. Areas in the thalamus

have previously been shown to have increased connectivity with DMN regions in individuals with ADHD (Tian et al., 2006; Tian et al., 2008), which would explain their inclusion in the ADHD DMN.

There was a consistent difference between the two groups in the strength of correlation of all DMN and TPN ROIs with the PCC, the seed used to create the masks. DMN ROIs in the ADHD group had a weaker correlation with the PCC and TPN ROIs in the ADHD group had a weaker anti-correlation with the PCC. This is likely a reflection of the observation that overall DMN/TPN anti-correlation was also weaker in individuals with ADHD. Strong anti-correlation between the DMN and TPN is a sign of healthy brain function (Fox et al., 2005) and is related to performance on vigilance tasks (Thompson et al., 2013). Indeed, it has been previously shown that individuals with ADHD show decreased anti-correlation between DMN and TPN activity (Sripada et al., 2014). This disruption has been shown to affect task performance and pharmaceutical solutions have been suggested to alleviate the atypical FC between the two networks (Querne et al., 2014; Rubia et al., 2009b). Our observations confirm a decreased anti-correlation in individuals with ADHD. Reproducing previous findings was a critical first step in analyzing the dynamics of the BOLD signal and investigating how QPPs may be contributing to differences observed through traditional static analyses of fMRI.

3.1.4.2 – Quasi-periodic patterns

Quasi-periodic patterns were observed in both the Control and ADHD groups. In each case, the spatiotemporal pattern captured in the QPP showed the DMN-to-TPN transition reported in the previous chapter and previous studies (Majeed et al., 2011; Yousefi et al., 2018; Abbas et al.,

2018a). The pattern lasted approximately 20 seconds and occurred quasi-periodically in the functional scans from both groups.

This was the first investigation of QPPs in individuals with a brain disorder. FC disruptions in the DMN and TPN have been widely reported in individuals with ADHD (Konrad & Eickhoff, 2010; Cortese et al., 2012; Hart et al., 2012). Given the involvement of the two networks in QPPs, it was pertinent to compare the spatiotemporal pattern of the QPPs between the Control and ADHD groups. A similar spatial comparison was carried out in the previous chapter., which assisted in explaining the FC changes that occur in task-performing individuals. Here, we hypothesize that any differences in the Control and ADHD QPPs may help explain the FC differences seen between the two groups.

Figure 3.1.2c and Supplementary Figure 4 demonstrate that the spatiotemporal pattern was largely similar in the Control and ADHD QPPs. However, the few observed differences were telling. Table 3.1.2 lists DMN or TPN ROIs that had anti-correlated timecourses between the Control and ADHD QPPs. Among the DMN ROIs, the cingulate gyrus and precuneus were also the regions that showed decreased FC within the DMN when FC was compared in Figure 4b. Among the TPN ROIs, the the middle and inferior frontal gyri showed decreased anti-correlation with DMN regions when FC was compared. Though the differences in the spatiotemporal pattern between the Control and ADHD QPPs were small, they aligned well with the region-to-region FC differences observed between the two groups. Hence, spatiotemporal differences in the QPPs between the two groups were able to predict FC differences in individuals with ADHD.

A key difference between the two QPPs was the magnitude of the difference between the DMN and TPN timecourses, as is demonstrated in Figure 3.1.2b on the right. The anti-correlation between the DMN and TPN was stronger in the Control QPP compared to the ADHD QPP. The pattern-finding algorithm used to acquire the QPPs averages occurrence of the spatiotemporal pattern over the course of the functional timeseries. Hence, the difference in magnitude of DMN/TPN anti-correlation between the two groups' QPPs is a reflection of a general trend in the data, rather than a consequence of the randomly-selected starting segment used to initiate the pattern-finding algorithm. This is a key difference in the QPPs acquired from the Control and ADHD groups, as it can have a strong effect on the overall contribution of QPPs to FC in the brain, discussed in the next section.

Comparison of the strength and frequency of the Control and ADHD QPPs in their respective functional scans showed no differences between the two groups (Figure 3.1.3). This is also an important observation as the different effects the two QPPs had on FC can be attributed only to the spatiotemporal differences outlined above, rather than any difference in the level of presence of QPPs in the functional scans. Figure 3.1.3 also demonstrated that the regression method used in this study was effective in significantly attenuating the presence of the QPPs in the scans. The efficacy of the regression was critical as it allowed the investigation of the contribution of QPPs to FC by essentially removing them from the BOLD signal.

3.1.4.3 – Functional connectivity

The region-to-region FC comparisons shown in Figure 3.1.4 required strict multiple comparisons correction due to the number of hypotheses being tested. However, comparison of the

distribution of FC strength within the DMN, within the TPN, and between the DMN and TPN only required testing one hypothesis each. This allowed us to conclude with confidence that the local FC within the DMN and TPN was significantly lower in individuals with ADHD. Additionally, FC analysis further demonstrated that the strength of anti-correlation between the DMN and TPN was weaker in the ADHD group. Observations of the overall differences in DMN and TPN FC between the two groups continue to align with previous reports (Konrad & Eickhoff, 2010; Weyandt et al., 2010; Sripada et al., 2014; Uddin et al., 2008).

Figure 3.1.4c and Figure 3.1.4d show that regression of the QPP from functional scans resulted in FC differences following a similar trend in both groups. Local connectivity in the DMN and TPN was reduced and anti-correlation between the DMN and TPN was weakened. This demonstrates that QPPs play a role in maintaining the FC within and across the DMN and TPN. Earlier, we saw that FC differences in individuals with ADHD follow the same trend. Our observations suggest that QPPs help maintain typical FC in the same regions that tend to develop atypical connectivity in ADHD. Hence, it may be that the FC differences in individuals with ADHD are the result of a failure of QPPs to maintain healthy FC as they do in healthy individuals.

Figure 3.1.4c and Figure 3.1.4d also show that the Control QPP contributes to FC within and across the DMN and TPN with far greater effect than the ADHD QPP. The number of connections that were significantly affected by regression of the Control QPP was 76% greater than the number of connections significantly affected by regression of the ADHD QPP. We know that the strength and frequency of both QPPs was similar in their respective functional scans. Hence this difference is likely a result of the spatiotemporal differences in the Control and

ADHD QPPs. The difference in magnitude of anti-correlation between the DMN and TPN within the spatiotemporal pattern of the QPP (Figure 3.1.2b, *right*) suggests that QPPs are contributing to an overall smaller percentage of the spontaneous BOLD signal fluctuations in individuals with ADHD. This would reduce their contribution to FC.

Figure 3.1.4b shows the difference in FC between the Control and ADHD groups. Notably, it distinguishes between the FC differences observed between the two groups before and after regression of native QPPs from the functional scans. Both the nature and the number of FC differences are different between these two comparisons. When the original functional scans were compared, the FC differences showed partial decrease in local connectivity in the DMN and reduced anti-correlation between DMN and TPN regions. These differences follow the trend of previous reports on FC disruptions in individuals with ADHD. However, when the QPP-regressed functional scans were compared, the trend of the differences was reversed and the number of FC differences increased: When comparing QPP-regressed Control scans to QPP-regressed ADHD scans, local connectivity in the DMN and TPN and anti-correlation between regions in the DMN and TPN increased. This is most likely due to the varying effects of the Control and ADHD QPPs on FC in the DMN and TPN. When the Control QPP was regressed from Control scans, it led to a large number of FC differences, as is visible in Figure 3.1.4c. When the ADHD QPP was regressed from ADHD scans, it led to a relatively smaller number of FC differences. Hence, the difference between the two comparisons in Figure 3.1.4b is a result of the ADHD QPP failing to contribute as strongly to FC in the DMN and TPN. Interestingly, comparison of FC between the Control and ADHD groups after native QPP regression demonstrates how QPPs are contributing to FC differently in individuals with ADHD. In fact, the

greater the increase in FC differences observed between the two groups after QPP regression, the more the QPP in individuals with ADHD is failing to contribute to FC. This further demonstrates the relevance of QPPs in understanding the mechanisms behind FC differences in individuals with ADHD.

3.1.4.4 – Implications for ADHD

The static FC differences in the ADHD group observed in our analysis have largely been reported in previous literature. FC in the DMN has been shown to be decreased in individuals with ADHD (Rubia et al., 2007; Uddin et al., 2008; Liddle et al., 2010; Wilson et al., 2011; Yu-Feng et al., 2007). Reviews of several fMRI studies on ADHD (Cortese et al., 2012; Hart et al., 2012) have revealed a consistent decrease in BOLD activation in attentional networks, loosely similar to the TPN investigated in this study. Studies have also shown decreased activation in attentional networks similar to the TPN during task-based fMRI scans (Schneider et al., 2010; Rubia et al., 2009b). Increase in FC between brain regions in the DMN and TPN, which we refer to instead as a decrease in DMN/TPN anti-correlation, has also been reported (Hoekzema et al., 2013; Konrad & Eickhoff, 2010).

Analysis of the dynamics of the BOLD signal have allowed researchers to understand the mechanisms behind FC differences seen in individuals with other brain disorders (Sakoglu et al., 2010; Damaraju et al., 2012; Damaraju et al., 2014; Jones et al., 2012; Holtzheimer & Mayberg, 2011). For example, Sakoglu et al. (2010) and Damaraju et al. (2012; 2014) demonstrated real-time inter-network interactions being disrupted during an auditory oddball task in individuals with Schizophrenia and the relative rigidity of time-varying network FC compared to healthy

controls. Jones et al. (2012) showed that static FC differences observable in individuals with Alzheimer's Disease may exist due to certain dominant sub-network configurations of the brain's DMN, only observable through dynamic analysis. Similarly, Holtzheimer and Mayberg (2011) argue that FC differences seen in individuals with Major Depressive Disorder are due to a tendency of network activity to linger in 'down states' longer compared relative to healthy controls, indiscernible through a static analysis of FC. However, analyses of the dynamics of BOLD signal in individuals with ADHD has been limited (Durstun et al., 2003).

Studies sensitive to the time-varying changes in BOLD in individuals with ADHD have mostly focused on task-based BOLD activation in relevant brain regions (Schneider et al., 2010; Rubia et al., 2009b; Liddle et al., 2011; Yang et al., 2011; Siqueira et al., 2014). Sonuga-Barke and Castellanos (2007) showed that in the context of pathological conditions, the dynamics of the DMN can affect attentional control in individuals. Outside the context of ADHD, Thompson et al. (2013) demonstrated that the dynamics of DMN and TPN activity can predict vigilance in performance on a psychomotor vigilance task. Given that QPPs can be used to study the dynamics of DMN activity in both resting-state and task-performing individuals, they have the potential to provide insight into the static FC differences observed in individuals with ADHD. We find that this is indeed the case. Since analyses focused on QPPs consider the time-varying component of BOLD signal, they can provide a more sensitive analysis of differences in individuals with ADHD. For example, the number of region-to-region FC differences observed between the Control and ADHD groups was small. However, when the same comparison was done after regression of the QPP, the number of FC differences between the two groups was appreciably larger.

It has been demonstrated that using static FC differences as a biomarker in individuals with ADHD is not yet the most accurate way to differentiate them from healthy controls: Brown et al. (2012) showed that personal characteristic data — such as age, gender, and performance on different IQ tests — was more accurate in predicting ADHD diagnosis than static FC differences. Analysis techniques that focus on the dynamics of the BOLD signal, such as the one shown in this study, may provide greater sensitivity to differences in individuals with ADHD. The FC analysis presented in Figure 3.1.4 shows a greater number of differences between groups compared to traditional methods, which may provide a more sensitive prediction of ADHD diagnosis. This introduces the possibility of using disruptions in QPPs as a potential biomarker of disease.

It is important to note that the results from this study do not address a critical question: Is the disruption in the QPPs causing the FC differences seen in ADHD, or is ADHD causing the disruption seen in the QPPs? However, the next chapter suggests that QPPs may have a neurophysiological driver in deep brain nuclei. If this is indeed the case, a hypothesized pathway of the etiology of ADHD would link initial disruptions in deep brain nuclei with abnormalities in the spatiotemporal pattern of QPPs, resulting in the FC differences seen in individuals with ADHD.

Local field potential (LFP) electrophysiological recordings in anesthetized rats conducted simultaneously with fMRI have shown that QPPs are correlated with infra-slow electrical activity (Pan et al., 2013). Infra-slow electrical activity is disrupted in individuals with ADHD: Helps et al. (2010) showed reduced attenuation of electroencephalography (EEG) power at infra-slow frequency bands (0.02–0.2Hz) in individuals with ADHD, which was associated with poor

performance on attentional tasks. Monto et al. (2008) also showed that psychophysical performance is related to infra-slow fluctuations in electrical activity measured through EEG. Future investigations of the relationship between QPPs, and FC, and electrical activity could enhance the understanding of the etiology of ADHD.

3.1.4.5 – Limitations

First, the dataset used in our analysis included scans collected at different facilities using different scanners and slightly different scan parameters. This has the potential to increase variability in the functional data, reducing the likelihood of observation of subtle differences between groups. However, the heterogeneity in the data also speaks to the robustness of the differences that were observed in individuals with ADHD. Second, though the Control group had an even distribution of males and females, the ADHD group was dominated (91%) by males. This is a reflection of the relatively higher clinical referral of boys when symptoms for ADHD are present, the existing bias in the ADHD literature towards male participants, and the tendency for females to be diagnosed with the Inattentive sub-type of ADHD, which was not used in this study (Biederman et al., 2002; Arnold, 1996; Gaub & Carlson, 1997; Sharp et al., 1999). Third, the selection of only the Combined sub-type of ADHD may have helped reduce variability in the results and made analysis more straightforward, but it may have also resulted in certain differences in individuals with other types of ADHD being ignored. However, given the dramatic effect of QPPs on FC in most regions in the DMN and TPN, we believe that separate analysis of different sub-types of ADHD may not have resulted in conclusions dramatically different than the ones presented in this study, as the overall trend of DMN/TPN FC differences would have been the same.

The regression method used to ‘remove’ the QPPs from the functional data inherently assumes that QPPs are an additive component to the remaining BOLD signal. This was also addressed in the previous chapter. The assumption is based on multi-modal experiments in rodents that support the notion that QPPs are additive to the BOLD signal (Thompson et al., 2014). Though further work with neural recordings in animal models is required to provide ‘ground truth’ comparisons, treating QPPs as an additive signal is a reasonable first approximation.

There were multiple justifications for consolidating the 273 ROIs from the Brainnetome atlas into the 36 ROIs that were used to construct the FC matrices. Most importantly, QPPs have been shown to mainly contribute to FC in the DMN and TPN (as shown in the previous chapter), which is also where most FC disruptions relevant to ADHD have been reported (Konrad & Eickhoff, 2010). Hence, a focus on DMN and TPN connectivity was appropriate when studying the relationship between QPPs and ADHD. Notably, only voxels in the ROIs that overlapped with the DMN or TPN masks were used, allowing the FC analysis to be specific to the two networks. Additionally, consolidation of ROIs into larger brain regions helped alleviate variability in the ROI timecourses, providing more reliable results. Finally, consolidation of the ROIs meant that the number of comparisons being performed to determine the statistical significance of a change in connectivity was reduced from 37264 to 648; a 98% decrease.

Finally, it is important to comment on the use of global signal regression during the preprocessing of all functional scans. It has been shown that global signal regression reduces variability in QPPs acquired from different individuals. In Yousefi et al. (2018), individuals were divided into two groups; those with low levels of global signal fluctuation and those with high levels of global signal fluctuation. Individuals with low levels of global signal fluctuation showed

the same anti-correlated behavior of the DMN and TPN reported in this study. Individuals with high levels of global signal fluctuation showed that the global signal had an additive effect on the QPP: Though the observed spatiotemporal pattern and its frequency of occurrence was relatively unchanged, the whole-brain global changes in BOLD obscured the underlying pattern. When global signal regression was conducted in the individuals with high levels of global signal fluctuation, their QPPs aligned with those of individuals with low levels of global signal fluctuation. A primary aim of this study was to understand the effects of QPP regression on FC in the brain. If global signal had not been regressed from the functional scans, it could have served as a confounding factor in the subsequent analysis. Depending on the levels of global signal fluctuation in each individual, the spatiotemporal pattern observed in QPPs would have varied and their regression would have affected static FC differently across individuals. Hence, for a study investigating the effect of QPP regression on FC, global signal regression in all functional scans was appropriate, especially given that there are several studies already demonstrating the effects of global signal regression on FC (Murphy & Fox, 2007).

3.1.5 – Conclusions

We confirm that FC within and across the DMN and TPN is disrupted in individuals with ADHD. Investigation of quasi-periodic patterns is an effective way to understand the dynamics of the BOLD signal underlying those FC differences. We find that QPPs help maintain connectivity in the same brain regions affected during ADHD. Disruptions in the spatiotemporal pattern of the QPPs may be leading to an inability of the QPPs to maintain healthy FC in those regions. This could potentially underlie the FC differences seen in individuals with ADHD and provide a more accurate understanding of the etiology of the neurodevelopmental disorder.

3.2 – Stroke

3.2.1 – Introduction

Stroke is a leading cause of adult disability, with paretic arm dysfunction being a primary contributor (Langhorne et al., 2009). Following stroke, brain regions both close and distant to the infarct undergo a reorganization of neural connections (Grefkes & Fink, 2014; Carrera & Tononi, 2014). Though the exact nature of this cortical reorganization is not fully understood, fMRI studies have shown that individuals with stroke have altered FC in affected areas of the brain (Van Meer et al., 2010; Carter et al., 2010). For individuals with motor impairment following stroke, FC disruptions will often be found within the sensorimotor network (SMN) (Schaechter, 2004).

As discussed in Chapter 1, static fMRI measures do not provide a complete picture on how large-scale brain activity is affected during a neurological disorder. An understanding of the dynamics of FC can be more informative on how stroke affects large-scale brain activity. For example, Jones et al. (2012) used dynamic graphical representations of brain connectivity to demonstrate that changes in FC observable in individuals with Alzheimer's Disease could partially be explained by differences in dwell time in the DMN's sub-network configurations. Damaraju et al. (2012) used dynamic analysis techniques in individuals with schizophrenia to show that there was a difference in the 'rigidity' of FC between brain regions in patients compared to controls — a conclusion that was not apparent with traditional fMRI analysis techniques. However, little is known about changes in the dynamics of FC in individuals with motor impairment due to stroke.

The previous section in this chapter showed that quasi-periodic patterns are a viable method to capture the dynamics of relevant large-scale brain activity in individuals with ADHD. It is possible that QPPs can serve a similar purpose in individuals with stroke. However, there is a key difference between using QPPs to study ADHD and motor impairment due to stroke. ADHD is associated with FC disruptions in the DMN and TPN (Konrad & Eickhoff, 2010). Individuals with motor impairment due to stroke have disruptions in FC within the SMN (Van Meer et al., 2010; Wang et al., 2010; Calautti & Baron, 2003). Though QPPs have been shown to contribute to FC in the DMN and TPN, their relationship with SMN FC is weak at best. Under the current hypothesis, QPPs should not be the underlying mechanism behind FC disruptions in individuals with motor impairment during stroke.

In this study, we investigate just that — with the objective to better understand how QPPs can assist in studying the dynamics of brain activity and when they cannot. QPPs are extracted from healthy individuals and individuals with stroke. Their spatiotemporal pattern and their strength and frequency in the functional scans are compared between the two groups. FC is compared between the Control and Stroke groups. The QPPs are then regressed from the BOLD signal and the FC comparison is conducted again. Finally, the effects of QPP regression on FC is measured to test the contributions of QPPs to FC in the brain. We find that given the QPPs' weak relationship with FC in the SMN, they are not a viable method to study FC disruptions in individuals with motor impairment due to stroke. In doing so, the results validate the methods used in the ADHD study from earlier in this chapter and demonstrate that QPPs are only relevant to neuropsychiatric disorders that show FC disruptions in the DMN and TPN.

3.2.2 – Methods

3.2.2.1 – Participants

The Control group consisted of 14 healthy individuals (aged 52 ± 15 years, 6 males). The Stroke group consisted of 14 individuals (aged 66 ± 10 years, 8 males) with a subcortical ischemic stroke in the right ($n = 7$) or left ($n = 7$) hemisphere of the brain. They were in the chronic stage (> 6 months, 52 ± 29 months after stroke) of recovery. Exclusion criteria included (1) hemorrhagic stroke, (2) history of multiple strokes, (3) neurodegenerative disorder or psychiatric diagnosis, (4) outside the age range of 18–85 years, and (5) contraindications to TMS. Written informed consent was obtained from all participants in accordance with the Declaration of Helsinki and all study procedures were approved by the Emory University Institutional Review Board.

3.2.2.2 – Data acquisition

All data was acquired using a 3T Siemens Scanner (Magnetom Trio, Siemens, Germany). For each individual, one anatomical scan and three resting-state functional scans were acquired. The anatomical scan was acquired through a T1-weighted three-dimensional magnetization-prepared rapid gradient echo (T1w 3D MPRAGE) sequence with TR 2300 ms, TE 2.89 ms, TI 800 ms, FOV 256 mm x 256 mm, and 1 mm isotropic voxels. The functional scans were acquired in 3 discontinuous 4-minute sessions using a Gradient-echo echo-planar imaging (EPI) sequence with TR 2000 ms, TE 28 ms, FOV 1152 mm x 1152 mm, matrix dimensions 64 x 64 x 64, slice

thickness 3 mm, and 3 mm isotropic voxels. Each of the three scans were concatenated for a combined 11 minutes (660 seconds) of usable functional data per participant.

All preprocessing steps carried out on the data are outlined in the preprocessing pipeline described in Appendix A.

3.2.2.3 – Functional connectivity

All functional scans were segmented using the Brainnetome region of interest atlas (Fan et al. 2016). Of the 273 regions of interest in the Brainnetome ROI atlas, only 253 were applicable to the functional data in this study as all cerebellar regions fell outside the field of view of the functional scans. The 253 remaining ROIs were consolidated into 55 ROIs based on their structural hierarchy, as specified by the Brainnetome atlas. For all analyses in this study, only the 8 regions of interest (ROIs) that comprised of the sensorimotor network were used. The timecourses of all ROIs in the SMN were calculated. Pearson correlations between the timecourses of all ROIs were conducted to represent the strength of FC between all ROI connections in the SMN. The correlation values were compiled into a FC matrix for each individual. FC between the Control and Stroke groups was then compared.

3.2.2.4 – Standardization of lesioned hemispheres

Of the 14 individuals in the Stroke group, 7 individuals had lesions in the right hemisphere, while 7 had lesions in the left hemisphere. To better assess the effect of motor impairment across individuals with stroke, the effect of lesion location had to be reduced by standardizing the lesioned hemisphere to the right hemisphere. Thus, for all individuals with lesions in the left

hemisphere. the timecourses for all regions in the right hemisphere were switched with the left hemisphere. This step was performed after calculating all ROI timecourses and before generating the FC matrices.

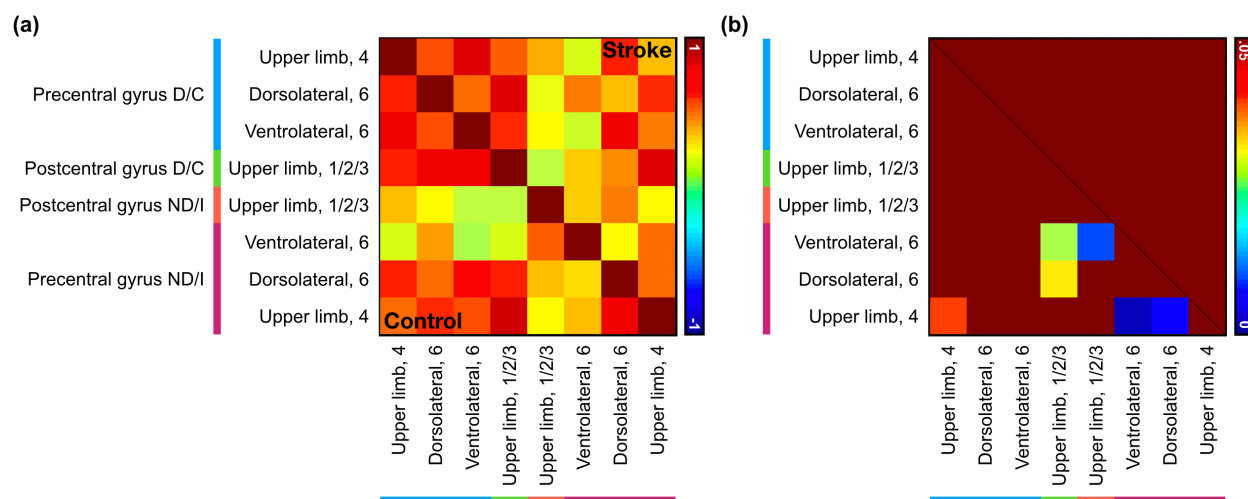
3.2.2.5 – Quasi-periodic patterns

Quasi-periodic patterns were acquired using the same methods as described in Chapter 2.1.2 and Chapter 3.1.2. For the Control and Stroke groups separately, all functional scans from unique individuals were concatenated and the pattern-finding algorithm was then applied. One representative QPP was chosen for the Control group and another for the Stroke group. The spatiotemporal pattern of the QPP and the strength and frequency of its occurrence in the functional scans was then compared. Finally, the Control and Stroke QPPs were regressed from the Control and Stroke scans respectively to study their contributions to FC. Strength of FC between all SMN ROIs before and after regression of the QPPs was compared for the Control and Stroke groups.

3.2.3 – Results

3.2.3.1 – Functional connectivity

Mean FC within the SMN in both the Control and Stroke groups was arranged into FC matrices and compared (Figure 3.2.1a). As was expected, all ROI timecourses in the SMN were positively correlated. In the Control group, intra-hemisphere SMN FC in the dominant hemisphere was positive (mean $r \pm SD = 0.70 \pm 0.079$). In the Stroke group, intra-hemisphere SMN FC in the corresponding contralesional hemisphere was also positive (mean $r \pm SD = 0.64 \pm 0.12$). Intra-hemisphere SMN FC for both groups was weaker and more varied in the non-dominant ($\mu = 0.43 \pm 0.20$) and ipsilesional ($\mu = 0.38 \pm 0.15$) hemispheres. Interhemispheric connectivity for both Control ($\mu = 0.43 \pm 0.25$) and Stroke ($\mu = 0.43 \pm 0.24$) is more varied than each's respective intrahemispheric connectivity. Interhemispheric connections include strong and very weak connections (correlation ~ 0) as can be seen qualitatively. Significant differences ($p < 0.05$) between SMN FC in Control and Stroke groups ($n = 14$) were found and compared (Figure 3.2.1b). There were 6 significant differences found: three interhemispheric differences ($p < 0.05$), three intrahemispheric differences in the non-dominant/ipsilesional hemispheres ($p < 0.01$), and no differences in the dominant/contralesional hemispheres.



Hemisphere convention: D = dominant, ND = non-dominant, C = contralesional, I = ipsilesional

Figure 3.2.1: FC Differences between Control and Stroke groups

(a) Mean functional connectivity between eight ROIs associated with the sensorimotor network across individuals in the Control group (*bottom-left*) and Stroke (*top-right*) group. The color bar corresponds to the range of correlation values. (b) Significant differences ($\alpha < 0.05$) in sensorimotor functional connectivity between Control and Stroke groups.

3.2.3.2 – Quasi-periodic patterns

As observed in Chapter 2 and earlier in Chapter 3, the QPP observed in both the Control and Stroke groups involved a transition between DMN and TPN activity spanning 20 seconds. The spatiotemporal pattern of the QPP did not differ between the Control and Stroke groups (Figure 3.2.2). The strength and frequency of the occurrence of QPPs was also similar (Figure 3.2.3). Overall, there were no significant differences between the QPPs observed in both groups.

Regression of QPPs from the functional scans was effective in removing the presence of the QPPs in the BOLD signal from both groups. When FC in the sensorimotor network was compared in the Control and Stroke groups before versus after regression of QPPs, no significant differences in FC could be seen. Removal of QPPs through regression did not affect FC in the same regions that showed FC differences when comparing FC between the Control and Stroke groups.

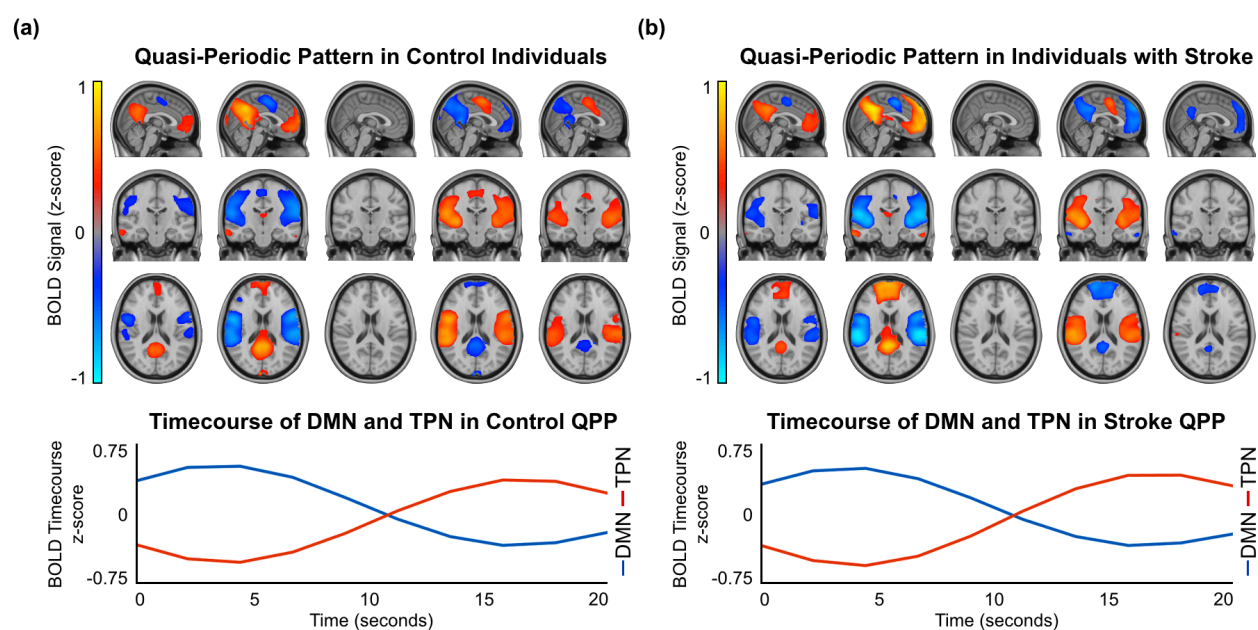


Figure 3.2.2: Spatiotemporal pattern of Control and Stroke QPPs

(a) *Top*: Spatiotemporal pattern of QPPs in the Control group. *Bottom*: Timecourse of the DMN and TPN in the Control QPP. (b) *Top*: Spatiotemporal pattern of QPPs in the Stroke group. *Bottom*: Timecourse of the DMN and TPN in the Stroke QPP. The quasi-periodic patterns did not show any observable spatiotemporal differences between the Control and Stroke groups.

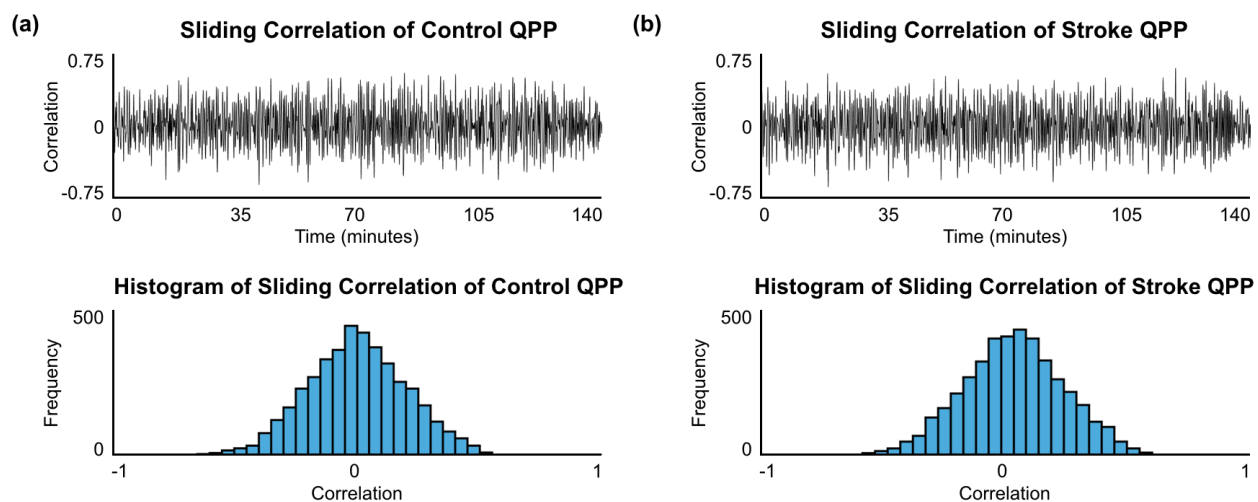


Figure 3.2.3: Strength and frequency of Control and Stroke QPPs

(a) Top: Sliding correlation vector of the Control QPP with all 14 scans in the Control group. **Bottom:** Histogram of the sliding correlation vector of the Control QPP with all 14 scans in the Control group. **(b) Top:** Sliding correlation vector of the Stroke QPP with all 14 scans in the Stroke group. **Bottom:** Histogram of the sliding correlation vector of the Stroke QPP with all 14 scans in the Stroke group.

3.2.4 – Discussion

Comparison of static functional connectivity led to observation of significant FC differences between the Stroke and Control groups in the sensorimotor network. This shows that lesions from stroke affecting motor behavior in individuals indeed disrupts the functional architecture of the SMN. Similar FC differences have been observed in previous studies and were hence expected in this analysis (Schaechter, 2004). QPPs were observable in both healthy individuals and individuals with motor impairment due to stroke. When the QPPs from the two groups were compared, no significant differences were observable. The spatiotemporal pattern involved a transition from the DMN to TPN in both groups and the strength and frequency of the QPPs was similar as well.

Studying large-scale brain activity dynamics in stroke through investigation of QPPs was useful in that it tells us how large-scale activity is *not* disrupted due to lesions from stroke. The lesions in this study resulted in motor impairments in the participants. Such effects are not directly related to the primary areas involved in the large-scale brain activity captured in QPPs, i.e., the DMN and TPN. Hence, the hypothesis was that the QPPs will be unaffected in the Stroke group.

This is helpful in understanding the large-scale brain activity disruptions behind motor impairment from stroke as it rules out atypical activity in brain regions not directly in the infarct. Particularly relevant to this dissertation, the observations are also helpful in understanding the role that QPPs play in maintaining healthy brain function. Chapter 2 shows that QPPs contribute to functional connectivity in the DMN and TPN. The previous section in this chapter shows that contribution of QPPs to FC deems them relevant to brain disorders involving the DMN and TPN.

This section shows that the contribution of QPPs to FC does not deem them relevant to brain disorders not involving the DMN and TPN.

It is important to note that the sample size in this experiment was drastically smaller than the previous experiments described in this dissertation. Compared to approximately 100 subjects per group in Chapter 2 and Chapter 3.1, the 14 subjects per group used in this experiment certainly provides weaker statistical robustness. However, the QPP acquisition in previous chapters was conducted using no more than 30 subjects per group; all 100 subjects were not needed when comparing the spatiotemporal pattern of the QPPs. More importantly, the stability of the spatiotemporal pattern in the observed QPP *increases* with the number of subjects used. If anything, using fewer individuals in this experiment should lead to greater variability between groups. Given that no variability was seen is a demonstration that the QPPs are indeed unaffected in the presence of motor impairment from stroke.

3.2.5 – Conclusions

We observe through static analysis of fMRI data that SMN FC is disrupted in individuals with motor impairment due to stroke. Investigation of quasi-periodic patterns in these individuals reveals that QPPs indeed do not influence FC in the SMN. This demonstrates that stroke may not be influencing large-scale brain activity dynamics in regions not directly associated with the infarct. These results also help narrow the focus of the role QPPs play in brain function by tying them closer to FC in the DMN and TPN and distancing them from FC in regions whose activity is not directly captured in the spatiotemporal pattern of the QPPs.

Chapter 4

Predicting neural drivers of quasi-periodic patterns

4.1 – Introduction	104
4.2 – Methods	107
4.2.1 - Animal preparation	107
4.2.2 – Acquisition of fMRI data	107
4.2.3 – Acquisition of quasi-periodic patterns	108
4.3 – Results	110
4.3.1 – Efficacy of DSP4 treatment	110
4.3.2 – Spatiotemporal pattern of QPPs	110
4.3.3 – Strength and frequency of QPPs	113
4.4 – Discussion	116
4.4.1 – A neural mechanism for QPPs	116
4.4.2 – Controlled input from the locus coeruleus	117
4.4.3 – Limitations and future directions	118
4.5 – Conclusions	119

4.1 – Introduction

The importance of studying large-scale brain activity has been extensively argued for in this dissertation. Human behavior and disease are represented in the dynamics of large-scale brain activity, which can be studied through the investigation of QPPs. Evidence shows that QPPs contribute to typical functional connectivity — a sign of healthy brain activity — and that disruption in QPPs may be a mechanism behind the altered FC seen in individuals with brain disorders. However, the mechanism behind the occurrence of QPPs remains to be investigated. In this chapter, I explore a working model hypothesizing that QPPs are the result of neuromodulatory input from subcortical nuclei, specifically from the locus coeruleus.

Deep brain nuclei have the capacity to influence large cortical regions through spatially patterned projections. The distribution of the receptors they target allow them to influence the activity of regions across the cortex through neuromodulation. The locus coeruleus, with its wide noradrenergic projections, is not unique in this ability. In fact, large-scale brain organization is affected by the manipulation of any major neuromodulator (Williams et al., 2002; Wiggins et al., 2012; Kelly et al., 2009). Hence, when it comes to investigating possible neural drivers of QPP activity, several subcortical nuclei are possible contenders. Indeed, it is arguably the case that activity from more than one subcortical nucleus is responsible for QPP activity. For purely experimental reasons, it is ideal to start investigation of a subcortical role on QPP activity with one nucleus. For the locus coeruleus to be chosen first, adequate justification was needed.

Evidence suggests that QPPs are related to arousal and vigilance, which are highly relevant to locus coeruleus activity (Aston-Jones et al., 1991; Aston-Jones et al., 1994). The locus coeruleus

is known to be a driver of attentional control in the brain (Aston-Jones et al., 1999). Work from our group provides an argument for a potential relationship between QPPs and attention and vigilance. Chapter 1 shows that QPPs occur with greater strength and frequency in individuals when they are performing a cognitively demanding task compared to when the same individuals are at rest. Chapter 2 shows that the spatiotemporal pattern of QPPs is disrupted in individuals with ADHD, a neuropsychiatric disorder highly relevant to attention and vigilance. Preliminary experiments not presented in this dissertation showed that QPPs in awake, resting-state rhesus macaques occur with greater strength and frequency compared to anesthetized macaques (Abbas et al., 2016).

Work by other groups furthers the case for a relationship between locus coeruleus activity and the role of QPPs. Pupil diameter, which has been shown to reflect LC activity (Gilzenrat et al., 2010; Joshi et al., 2016), is correlated with changes in FC (Murphy et al., 2010; Chang et al., 2016). Locus coeruleus activity also influences trial-to-trial variability in task fMRI, which is tied to activity in the DMN (Kelly et al., 2008). The power of cortical delta band synchronization, which leads to stronger FC, is increased by locus coeruleus activity (Lu et al., 2007; Pan et al., 2011; Safaai et al., 2015). When noradrenergic neurons are stimulated using DREADDs (designer receptors exclusively activated by designer drugs), they exhibit distinct activation timecourses, the spatial distribution of which resemble resting-state network and QPPs (Das et al., 2017). There is compelling evidence for a relationship between the locus coeruleus and QPP activity. Hence, the locus coeruleus is a strong contender for a driver of the large-scale brain activity dynamics captured within QPPs.

In this experiment, we search for QPPs in three groups of rats. The first is a group of Control rats, with which we expect to replicate the observations from previous studies observing QPPs in rodents (Majeed et al., 2009; Majeed et al., 2011). The second group is rats that have been treated with DSP4 (N-(2-chloroethyl)-N-ethyl-2-bromobenzylamine), a selective locus coeruleus neurotoxin. DSP4 decreases noradrenergic innervation of the cortex to 10-20% of its normal value and reduces the LC basal firing rate by 50% (Jonsson et al., 1981). The third group is rats that have been treated with Atomoxetine, a norepinephrine re-uptake inhibitor. Atomoxetine drastically increases extracellular norepinephrine levels and signaling in the cortex (Bymaster et al., 2002). We compare the results of the pattern-finding algorithm on all three groups, with the hypothesis that previous findings on the spatiotemporal pattern of QPPs will only be replicated in the Control group. If QPP activity is indeed affected by disruption of neuromodulation by locus coeruleus activity, it will be compelling evidence that QPPs are tied to neuromodulatory input from deep brain nuclei.

4.2 – Methods

4.2.1 - Animal preparation

A total of 24 adult male Sprague-Dawley rats weighing between 200 g and 250 g were used for this study. The 24 rats were divided evenly into three groups of 8: Control, DSP4, and Atomoxetine. The DSP4 group was given a subcutaneous injection of 50 mg/kg DSP4 10 days prior to MRI data acquisition, which is known to reduce norepinephrine levels in the brain by up to 90% in that time period (Jaim-Etcheverry & Mari, 1980). The Atomoxetine group was given a subcutaneous injection of 1 mg/kg Atomoxetine 30 minutes prior to MRI data acquisition (Bymaster et al., 2002). All experimental procedures were carried out following approval by the Institutional Animal Care and Use Committee of Emory University.

4.2.2 – Acquisition of fMRI data

Prior to MRI data acquisition, all rats were placed in a 5% isoflurane chamber until fully anesthetized, after which they were placed onto a cradle. Anesthesia was maintained through a supply of 2% isoflurane in the cradle. A respiratory pressure transducer was placed under the chest for respiratory monitoring. A pulse oximeter was attached to the hind paw for oxygen and heart rate monitoring. A rectal thermometer probe was used for temperature monitoring. Body temperature was maintained using a heated water circulator. A subcutaneous injection providing a continuous supply of 0.05 mg/kg dexmedetomidine was inserted into the thigh. After the anatomical scan, isoflurane was slowly decreased to 0.5%, relying solely on the

dexmedetomidine supply to keep the rat sedated. The physiological state of the animal was recorded every 15 minutes.

For MRI data acquisition, a 9.4 Tesla Bruker BioSpec[®] scanner with a 20-cm horizontal bore running ParaVision 5.1 was used. Each rat underwent one anatomical scan (FLASH3D sequence; TR 70ms, TE 4ms, FOV 3.2cm, matrix size 128x128x128) and 1-*n* functional scans (GE-EPI sequence; TR 1000ms, TE 14.5ms, FOV 3.2cm, matrix size 64x64x30), with *n* determined by the physiological state of the animal in the scanner and the quality of the data being acquired. All scans with motion greater than 0.5 mm or 0.025 radians were discarded. Only scans with isoflurane levels less than 0.5% were used. This appreciably decreased the number of scans used in the study compared to the number of scans collected. A total of 15 functional scans from 8 rats were acquired for the Control group, 10 functional scans from 8 rats for the DSP4 group, and 9 functional scans from 8 rats for the Atomoxetine group. All data was preprocessed according to the preprocessing pipeline detailed in Appendix A.

4.2.3 – Acquisition of quasi-periodic patterns

The acquisition of QPPs follows what has been described in previous chapters. Since the rat fMRI data was not registered to a standard space in order to maintain data quality, the pattern-finding algorithm was applied to each scan separately. For every scan, the pattern-finding algorithm was applied 100 times using unique, randomly-selected starting timepoints. From the results, the output with the greatest average correlation in all peaks in the QPP's sliding correlation vector was chosen as the representative QPP from that functional scan. The spatiotemporal pattern of the resulting QPP and its strength and frequency of occurrence in the

functional scans in the Control group was compared to previously observed results in Majeed et al. (2011) and the QPPs acquired from the DSP4 and Atomoxetine groups.

After scanning, the brains of the Control and DSP4 group rats were collected through rapid decapitation after deep anesthetization with isoflurane. High Performance Liquid Chromatography (HPLC) was used to test for both norepinephrine and dopamine levels in the brain. The hippocampus and prefrontal cortex of each hemisphere were rapidly dissected and snap-frozen in isopentane cooled on dry ice. The samples were stored at -80°C until processing. For tissue processing, samples were thawed on ice and sonicated at 4°C in 0.1 N perchloric acid (10 l/mg tissue) for 12 sec of 0.5 sec pulses. Sonicated samples were centrifuged (16100 rcf) for 30 min at 4°C . The supernatant was centrifuged through $0.45\ \mu\text{m}$ filters at 4000 rcf for 10 min at 4°C . Norepinephrine and metabolites were measured by electrochemical detection using an ESA 5600A CoulArray detection system (Chalermphanupap et al., 2018). Analytes were identified by matching criteria of retention time and sensor ratio measures to known standards (Sigma-Aldrich). Compounds were quantified by comparing peak areas to those of standards on the dominant sensor. If the DSP4 treatment was successful, the rats in the DSP4 group were predicted to show significantly lower levels of norepinephrine when compared to the Control group while showing the same level of dopamine.

4.3 – Results

4.3.1 – Efficacy of DSP4 treatment

HPLC results showed that norepinephrine levels in the DSP4 group were significantly decreased in the prefrontal cortex and hippocampus when compared to the Control group (Figure 4.1a; Figure 4.1b). Dopamine levels in the prefrontal cortex and hippocampus were similar in both groups (Figure 4.1c; Figure 4.1d). This demonstrated that the DSP4 treatment was successful in inhibiting the effect of the locus coeruleus on cortical activity through a depletion of norepinephrine levels in the brain.

4.3.2 – Spatiotemporal pattern of QPPs

Application of the pattern-finding algorithm to the Control group resulted in the observation of a distinct spatiotemporal pattern spanning approximately 5 seconds. The observed spatiotemporal pattern showed activity similar to the QPPs observed in Majeed et al. (2009) and Majeed et al. (2011), which were reports of the first observations of QPPs in rodents. A representative visualization of the QPPs observed in the Control group is provided in Figure 4.2b, which can be compared to the QPP reported in Majeed et al. (2011) in Figure 4.2a.

A similar spatiotemporal pattern was not observable in either the DSP4 group or the Atomoxetine group. There was significant variability between the spatiotemporal patterns acquired through the application of the pattern-finding algorithm. The pattern shown in Figure 4.2c for the DSP4 group and Figure 4.2d for the Atomoxetine group are examples of the results observed. In both cases, no reliably recurring sequence of events was distinguishable. The spatiotemporal patterns

observed were not consistent across subjects in the groups. Lastly, they were not similar to the sequence of events reliably captured in the rats from the Control group.

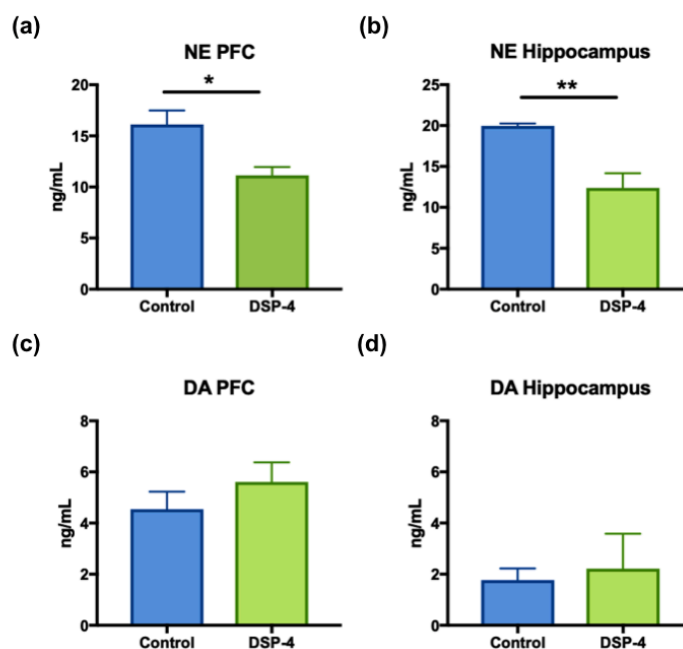


Figure 4.1: HPLC results in rats from the Control and DSP4 groups

(a) Administration of DSP4 resulted in a significant decrease in levels of norepinephrine in the prefrontal cortex in the DSP4 group compared to the Control group. (b) Administration of DSP4 resulted in a significant decrease in levels of norepinephrine in the hippocampus in the DSP4 group compared to the Control group. (c) Administration of DSP4 did not affect dopamine levels in the prefrontal cortex in the DSP4 group compared to the Control group. (d) Administration of DSP4 did not affect dopamine levels in the hippocampus in the DSP4 group compared to the Control group.

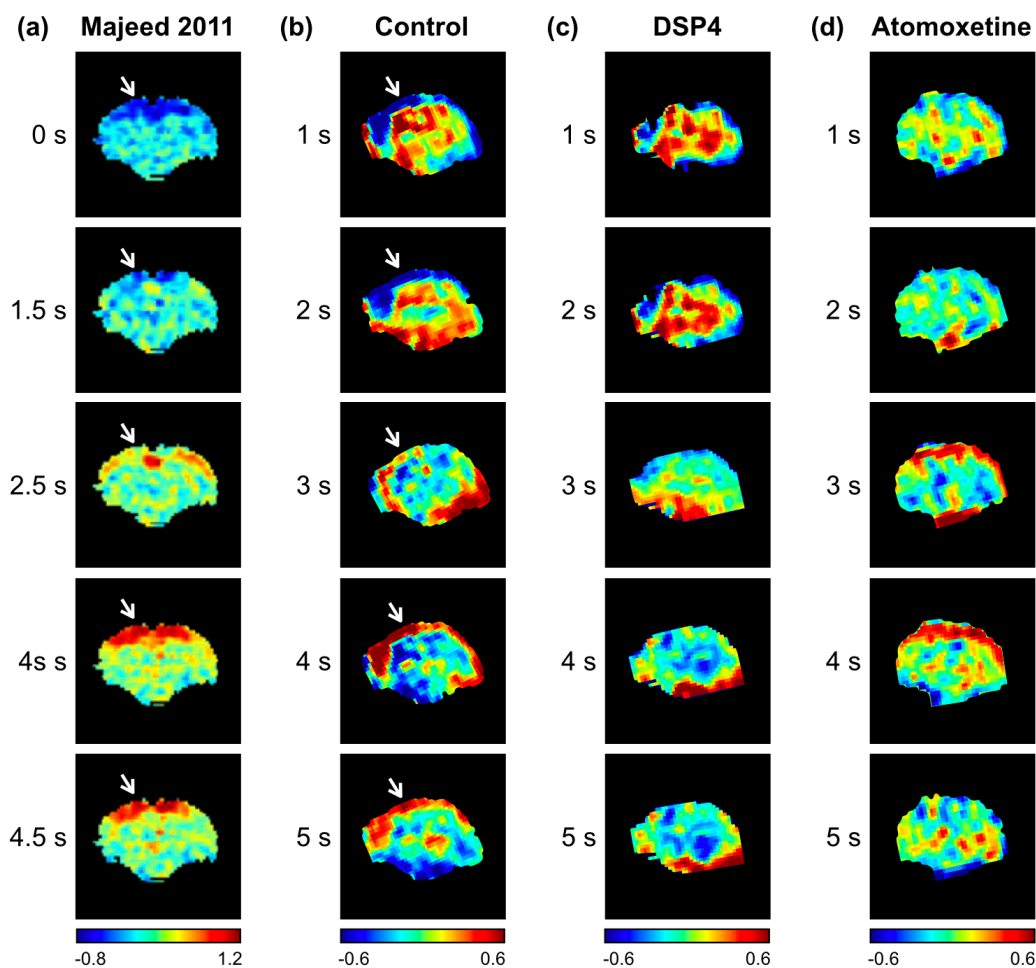


Figure 4.2: Spatiotemporal comparison of QPPs in rats

(a) Previously reported spatiotemporal pattern of QPPs reported in Majeed et al. (2011). Arrows indicate regions of the brain that dominate QPP activity. **(b)** Representative spatiotemporal pattern observed in the Control group's QPPs from this experiment. Similar to (a), the arrows point to brain regions whose activity dominates the QPP. **(c)** Spatiotemporal pattern resulting from application of the pattern-finding algorithm to a functional scan from one rat in the DSP4 group. **(d)** Spatiotemporal pattern resulting from application of the pattern-finding algorithm to a functional scan from one rat in the Atomoxetine group.

4.3.3 – Strength and frequency of QPPs

Example sliding correlations of the QPPs acquired from the Control, Atomoxetine, and DSP4 groups are plotted in Figure 4.3. The sliding correlation vector demonstrates the strength and frequency of the occurrence of QPPs in the functional scans. The figure shows that the strength and frequency of the QPP observed in the Control rats (Figure 4.3a) is significantly higher in the Control group compared to the Atomoxetine group (Figure 4.3b) and the DSP4 group (Figure 4.3c). Histograms of the cumulative sliding correlation vectors acquired from each group are plotted in Figure 4.4. Similar to previous chapters, short, wide histograms indicate a greater strength and frequency of the QPPs in the functional scans, while tall, narrow histograms indicate weaker strength and frequency of the QPPs in the functional scans. The figure shows that, overall, the strength and frequency of the QPPs observed in the Control group (Figure 4.4a) was greater than the Atomoxetine group (Figure 4.4b) and the DSP4 (Figure 4.4c). Both Figure 4.3 and Figure 4.4 show that QPP activity is drastically diminished in the Atomoxetine and DSP4 groups compared to the Control group.

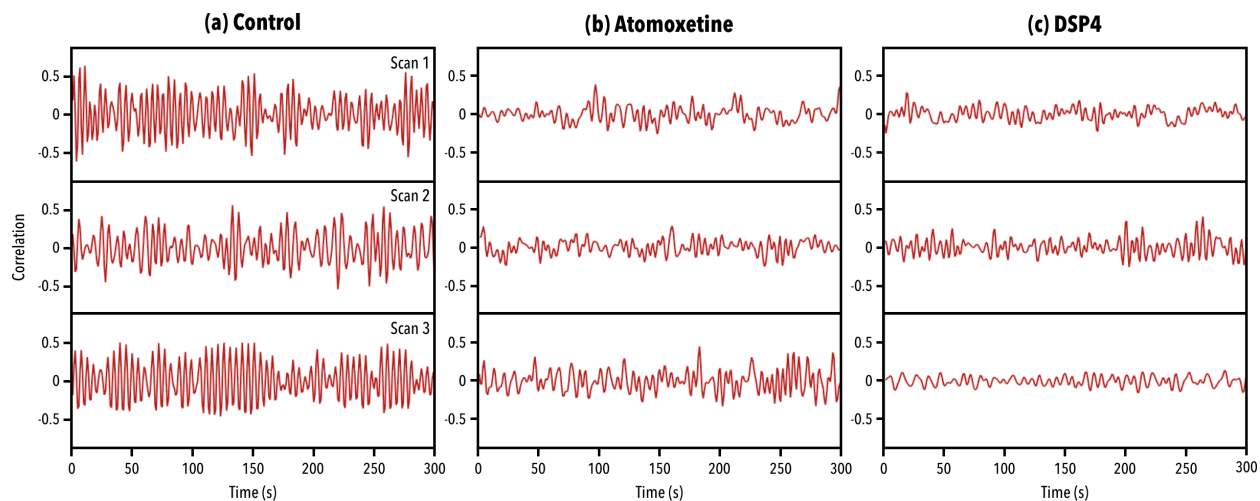


Figure 4.3: Examples of QPP sliding correlation vectors in rats

(a) Examples of sliding correlation of the Control QPP in the functional scans of the Control rats they were acquired from. **(b)** Examples of sliding correlation of the Atomoxetine spatiotemporal pattern in the functional scans of the Atomoxetine-administered rats it was acquired from. **(c)** Examples of sliding correlation of the DSP4 spatiotemporal pattern in the functional scans of the DSP4-administered rats it was acquired from.

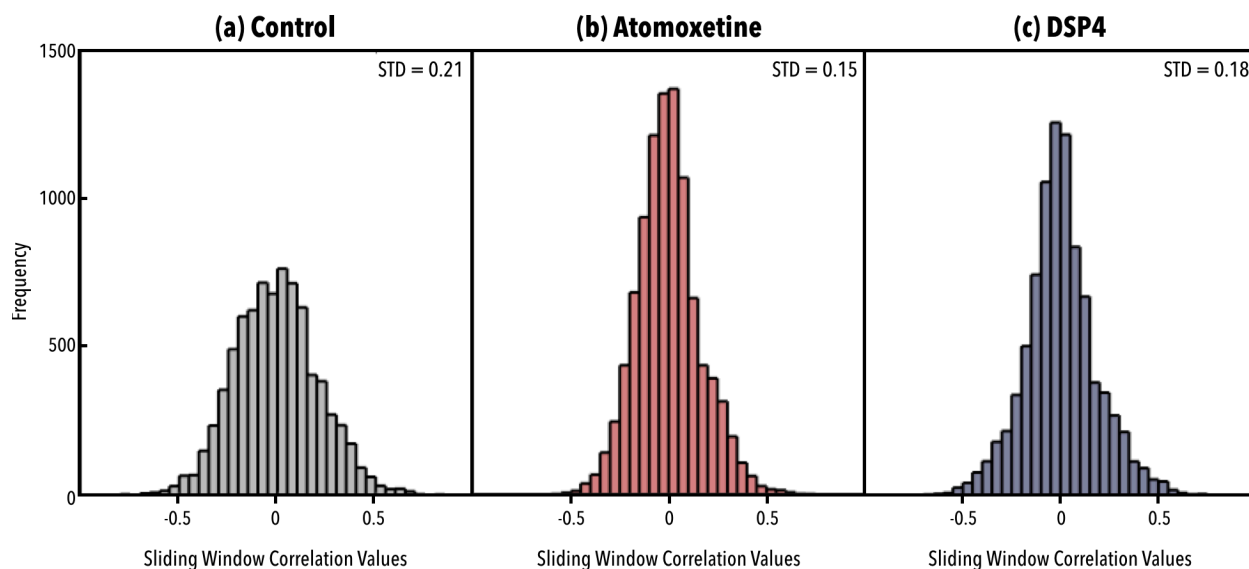


Figure 4.4: Histograms of cumulative sliding correlation vectors in rats

(a) Cumulative sliding correlation of all QPPs acquired from the Control group with the functional scans they were acquired from. **(b)** Cumulative sliding correlation of all spatiotemporal patterns acquired from the Atomoxetine group with the functional scans they were acquired from. **(c)** Cumulative sliding correlation of all spatiotemporal patterns acquired from the DSP4 group with the functional scans they were acquired from. Overall, the distribution of values in (a) show further deviation from zero in the sliding correlation vectors. This indicates a stronger presence of the QPPs in the functional scans in the Control group compared to the Atomoxetine or DSP4 groups.

4.4 – Discussion

The results from this experiment demonstrate that the spatiotemporal pattern captured in QPPs and the strength and frequency of its occurrence in large-scale brain activity dynamics is tied to neuromodulation by deep brain nuclei, specifically noradrenergic projections from the locus coeruleus. Here, we show that both inhibition of locus coeruleus activity through administration of a selective locus coeruleus neurotoxin and augmentation of locus coeruleus activity through administration of a norepinephrine re-uptake inhibitor disrupts the spatiotemporal pattern observed in the QPPs. The results are a step forward in determining the neural mechanisms behind the occurrence of QPPs in large-scale brain activity dynamics.

4.4.1 – A neural mechanism for QPPs

Three main hypotheses can be proposed regarding the neural mechanisms behind QPP activity. The first suggests that quasi-periodic patterns are a direct result of neuromodulatory input from deep brain nuclei with the capacity to cause large-scale fluctuations in brain activity through patterned projections to the cortex. This hypothesis is supported by the results observed in this study. The second hypothesis suggests that quasi-periodic patterns could solely be a result of organization of brain activity within the cortex. Such organization would be an emergent phenomenon from ongoing brain function. This is marginally supported by the observation that QPPs become a unilateral pattern rather than a bilateral pattern following callosotomy in rats (Magnuson et al., 2014), suggesting that QPPs rely on circuitry within the cortex for the spatiotemporal pattern observed. The third — and most likely — hypothesis is that QPPs are the

result of a combination of patterned projections of neuromodulatory input from deep brain nuclei *and* innate cortical circuitry to create the distinct spatiotemporal pattern observed in the brain.

4.4.2 – Controlled input from the locus coeruleus

The locus coeruleus is known to have specific modes of activity: *Phasic* firing of locus coeruleus neurons is tied to instances of high vigilance or task performance, while *tonic* firing of locus coeruleus neurons is related to the absence of a specific task — which in this context can be referred to as resting-state behavior (Aston-Jones & Cohen, 2005). Given the overall hypothesis that QPP activity is regulated through controlled input from the locus coeruleus, we can speculate that shifts in the nature with which locus coeruleus neurons are firing can have drastic effects on QPPs. DSP4 and Atomoxetine have opposite effects on the noradrenergic circuitry in the brain. DSP4 drastically decreases the influence of norepinephrine in the brain. If norepinephrine projections are indeed necessary to affect neuronal excitability and create the spatiotemporal pattern observed in QPPs, then administration of DSP4 should inhibit any such effect, and the presence of QPPs in the functional scan should be diminished. This was evident in the observations from the experiment. On the other hand, Atomoxetine drastically increases the influence of norepinephrine in the brain. If QPPs rely on noradrenergic input for their propagation in the BOLD signal, it is possible that increasing norepinephrine levels would lead to an increase in the strength and frequency of QPPs. However, administration of Atomoxetine had the same effect on QPPs as DSP4 administration. This suggests that a balanced output from the locus coeruleus may be what is necessary in creating the spatiotemporal pattern observed in the QPPs: Regardless of whether synapses are being flooded with norepinephrine or if they are being deprived of it, QPPs disruption would be observed in either scenario.

4.4.3 – Limitations and future directions

The results from the experiment outlined in this chapter are not meant to be conclusive on the relationship between subcortical neuromodulation and QPP activity. Rather, the observations are the first step in providing evidence for the argument that QPPs could have a neural driver in deep brain regions. Administration of a locus coeruleus neurotoxin such as DSP4 or a norepinephrine re-uptake inhibitor such as Atomoxetine is a drastic and coarse modulation of the norepinephrine system of the rat brain. It only suggests that there is a relationship between large-scale BOLD activity and neuromodulation from the locus coeruleus. However, the nature of this relationship is not discernible from such an experiment. The use of locus coeruleus-specific optogenetic and DREADD chemogenetic viruses would allow a more controlled manipulation of locus coeruleus activity, enabling researchers to measure the effect of its activity on QPPs in real time. The use of dopamine beta hydroxylase knockout mice is another avenue through which the effect of the norepinephrine system on QPP activity and large-scale brain activity dynamics can be investigated.

4.5 – Conclusions

Here we showed that pharmacological disruption of the norepinephrine system through modulation of locus coeruleus activity in the rat brain affects the spatiotemporal pattern of QPPs in the BOLD signal and the strength and frequency with which they occur in the functional scan. This suggests a possible neural driver of QPP activity. In doing so, it ties neural activity at the scale of individual brain regions (such as the locus coeruleus) to large-scale brain activity dynamics (such as the spatiotemporal pattern captured within QPPs).

Chapter 5

Conclusions on Quasi-periodic patterns

To arrive at a complete theory of any phenomenon, its mechanisms must be understood across scale and time. The unique complexity of understanding the brain stems from the plethora of scales at which its activity occurs, and the breadth of sophistication present at each of those scales. To address this challenge, neuroscientists have in turn developed a plethora of methods to investigate brain activity, each unraveling complexity at a specific scale. From there, neuroscientists' responsibilities become two-fold: First, they must understand brain activity at every scale. Second, they must integrate knowledge from all scales. By doing so, they will then be able to present a unified theory of the brain.

This dissertation focuses on large-scale brain activity involving functionally diverse cortical regions from across the brain. Such large-scale activity was not a primary focus of classical neuroscience, mainly due to the lack of existing techniques to investigate brain activity at this scale. With the development of non-invasive whole-brain imaging modalities such as fMRI, large-scale brain activity became a topic of interest. If understanding the brain indeed requires that it be understood at every scale, then investigation of large-scale brain activity would be highly relevant.

The methods used to analyze large-scale brain activity in data collected through fMRI have been developing over the last few decades. Static fMRI analyses allow researchers to understand overall relationships between brain regions and to form an understanding of the brain's functional architecture, including how it is disrupted during disease. However, static analyses of fMRI are not able to fully capture the time-varying nature of large-scale brain activity. Dynamic analysis of fMRI allows researchers to study large-scale brain activity in real time and learn how the structure of functional networks varies in the brain, including how it changes during disease.

But given the complexity in the dynamics of large-scale brain activity, a dynamic analysis of fMRI comes with its challenges.

Delving into the spatiotemporal dynamics of large-scale brain activity requires consideration of an entirely new dimension: Time. An overview of recently developed methods to tackle this is provided in Chapter 1. These methods are helping tackle the complexity of time-varying brain activity. This dissertation focuses on one of those techniques; i.e., searching for patterns. If there are sequences of events in the dynamics of large-scale brain activity that tend to reliably recur in the BOLD signal, it is possible they may be serving a purpose in healthy brain function. Upon the application of an automated pattern-finding algorithm, our group demonstrated that such a spatiotemporal pattern indeed exists. This quasi-periodic pattern became a topic of interest. The next step was understanding its purpose.

Chapter 2 of this dissertation describes in detail the spatiotemporal pattern of large-scale brain activity dynamics captured in QPPs. Figure 2.1 outlines the brain regions dominating the pattern and the order in which they are involved. It shows how closely QPPs are tied to two central functional networks in the brain; the DMN and TPN. Figure 2.2 illustrates the strength and frequency with which QPPs occur in fMRI data. Together, Figure 2.1 and Figure 2.2 further demonstrate how QPPs change in varying brain states by outlining differences in the QPPs when individuals are performing a cognitively demanding task as opposed to resting. This was the first investigation of how QPPs may differ across brain states. Chapter 2 also discusses the purpose of QPPs in the BOLD signal by exploring their relationship with static functional connectivity. Figure 2.3 and Figure 2.4 show that QPPs contribute to typical functional connectivity in the brain, specifically within and between the DMN and TPN. At the conclusion of Chapter 2, we

have an understanding of the large-scale brain activity dynamics captured in QPPs along with evidence that they assist in maintaining healthy brain function by contributing to functional connectivity in two important brain networks.

These findings open several avenues for further research. The spatiotemporal differences observed in the QPPs between resting-state and task-performing individuals were specific to the memory task being performed, i.e., the differences corresponded to the changes in brain activity expected during the altered brain state. The observation and description of the spatiotemporal differences in QPPs in further brain states will reveal more about their purpose and how they may be working towards it. This includes searching for QPPs in individuals conducting a wide variety of tasks; a straightforward analysis given that the Human Connectome Project data used for the study in Chapter 2 extends to include several other cognitive tasks (Barch et al., 2013). Furthermore, fMRI data collected from individuals who are either asleep or anesthetized would help in obtaining a better grasp on how QPPs may be relevant to arousal and vigilance, which could lead to a more solidified understanding of the role QPPs play in brain function.

Chapter 3 further delves into the role of QPPs play in maintaining healthy brain activity. By investigating how QPPs are affected in individuals with brain disorders, a more precise understanding of their function can be obtained. Chapter 2 had just demonstrated that QPPs contribute to functional connectivity primarily in the DMN and TPN. Chapter 3 hypothesizes that the large-scale brain activity dynamics captured in QPPs are only relevant to disorders involving the two functional networks, such as ADHD. Consequently, this would predict that QPPs are not directly relevant to disorders that do not involve the DMN and TPN, such as a stroke affecting motor control.

The first section of Chapter 3 investigates QPPs in individuals with ADHD and compares them to QPPs acquired from healthy controls. This was the first investigation of how QPPs may be altered in individuals with a brain disorder. Figure 3.1.1 outlines how static functional connectivity strength within regions in the DMN and TPN is decreased in individuals with ADHD and how the strength of anti-correlation between the two networks becomes weaker. These findings followed the trend of existing knowledge on static functional connectivity differences between individuals with ADHD and healthy controls. Figure 3.1.2 shows how the large-scale brain activity dynamics captured in QPPs differ between the Control group and the ADHD group. Though the spatiotemporal pattern of the QPPs is mostly similar, some distinct differences were apparent. Figure 3.1.4 shows how those differences could be leading to the observed static functional connectivity differences between the Control and ADHD groups. It also shows that QPPs contribute to functional connectivity strength within regions in the DMN and TPN and to the strength of anti-correlation between the two networks. The first section of Chapter 3 provides a clearer understanding of the role QPPs play in maintaining healthy brain function through an investigation of how they relate to a neuropsychiatric disorder involving the DMN and TPN.

The second section of Chapter 3 investigates QPPs in individuals with motor impairment due to stroke. Figure 3.2.1 shows how functional connectivity strength within the sensorimotor network is disrupted in individuals with stroke. The individuals with stroke who participated in this study did not have differences in functional connectivity within and between the DMN and TPN, which is where QPP activity is relevant to functional connectivity strength. Figure 3.2.2 illustrates that the spatiotemporal pattern of the QPP is unchanged between the Control and

Stroke groups. Figure 3.2.3 shows that the strength and frequency with which QPPs occur is unchanged between the Control and Stroke groups. Findings from the second section of Chapter 3 help focus the understanding of the role QPPs serve in healthy brain function by demonstrating where their activity is not relevant through an investigation of how they relate to a brain disorder not involving the DMN and TPN.

Chapter 3 provides further evidence that QPPs are relevant specifically to functional connectivity in the DMN and TPN through the observation that the spatiotemporal pattern of QPPs is disrupted in individuals with ADHD, but not in individuals with stroke. This line of evidence can be built upon through investigation of QPPs in individuals with neuropsychiatric disorders such as Alzheimer's Disease or Major Depressive Disorder, which also show altered functional connectivity in the DMN and TPN. Given that datasets for both Alzheimer's and Depression are freely available, this would require a simple repetition of the analyses carried out in Chapter 3 onto new fMRI datasets. The same could then be done with an fMRI dataset comprising of individuals with neuropsychiatric disorders such as Schizophrenia, which does not show disruptions in DMN and TPN connectivity. If differences in the QPPs are seen in the case of Alzheimer's and Depression, but not in individuals with Schizophrenia, it would further confirm the observations reported in Chapter 3. A commendable next step would then be to try and investigate the BOLD spatiotemporal dynamics that lead to the functional connectivity differences seen in individuals with neuropsychiatric disorders unrelated to the DMN and TPN. Part of our overall hypothesis states that QPPs contribute to static functional connectivity observed within and between the DMN and TPN. Of course, functional connectivity is not exclusive to those two networks. If there is a dynamic process contributing to connectivity in one

network, there may be other dynamic processes contributing to functional connectivity in other parts of the brain. Discovery of novel recurring spatiotemporal events — separate from the QPPs described here — which contribute to functional connectivity in areas unrelated to the DMN and TPN would greatly augment the claims presented in this dissertation.

Chapter 4 ties the spatiotemporal dynamics captured in QPPs to brain activity at smaller scales. By disrupting the activity at the level of the locus coeruleus, its effect on large-scale brain activity captured in QPP is investigated. We see that pharmacological manipulation of the noradrenergic system of the brain — driven by the locus coeruleus — either through administration of a selective locus coeruleus neurotoxin or a norepinephrine re-uptake inhibitor leads to a disruption in QPP activity. Figure 4.1 shows how results from the pattern-finding algorithm change in the treatment groups in terms of the spatiotemporal pattern that is outputted. Figure 4.2 shows how the strength and frequency of the observed spatiotemporal pattern is reduced in the treatment groups compared to the control group. Chapter 4 helps form an understanding of the relationship between locus coeruleus activity and QPPs. This assists in further uncovering the nature of QPPs and the role they play in maintaining healthy brain function. It also serves as insight into how neuromodulatory input from deep brain nuclei may be affecting large-scale brain activity dynamics in general. This contributes to the overall aim of this dissertation, which is to investigate large-scale brain activity and how it is connected to other scales of brain activity. Chapters 2 and 3 explore large-scale brain activity dynamics and what purpose they might be serving in the brain. They do not delve into the relationship of large-scale brain activity with brain activity at other scales. Chapter 4, by investigating the relationship between large-scale brain activity and brain activity at the scale of individual deep brain nuclei,

begins to explain the mechanisms of connection between large-scale and medium-scale brain activity.

Through investigation of the dynamics of large-scale brain activity in healthy individuals, the dissertation concludes that quasi-periodic patterns are a reliably observable phenomenon in the brain, contributing to functional connectivity in the default mode and task positive networks. Through investigation of QPPs in individuals with neurological disorders, the dissertation concludes that the contribution of QPPs to functional connectivity assists in maintaining healthy brain function, which is disrupted during disease. Through investigation of the relationship of QPPs to locus coeruleus activity, the dissertation concludes that QPP activity is dependent on healthy function in a subcortical nucleus. In doing so, it establishes a relationship between large-scale brain activity and brain activity occurring at smaller scales. Overall, the dissertation provides compelling evidence that studying large-scale brain activity in the form of repeating patterns can assist with understanding healthy brain function and how it is disrupted during disease.

Appendix A: fMRI Preprocessing Pipeline

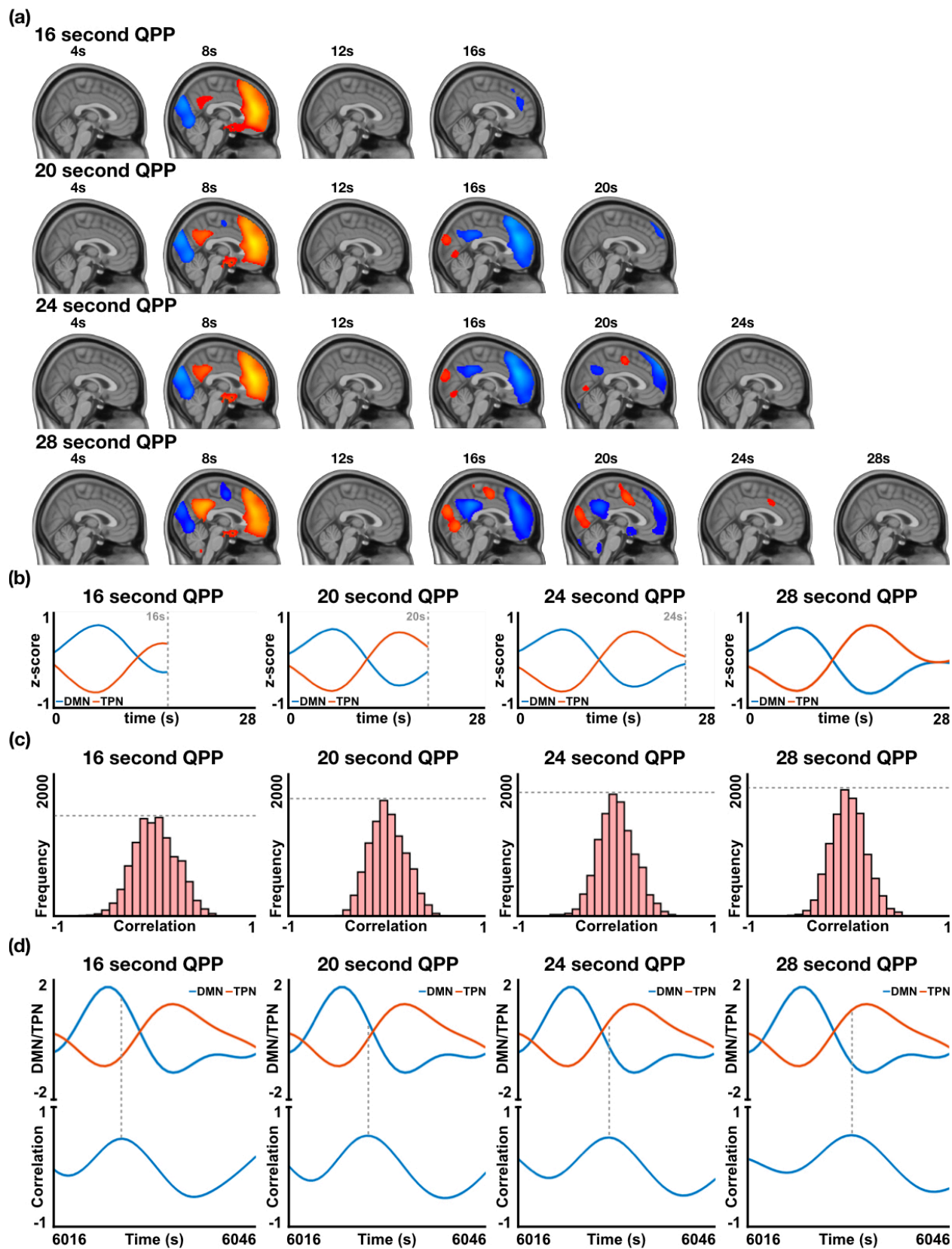
An automated preprocessing pipeline was created to manage preprocessing for all fMRI data analyzed in this dissertation. The code for the pipeline was published online, which has helped other research groups work with fMRI datasets for the first time. The preprocessing pipeline as it applies to rodent data was also published in a methods paper by the lab (Pan et al., 2017). An overview of the steps in the preprocessing pipeline are also provided in this appendix. All preprocessing was conducted using FSL 5.0 (Jenkinson et al., 2012) and Matlab (Mathworks, Natick, MA).

In the case of the human data analyzed in Chapters 2 and 3, all anatomical scans were registered to the 2 mm Montreal Neurological Institute (MNI) brain atlas using FSL's registration tool, FLIRT (Jenkinson & Smith, 2001; Jenkinson et al., 2002). Then, they were skull-stripped using FSL's brain extraction tool, BET. Next, they were tissue segmented into white matter, gray matter, and cerebrospinal fluid using FSL's segmentation tool, FAST (Zhang et al., 2001). In the case of the rat data analyzed in Chapter 4, all anatomical scans were skull-stripped using a manually drawn brain mask. They were not registered to a standard space or segmented into individual tissue types.

If the functional data was collected using a sequence that scanned one brain slice at a time, the functional scans were first slice time corrected using FSL's slicetimer tool. This was applicable to the ADHD and Stroke datasets used in Chapter 3. Second, all functional scans were motion corrected using FSL's motion correction tool, MCFLIRT (Jenkinson et al., 2002). In the case of rats, motion regression was also carried out using the motion parameters outputted from MCFLIRT. Third, all functional scans were registered to the same physical space as the anatomical data using FLIRT. This was not applicable to the rat data in Chapter 4. Fourth, they

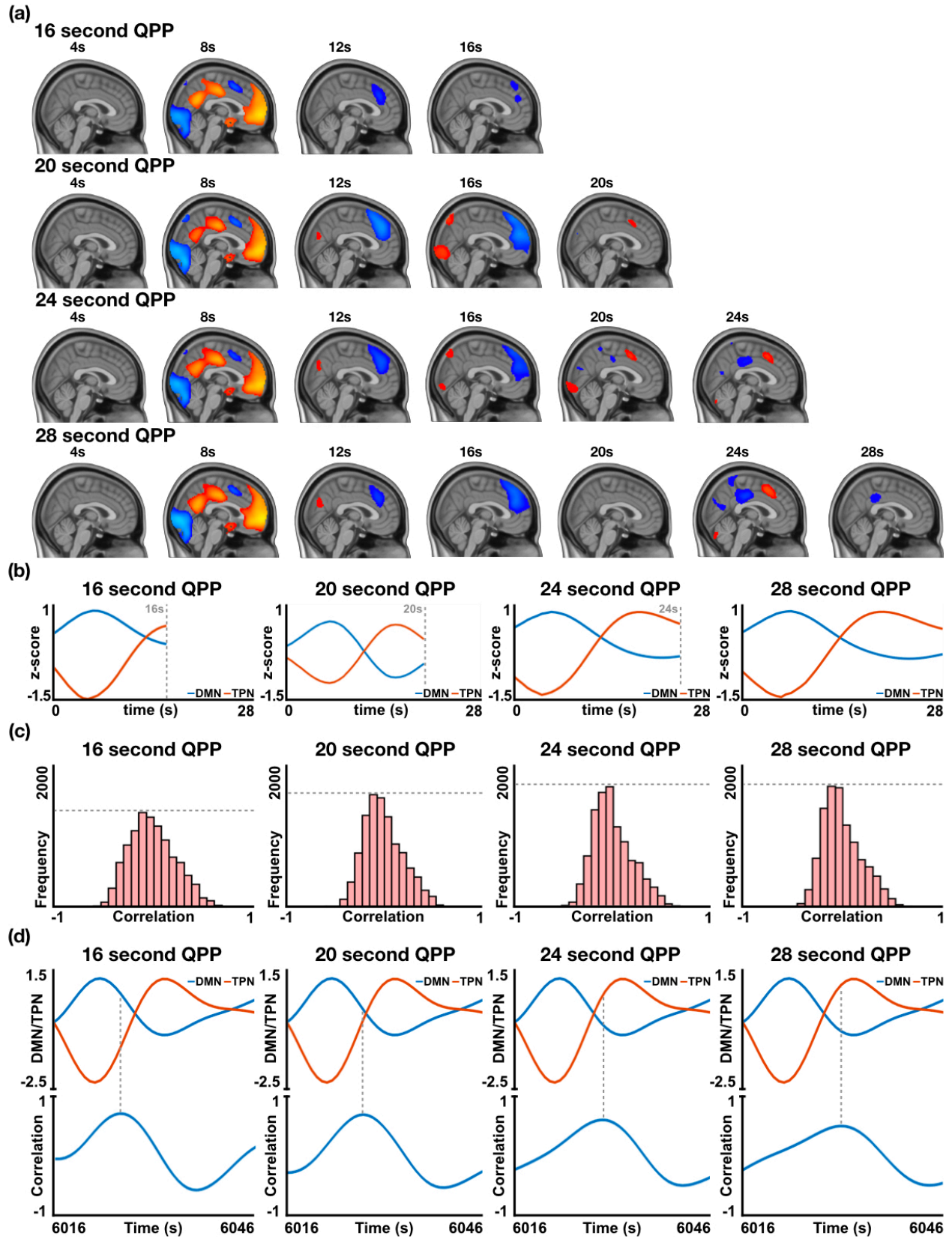
were spatially smoothed with a 6 mm Gaussian kernel in the case of the human data in Chapters 2 and 3 and a 0.5 mm Gaussian kernel in the case of the rat data in Chapter 4 using FSLMATHS. This significantly increases the signal to noise ratio of the BOLD signal. Fifth, Matlab was used to apply a Fast Fourier Transform bandpass temporal filter between 0.01 and 0.08 Hz in the case of the human data in Chapters 2 and 3 and 0.01 to 0.25 Hz in the case of the rat data in Chapter 4. Sixth, global, white matter, and cerebrospinal signals were regressed. Only global signal was regressed for rats as the white matter and cerebrospinal fluid form a significantly smaller portion of the image. Finally, all voxel timecourses were z-scored.

Appendix B: Supplementary Figures



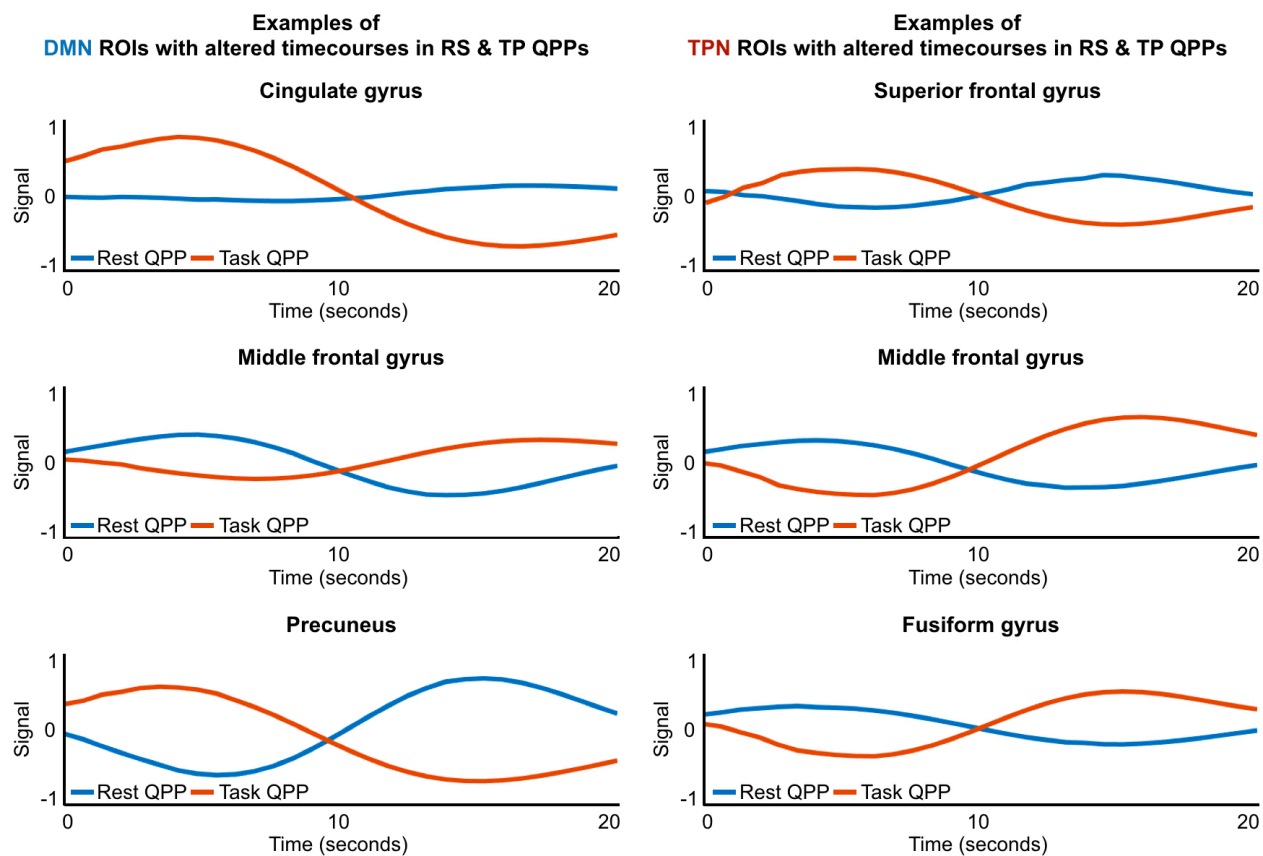
Supplementary Figure 1: Length of QPPs in RS individuals

In resting-state individuals, the effect of inputting different window lengths when searching for QPPs using the spatiotemporal pattern-finding algorithm, with the purpose of determining an apt QPP length to use for this study. (a) Spatiotemporal pattern of four QPPs with lengths 16s, 20s, 24s, and 28s (top to bottom). (b) Timecourses of the DMN and TPN during each of the QPPs. As can be observed, 16s is too short of a length to capture a complete transition between DMN and TPN dominance, hence this length can be discarded in our search for an apt QPP length. (c) Histogram of the cumulative sliding correlation of the QPP with the 25 concatenated scans it was acquired from. Of the three QPP lengths remaining, the strongest correlation (as determined by the widest distribution) is shown by the 20s QPP. With increasing QPP length, the strength of the sliding correlation decreases. (d) Top: Timecourse of the DMN and TPN at an instance in the functional data where a DMN to TPN transition is occurring. Bottom: Sliding correlation of the QPP with the functional scan at the same instance where a DMN to TPN transition is occurring. For an ideal QPP length, peaks in the sliding correlation vector should occur in the center of the QPP, which is the exact instance at which the DMN/TPN switch occurs. The 20s and 24s QPPs both pass this test with similar performance. Given the tests carried out in (b), (c), and (d), the 20s QPP stands out as an ideal length of a QPP in resting-state individuals.



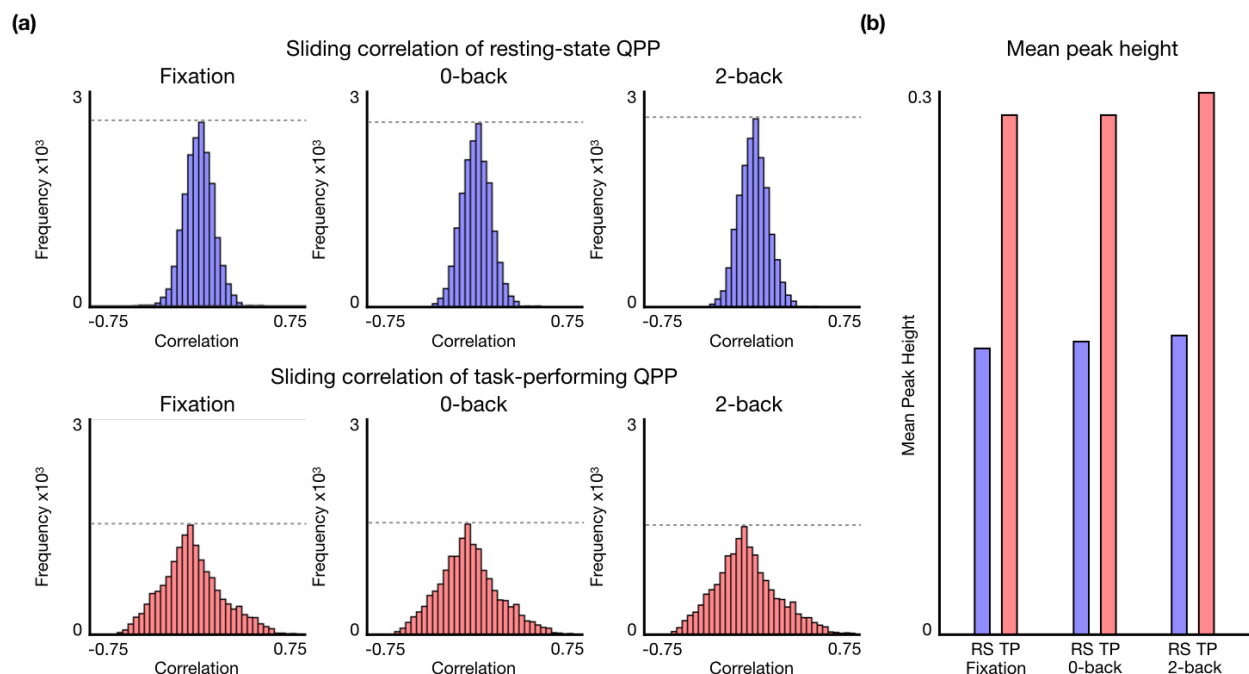
Supplementary Figure 2: Length of QPPs in TP individuals

In task-performing individuals, the effect of inputting different window lengths when searching for QPPs using the spatiotemporal pattern-finding algorithm, with the purpose of determining an apt QPP length to use for this study. (a) Spatiotemporal pattern of four QPPs with lengths 16s, 20s, 24s, and 28s (top to bottom). (b) Timecourses of the DMN and TPN during each of the QPPs. As can be observed, 16s is too short of a length to capture a complete transition between DMN and TPN dominance, hence this length can be discarded in our search for an apt QPP length. (c) Histogram of the cumulative sliding correlation of the QPP with the 25 concatenated scans it was acquired from. Of the three QPP lengths remaining, the strongest correlation (as determined by the widest distribution) is shown by the 20s QPP. With increasing QPP length, the strength of the sliding correlation decreases. (d) Top: Timecourse of the DMN and TPN at an instance in the functional data where a DMN to TPN transition is occurring. Bottom: Sliding correlation of the QPP with the functional scan at the same instance where a DMN to TPN transition is occurring. For an ideal QPP length, peaks in the sliding correlation vector should occur in the center of the QPP, which is the exact instance at which the DMN/TPN switch occurs. The 20s QPP passes this test with the best performance. Given the tests carried out in (b), (c), and (d), the 20s QPP stands out as an ideal length of a QPP in task-performing individuals.



Supplementary Figure 3: Timecourses of ROIs anti-correlated across QPPs

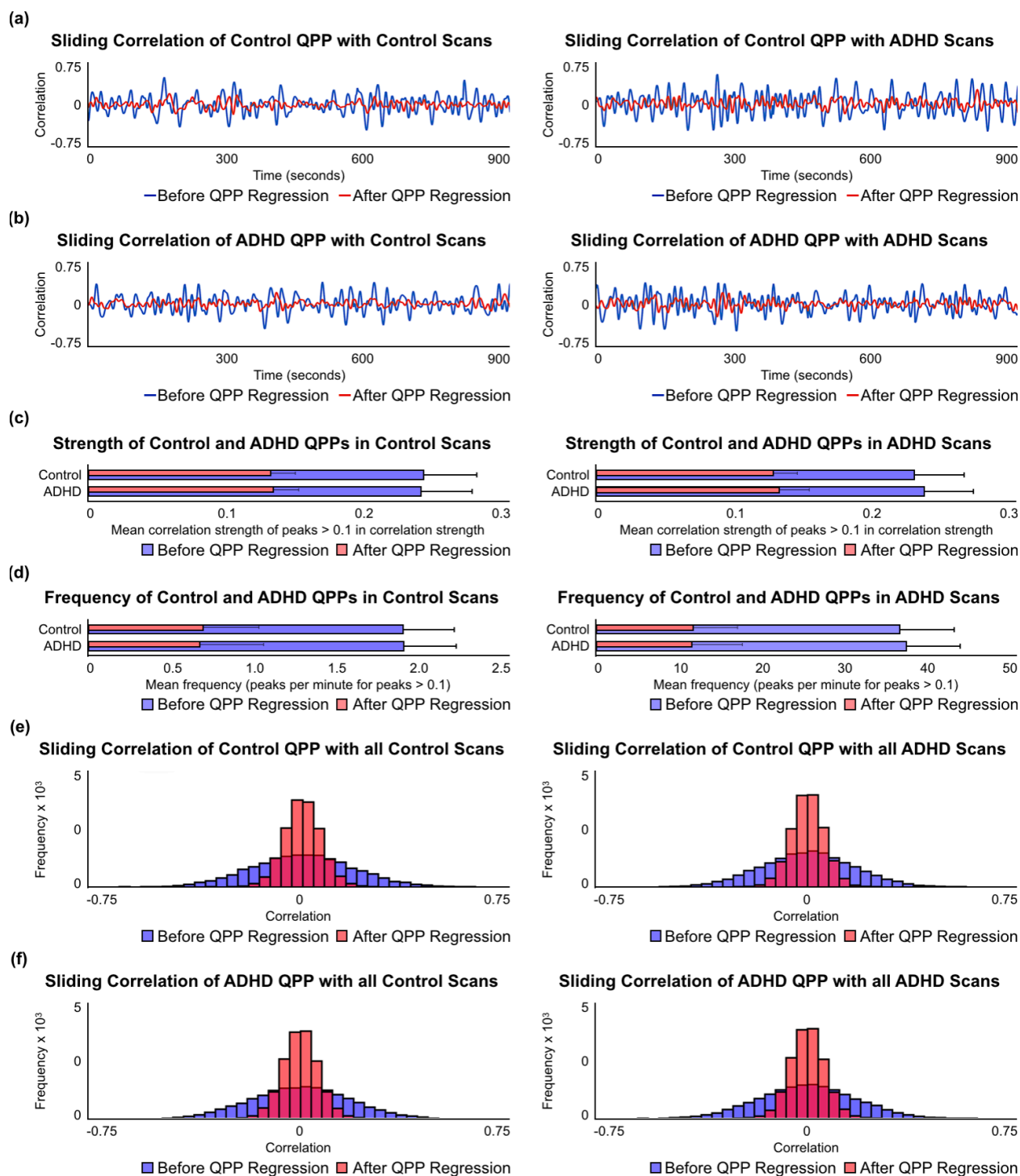
Timecourses of example ROIs that were identified as behaving differently in the resting-state QPP versus the task-performing QPP. Blue lines show how the ROI behaved during the resting-state QPP while red lines show how the ROI behaved during the task-performing QPP.



Supplementary Figure 4: Effect of task blocks on QPP strength and frequency

Effects of fixation, 0-back, and 2-back blocks on the occurrence of resting-state and task-performing QPPs in task-performing scans. The sliding correlation vectors of each of the QPPs were separated into areas that corresponded with the 15s fixation blocks and 25s 0-back and 2-back blocks in each scan. (a) Top: Histograms of the cumulative sliding correlation of the resting-state QPP with instances in all the task-performing scans that corresponded with fixation (left), the 0-back working memory task (middle), and the 2-back working memory task (right). There was no significant difference in the distribution of the sliding correlation vector of the resting-state QPP in each of the blocks. Bottom: Histograms of the cumulative sliding correlation of the task-performing QPP with instances in all the task-performing scans that corresponded with fixation (left), the 0-back working memory task (middle), and the 2-back working memory task (right). There was no significant difference in the distribution of the sliding correlation

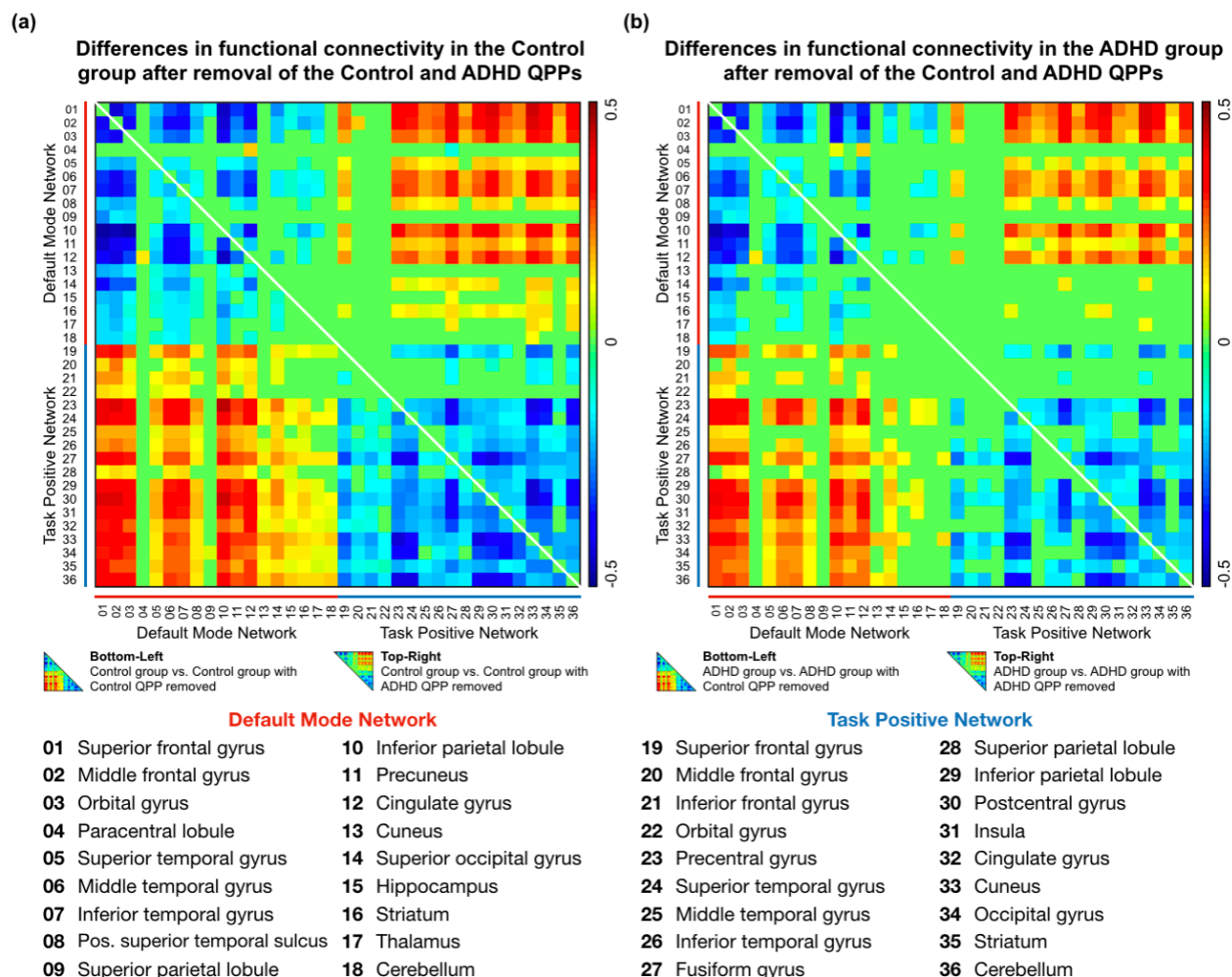
vector of the task-performing QPP in each of the blocks. As previously shown in Figure 2, the presence of the task-performing QPP was stronger in the task-performing scans compared to the resting-state QPP. (b) Mean correlation strength for all peaks > 0.1 in the sliding correlation vectors of the resting-state and task-performing QPPs in each of the blocks during all the task-performing scans. There was no significant difference in the mean peak height of either the resting-state or task-performing QPPs across the blocks in the task-performing scans. As previously shown in Figure 2, the mean peak heights of the task-performing QPP in task-performing scans is greater than those of the resting-state QPP.



Supplementary Figure 5: Strength and frequency of QPPs in Control and ADHD.

Comparison of the strength and frequency of QPPs between the Control and ADHD groups before and after removal of QPPs. This is a partial repetition of Figure 3 in the

main text. However, here we compare the strength and frequency of QPPs in their non-native scans. (a) Example sliding correlation vectors of the Control QPP with three randomly-selected concatenated functional scans from the Control group (left) and the ADHD group (right) before (blue) and after (red) regression of the Control QPP. (b) Example sliding correlation vectors of the ADHD QPP with three randomly-selected concatenated functional scans from the Control group (left) and the ADHD group (right) before (blue) and after (red) regression of the Control QPP. (c) Mean correlation strength of peaks > 0.1 in the cumulative sliding correlation of the Control and ADHD QPPs with all Control scans (left) and all ADHD scans (right) before QPP removal (blue) and after QPP removal (red). (d) Mean frequency (peaks per minute) of peaks with correlation strength > 0.1 in the cumulative sliding correlation of the Control and ADHD QPPs with all Control scans (left) and all ADHD scans (right) before QPP removal (blue) and after QPP removal (red). (e) Histogram of the cumulative sliding correlation of the Control QPP with all Control scans (left) and all ADHD scans (right) before QPP removal (blue) and after QPP removal (red). (f) Histogram of the cumulative sliding correlation of the ADHD QPP with all Control scans (left) and all ADHD scans (right) before QPP removal (blue) and after QPP removal (red). There were no significant differences in strength and frequency of either QPPs in each of the groups.



Supplementary Figure 6: FC changes in Control and ADHD after QPP regression

FC in 36 ROIs within the DMN and TPN after regression of QPPs. Parts of these matrices have also been shown in Figure 4 in the main text. However, here we show the effects of regressing non-native QPPs from the functional scans in each group. (a) Differences in FC in the Control scans after regression of the Control (bottom-left) and ADHD (top-right) QPPs. (b) Differences in FC in the ADHD scans after regression of the Control (bottom-left) and ADHD (top-right) QPPs. When the Control QPP was removed from the Control data, there were 494 significant changes in FC within and across the DMN and TPN. When the ADHD QPP was removed from the Control data, there were

362 significant changes in FC. When the Control QPP was removed from the ADHD group, there were 361 significant changes in FC. Lastly, when the ADHD QPP was removed from the ADHD scans, there were only 280 significant changes in FC.

Appendix C: Supplementary Tables

Supplementary Table 1: DMN ROIs in the Control and ADHD groups

Regions of interest from the 273 ROI Brainnetome atlas from Fan et al. (2016) that were in the DMN in Control individuals and individuals with ADHD. The table shows the number of voxels in each ROI that overlapped with the DMN mask as well as how many voxels ended up in the brain regions that made up the consolidated DMN atlas. Additionally, the table shows the mean correlation with the PCC with each ROI as well as the brain regions that made up the consolidated DMN atlas.

Region of Interest	Control Group		ADHD Group	
	Voxels	Correlation	Voxels	Correlation
superior frontal gyrus, part 2 (dorsolateral area 8), left	402	0.33	215	0.25
superior frontal gyrus, part 2 (dorsolateral area 8), right	456	0.33	127	0.24
superior frontal gyrus, part 3 (lateral area 9), left	105	0.29	22	0.23
superior frontal gyrus, part 3 (lateral area 9), right	363	0.29	0	N/A
superior frontal gyrus, part 6 (medial area 9), left	8	0.27	23	0.23
superior frontal gyrus, part 6 (medial area 9), right	152	0.28	25	0.23
superior frontal gyrus, part 7 (medial area 10), left	655	0.33	666	0.27
superior frontal gyrus, part 7 (medial area 10), right	771	0.35	436	0.27
middle frontal gyrus, part 1 (dorsal area 9/46), left	58	0.30	71	0.24
middle frontal gyrus, part 1 (dorsal area 9/46), right	215	0.32	39	0.23
middle frontal gyrus, part 3 (area 46), left	3	0.28	4	0.23
middle frontal gyrus, part 3 (area 46), right	27	0.29	0	N/A
middle frontal gyrus, part 5 (ventrolateral area 8), left	234	0.31	149	0.25
middle frontal gyrus, part 5 (ventrolateral area 8), right	24	0.28	0	N/A

Region of Interest	Control Group		ADHD Group	
	Voxels	Correlation	Voxels	Correlation
middle frontal gyrus, part 6 (ventrolateral area 6), right	28	0.30	0	N/A
middle frontal gyrus, part 7 (lateral area 10), left	211	0.31	187	0.26
middle frontal gyrus, part 7 (lateral area 10), right	401	0.35	130	0.25
orbital gyrus, part 1 (medial area 14), left	509	0.38	509	0.33
orbital gyrus, part 1 (medial area 14), right	670	0.40	670	0.33
orbital gyrus, part 4 (medial area 11), left	269	0.33	137	0.26
orbital gyrus, part 4 (medial area 11), right	499	0.36	344	0.28
orbital gyrus, part 5 (area 13), left	62	0.30	68	0.25
orbital gyrus, part 5 (area 13), right	13	0.28	36	0.23
paracentral lobule, part 1 (area 1/2/3 lower limb), left	25	0.34	80	0.30
paracentral lobule, part 1 (area 1/2/3 lower limb), right	85	0.35	154	0.31
paracentral lobule, part 2 (area 4 lower limb), left	26	0.34	53	0.31
paracentral lobule, part 2 (area 4 lower limb), right	13	0.32	32	0.29
superior temporal gyrus, part 4 (caudal area 22), left	0	0	N/A	N/A
superior temporal gyrus, part 4 (caudal area 22), right	1	1	0.23	0.23
middle temporal gyrus, part 1 (caudal area 21), left	69	0.29	75	0.24
middle temporal gyrus, part 1 (caudal area 21), right	235	0.32	7	0.22
middle temporal gyrus, part 2 (rostral area 21), left	92	0.29	97	0.24
middle temporal gyrus, part 2 (rostral area 21), right	61	0.29	8	0.22
middle temporal gyrus, part 3 (dorsolateral area 37), left	0	N/A	8	0.24
middle temporal gyrus, part 4 (anterior superior temporal sulcus), right	21	0.30	0	N/A
inferior temporal gyrus, part 4 (intermediate lateral area 20), left	91	0.29	106	0.24
inferior temporal gyrus, part 4 (intermediate lateral area 20), right	73	0.30	6	0.22

Region of Interest	Control Group				ADHD Group			
	Voxels		Correlation		Voxels		Correlation	
inferior temporal gyrus, part 6 (caudolateral of area 20), right	56	221	0.30	0.29	0	128	N/A	0.23
inferior temporal gyrus, part 7 (caudoventral of area 20), left	0		N/A		5		0.23	
inferior temporal gyrus, part 7 (caudoventral of area 20), right	1		0.28		11		0.24	
superior parietal lobule, part 2 (caudal area 7), left	0	0	N/A	N/A	4	4	0.23	0.23
inferior parietal lobule, part 1 (caudal area 39), right	486		0.39		443		0.32	
inferior parietal lobule, part 2 (rostradorsal area 39), left	145		0.34		171		0.30	
inferior parietal lobule, part 2 (rostradorsal area 39), right	628	2770	0.39	0.36	597	3033	0.33	0.31
inferior parietal lobule, part 4 (caudal area 40), left	222		0.33		341		0.29	
inferior parietal lobule, part 5 (rostroventral area 39), left	824		0.37		994		0.33	
inferior parietal lobule, part 5 (rostroventral area 39), right	465		0.36		487		0.29	
precuneus, part 1 (medial area 7), left	237		0.38		244		0.34	
precuneus, part 1 (medial area 7), right	187		0.37		160		0.32	
precuneus, part 2 (medial area 5), left	91		0.40		158		0.36	
precuneus, part 2 (medial area 5), right	150	3560	0.43	0.47	213	3926	0.39	0.43
precuneus, part 3 (dorsomeidal parietooccipital sulcus),	609		0.43		707		0.41	
precuneus, part 3 (dorsomeidal parietooccipital sulcus), right	584		0.48		742		0.44	
precuneus, part 4 (area 31), left	755		0.62		755		0.60	
precuneus, part 4 (area 31), right	947		0.62		947		0.59	
cingulate gyrus, part 1 (dorsal area 23), left	477		0.82		477		0.81	
cingulate gyrus, part 1 (dorsal area 23), right	412		0.80		412		0.80	
cingulate gyrus, part 2 (rostroventral area 24), left	40		0.49		63		0.43	
cingulate gyrus, part 2 (rostroventral area 24), right	47		0.30		92		0.27	

Region of Interest	Control Group		ADHD Group	
	Voxels	Correlation	Voxels	Correlation
cingulate gyrus, part 3 (pregenual area 32), left	76	0.30	234	0.27
cingulate gyrus, part 3 (pregenual area 32), right	1	0.28	53	0.24
cingulate gyrus, part 4 (ventral area 23), left	232	0.58	253	0.55
cingulate gyrus, part 4 (ventral area 23), right	262	0.60	263	0.58
cingulate gyrus, part 6 (caudal area 24), left	409	0.51	489	0.49
cingulate gyrus, part 6 (caudal area 24), right	357	0.53	416	0.51
cingulate gyrus, part 7 (subgenual area 32), left	535	0.36	555	0.32
cingulate gyrus, part 7 (subgenual area 32), right	342	0.34	413	0.30
cuneus, part 2 (rostral cuneus gyrus), left	9	0.34	12	0.31
cuneus, part 2 (rostral cuneus gyrus), right	92	0.38	115	0.34
cuneus, part 5 (ventomedial parietooccipital sulcus), left	79	0.33	163	0.29
cuneus, part 5 (ventomedial parietooccipital sulcus), right	332	0.41	435	0.38
superior occipital gyrus, part 1 (medial superior occipital gyrus), left	4	0.28	9	0.25
superior occipital gyrus, part 1 (medial superior occipital gyrus), right	0	N/A	1	0.23
superior occipital gyrus, part 2 (lateral superior occipital gyrus), left	1	0.28	21	0.26
superior occipital gyrus, part 2 (lateral superior occipital gyrus), right	184	0.33	136	0.29
hippocampus, part 2 (caudal hipp), left	2	0.30	7	0.27
striatum, part 3 (nucleus accumbens), right	0	N/A	3	0.22
thalamus, part 4 (rostral temporal thalamus), left	0	N/A	11	0.25
thalamus, part 4 (rostral temporal thalamus), right	0	N/A	9	0.25
thalamus, part 6 (occipital thalamus), left	0	N/A	2	0.23
thalamus, part 7 (caudal temporal thalamus), left	0	N/A	7	0.24

Region of Interest	Control Group		ADHD Group	
	Voxels	Correlation	Voxels	Correlation
thalamus, part 7 (caudal temporal thalamus), right	0	N/A	4	0.24
Cerebellar lobule I-IV, left	1	0.27	1	0.22
Cerebellar lobule I-IV, right	1	0.28	0	N/A

Supplementary Table 2: TPN ROIs in individuals with ADHD

Regions of interest from the 273 ROI Brainnetome atlas from Fan et al. (2016) that were in the TPN in Control individuals and individuals with ADHD. The table shows the number of voxels in each ROI that overlapped with the TPN mask as well as how many voxels ended up in the brain regions that made up the consolidated TPN atlas. Additionally, the table shows the mean correlation with the PCC with each ROI as well as the brain regions that made up the consolidated TPN atlas.

Region of Interest	Control Group		ADHD Group	
	Voxels	Correlation	Voxels	Correlation
superior frontal gyrus, part 1 (medial area 8), left	112	-0.27	45	-0.21
superior frontal gyrus, part 1 (medial area 8), right	97	-0.27	41	-0.21
superior frontal gyrus, part 4 (dorsolateral area 6), left	190	-0.26	267	-0.21
superior frontal gyrus, part 4 (dorsolateral area 6), right	6	-0.26	126	-0.21
superior frontal gyrus, part 5 (medial area 6), left	256	-0.28	142	-0.22
superior frontal gyrus, part 5 (medial area 6), right	266	-0.28	157	-0.21
middle frontal gyrus, part 2 (inferior frontal junction), left	1	-0.26	0	N/A
middle frontal gyrus, part 2 (inferior frontal junction), right	0	N/A	2	-0.21

Region of Interest	Control Group				ADHD Group			
	Voxels		Correlation		Voxels		Correlation	
middle frontal gyrus, part 4 (ventral area 9/46), right	0	24	N/A	-0.25	233	361	-0.22	-0.21
middle frontal gyrus, part 5 (ventrolateral area 8), right	0		N/A		3		-0.21	
middle frontal gyrus, part 6 (ventrolateral area 6), left	23		-0.25		123		-0.22	
inferior frontal gyrus, part 1 (dorsal area 44), left	152		-0.32		171		-0.28	
inferior frontal gyrus, part 1 (dorsal area 44), right	5		-0.26		62		-0.25	
inferior frontal gyrus, part 2 (inferior frontal sulcus), left	0		N/A		1		-0.22	
inferior frontal gyrus, part 2 (inferior frontal sulcus), right	0		N/A		175		-0.22	
inferior frontal gyrus, part 3 (caudal area 45), left	69		-0.27		160		-0.24	
inferior frontal gyrus, part 3 (caudal area 45), right	4		-0.26		55		-0.22	
inferior frontal gyrus, part 4 (rostral area 45), left	3	1367	-0.26	-0.29	22	2003	-0.21	-0.24
inferior frontal gyrus, part 4 (rostral area 45), right	0		N/A		102		-0.21	
inferior frontal gyrus, part 5 (opercular area 44), left	388		-0.29		243		-0.23	
inferior frontal gyrus, part 5 (opercular area 44), right	314		-0.29		448		-0.25	
inferior frontal gyrus, part 6 (ventral area 44), left	297		-0.34		297		-0.31	
inferior frontal gyrus, part 6 (ventral area 44), right	135		-0.31		267		-0.28	
orbital gyrus, part 6 (lateral area 12/47), left	52		-0.26		9		-0.21	
orbital gyrus, part 6 (lateral area 12/47), right	15	67	-0.26	-0.26	41	50	-0.23	-0.22
precentral gyrus, part 1 (area 4 head and face), left	420		-0.29		145		-0.26	
precentral gyrus, part 1 (area 4 head and face), right	223		-0.27		212		-0.23	
precentral gyrus, part 2 (caudal dorsolateral area 6), left	266		-0.27		210		-0.22	
precentral gyrus, part 2 (caudal dorsolateral area 6), right	45		-0.26		53		-0.21	
precentral gyrus, part 3 (area 4 upper limb), right	53	2582	-0.26	-0.30	0	2281	N/A	-0.26

Region of Interest	Control Group				ADHD Group			
	Voxels		Correlation		Voxels		Correlation	
precentral gyrus, part 5 (area 4 tongue and larynx), left	437		-0.33		410		-0.26	
precentral gyrus, part 5 (area 4 tongue and larynx), right	367		-0.35		367		-0.31	
precentral gyrus, part 6 (caudal ventrolateral area 6), left	566		-0.33		453		-0.29	
precentral gyrus, part 6 (caudal ventrolateral area 6), right	205		-0.29		431		-0.27	
superior temporal gyrus, part 2 (area 41/42), left	111		-0.26	-0.27	1		-0.20	
superior temporal gyrus, part 2 (area 41/42), right	266		-0.27		11		-0.21	
superior temporal gyrus, part 3 (area TE), left	386		-0.28		251		-0.24	
superior temporal gyrus, part 3 (area TE), right	552		-0.32		392		-0.26	
superior temporal gyrus, part 4 (caudal area 22), left	1		-0.25		59		-0.23	
superior temporal gyrus, part 4 (caudal area 22), right	187	1618	-0.28		0	852	N/A	-0.23
superior temporal gyrus, part 5 (lateral area 38), left	28		-0.27		44		-0.23	
superior temporal gyrus, part 5 (lateral area 38), right	19		-0.27		14		-0.22	
superior temporal gyrus, part 6 (rostral area 22), left	30		-0.27		58		-0.23	
superior temporal gyrus, part 6 (rostral area 22), right	38		-0.28		22		-0.22	
middle temporal gyrus, part 3 (dorsolateral area 37), left	0		N/A		12		-0.21	
middle temporal gyrus, part 3 (dorsolateral area 37), right	0	0	N/A	N/A	3	15	-0.21	-0.21
inferior temporal gyrus, part 2 (extreme lateroventral area 37), left	99		-0.27		105		-0.24	
inferior temporal gyrus, part 5 (ventrolateral area 37), left	153	253	-0.26	-0.26	246	386	-0.23	-0.23
inferior temporal gyrus, part 5 (ventrolateral area 37), right	1		-0.25		35		-0.21	
fusiform gyrus, part 1 (rostroventral area 20), left	0		N/A		3		-0.20	
fusiform gyrus, part 2 (medioventral area 37), left	695		-0.30		653		-0.24	
fusiform gyrus, part 2 (medioventral area 37), right	515	1771	-0.30	-0.29	577	1857	-0.25	-0.23

Region of Interest	Control Group		ADHD Group					
	Voxels	Correlation	Voxels	Correlation				
fusiform gyrus, part 3 (ventrolateral area 37), left	400	-0.29	401	-0.23				
fusiform gyrus, part 3 (ventrolateral area 37), right	161	-0.27	223	-0.24				
superior parietal lobule, part 1 (rostral area 7), left	0	N/A	117	-0.22				
superior parietal lobule, part 1 (rostral area 7), right	0	N/A	41	-0.21				
superior parietal lobule, part 2 (caudal area 7), left	0	N/A	6	-0.21				
superior parietal lobule, part 2 (caudal area 7), right	0	24	N/A	-0.25	23	393	-0.21	-0.21
superior parietal lobule, part 3 (lateral area 5), left	18	-0.25	26	-0.21				
superior parietal lobule, part 4 (postcentral area 7), left	0	N/A	38	-0.21				
superior parietal lobule, part 5 (intraparietal area 7), left	6	-0.24	132	-0.22				
inferior parietal lobule, part 3 (rostrrodorsal area 40), left	241	-0.28	10	-0.21				
inferior parietal lobule, part 3 (rostrrodorsal area 40), left	0	N/A	567	-0.25				
inferior parietal lobule, part 3 (rostrrodorsal area 40), right	29	-0.25	530	-0.24				
inferior parietal lobule, part 4 (caudal area 40), right	0	1303	N/A	-0.27	197	2262	-0.24	-0.24
inferior parietal lobule, part 6 (rostroventral area 40), left	381	-0.28	217	-0.22				
inferior parietal lobule, part 6 (rostroventral area 40), right	652	-0.27	751	-0.24				
postcentral gyrus, part 1 (area 1/2/3 upper limb), left	235	-0.26	168	-0.23				
postcentral gyrus, part 1 (area 1/2/3 upper limb), right	125	-0.26	5	-0.21				
postcentral gyrus, part 2 (area 1/2/3 tongue and larynx), left	540	-0.28	143	-0.22				
postcentral gyrus, part 2 (area 1/2/3 tongue and larynx), right	511	-0.29	247	-0.24				
postcentral gyrus, part 3 (area 2), left	148	-0.27	556	-0.24				
postcentral gyrus, part 3 (area 2), right	16	-0.25	27	-0.21				
insular, part 1 (hypergranular insula), left	69	-0.27	11	-0.21				

Region of Interest	Control Group		ADHD Group	
	Voxels	Correlation	Voxels	Correlation
insular, part 1 (hypergranular insula), right	110	-0.28	0	N/A
insular, part 2 (ventral agranular insula), left	1	-0.25	0	N/A
insular, part 2 (ventral agranular insula), right	0	N/A	9	-0.22
insular, part 3 (dorsal agranular insula), left	231	-0.29	95	-0.21
insular, part 3 (dorsal agranular insula), right	215	-0.29	213	-0.25
insular, part 4 (ventral granular insula), left	158	-0.28	76	-0.23
insular, part 4 (ventral granular insula), right	163	-0.28	53	-0.22
insular, part 5 (dorsal granular insula), left	231	-0.30	102	-0.24
insular, part 5 (dorsal granular insula), right	260	-0.32	204	-0.25
insular, part 6 (dorsal dysgranular insula), left	362	-0.33	350	-0.25
insular, part 6 (dorsal dysgranular insula), right	313	-0.34	313	-0.28
cingulate gyrus, part 5 (caudodorsal area 24), left	5	-0.25	0	N/A
cingulate gyrus, part 5 (caudodorsal area 24), right	19	-0.26	0	N/A
cuneus, part 1 (caudal lingual gyrus), left	152	-0.27	72	-0.22
cuneus, part 1 (caudal lingual gyrus), right	142	-0.28	72	-0.22
cuneus, part 2 (rostral cuneus gyrus), left	2	-0.26	0	N/A
cuneus, part 2 (rostral cuneus gyrus), right	36	-0.25	2	-0.21
cuneus, part 3 (caudal cuneus gyrus), right	29	-0.25	0	N/A
cuneus, part 4 (rostral lingual gyrus), left	390	-0.29	452	-0.25
cuneus, part 4 (rostral lingual gyrus), right	406	-0.29	480	-0.24
cuneus, part 5 (ventomedial parietooccipital sulcus), left	0	N/A	33	-0.21
cuneus, part 5 (ventomedial parietooccipital sulcus), right	0	N/A	1	-0.20

Region of Interest	Control Group				ADHD Group			
	Voxels		Correlation		Voxels		Correlation	
occipital gyrus, part 1 (middle occipital gyrus), left	68		-0.25		71		-0.21	
occipital gyrus, part 1 (middle occipital gyrus), right	52		-0.25		0		N/A	
occipital gyrus, part 2 (area V5/MT), left	317		-0.27		204		-0.22	
occipital gyrus, part 2 (area V5/MT), right	269	1259	-0.27	-0.26	590	1175	-0.25	-0.22
occipital gyrus, part 3 (occipital polar cortex), right	12		-0.25		0		N/A	
occipital gyrus, part 4 (inferior occipital gyrus), left	189		-0.27		11		-0.21	
occipital gyrus, part 4 (inferior occipital gyrus), right	352		-0.27		299		-0.23	
striatum, part 2 (globus pallidus), left	4		-0.25		0		N/A	
striatum, part 2 (globus pallidus), right	67		-0.27		58		-0.22	
striatum, part 4 (ventromedial putamen), left	3		-0.25		0		N/A	
striatum, part 4 (ventromedial putamen), right	8	413	-0.26	-0.26	2	206	-0.21	-0.22
striatum, part 6 (dorsolateral putamen), left	134		-0.26		0		N/A	
striatum, part 6 (dorsolateral putamen), right	197		-0.28		146		-0.23	
Cerebellar lobule I-IV, right					1		-0.20	
Cerebellar lobule V, left	1		-0.25		40		-0.21	
Cerebellar lobule V, right	62		-0.26		147		-0.23	
Cerebellar lobule VI, left	657		-0.29		889		-0.24	
Cerebellar lobule VI, vermis	9		-0.25		33		-0.21	
Cerebellar lobule VI, right	739	2073	-0.30	-0.27	656	2326	-0.25	-0.22
Cerebellar Crus I, left	80		-0.27		151		-0.22	
Cerebellar Crus I, right	525		-0.29		292		-0.24	
Cerebellar lobule VIIb, left	0		N/A		31		-0.21	

Region of Interest	Control Group		ADHD Group	
	Voxels	Correlation	Voxels	Correlation
Cerebellar lobule VIIIA, left	0	N/A	9	-0.21
Cerebellar lobule VIIIA, right	0	N/A	77	-0.21

Supplementary Table 3: ROIs in DMN and TPN and their correlation across QPPs

A list of regions of interest in the Brainnetome ROI atlas, whether they were included in the Control or ADHD DMN or TPN, and their correlation between the Control and ADHD quasi-periodic patterns. Among the four sub-columns for Correlation, the first shows the correlation value for each ROI, the second shows the mean correlation for all ROIs that were in the collective DMN from both groups, the third shows the mean correlation for all ROIs that were in the collective TPN from both groups, and the fourth shows the mean correlation for all ROIS in the respective anatomical region of the brain.

Region of Interest	Control		ADHD		Correlation
	DMN	TPN	DMN	TPN	
superior frontal gyrus, part 1 (medial area 8), left			✓	✓	0.46
superior frontal gyrus, part 1 (medial area 8), right			✓	✓	0.08
superior frontal gyrus, part 2 (dorsolateral area 8), left	✓	✓			0.98
superior frontal gyrus, part 2 (dorsolateral area 8), right	✓	✓			0.99
superior frontal gyrus, part 3 (lateral area 9), left	✓	✓			1.00
superior frontal gyrus, part 3 (lateral area 9), right	✓				1.00

Region of Interest	Control		ADHD		Correlation
	DMN	TPN	DMN	TPN	
superior frontal gyrus, part 4 (dorsolateral area 6), left			✓	✓	0.99
superior frontal gyrus, part 4 (dorsolateral area 6), right			✓	✓	0.75
superior frontal gyrus, part 5 (medial area 6), left			✓	✓	1.00
superior frontal gyrus, part 5 (medial area 6), right			✓	✓	0.99
superior frontal gyrus, part 6 (medial area 9), left	✓	✓			0.97
superior frontal gyrus, part 6 (medial area 9), right	✓	✓			1.00
superior frontal gyrus, part 7 (medial area 10), left	✓	✓			1.00
superior frontal gyrus, part 7 (medial area 10), right	✓	✓			1.00
middle frontal gyrus, part 1 (dorsal area 9/46), left	✓	✓			0.96
middle frontal gyrus, part 1 (dorsal area 9/46), right	✓	✓			0.96
middle frontal gyrus, part 2 (inferior frontal junction), left			✓		0.95
middle frontal gyrus, part 2 (inferior frontal junction), right				✓	1.00
middle frontal gyrus, part 3 (area 46), left	✓	✓			1.00
middle frontal gyrus, part 3 (area 46), right	✓				0.99
middle frontal gyrus, part 4 (ventral area 9/46), left					0.08
middle frontal gyrus, part 4 (ventral area 9/46), right				✓	-0.27
middle frontal gyrus, part 5 (ventrolateral area 8), left	✓	✓			0.99

Region of Interest	Control		ADHD		Correlation
	DMN	TPN	DMN	TPN	
middle frontal gyrus, part 5 (ventrolateral area 8), right	✓			✓	0.99
middle frontal gyrus, part 6 (ventrolateral area 6), left			✓	✓	0.12
middle frontal gyrus, part 6 (ventrolateral area 6), right	✓				0.97
middle frontal gyrus, part 7 (lateral area 10), left	✓	✓			1.00
middle frontal gyrus, part 7 (lateral area 10), right	✓	✓			1.00
inferior frontal gyrus, part 1 (dorsal area 44), left			✓	✓	1.00
inferior frontal gyrus, part 1 (dorsal area 44), right			✓	✓	0.99
inferior frontal gyrus, part 2 (inferior frontal sulcus), left				✓	0.83
inferior frontal gyrus, part 2 (inferior frontal sulcus), right				✓	-0.52
inferior frontal gyrus, part 3 (caudal area 45), left			✓	✓	0.77
inferior frontal gyrus, part 3 (caudal area 45), right			✓	✓	0.94
inferior frontal gyrus, part 4 (rostral area 45), left			✓	✓	-0.18
inferior frontal gyrus, part 4 (rostral area 45), right				✓	0.83
inferior frontal gyrus, part 5 (opercular area 44), left			✓	✓	0.97
inferior frontal gyrus, part 5 (opercular area 44), right			✓	✓	0.95
inferior frontal gyrus, part 6 (ventral area 44), left			✓	✓	1.00
inferior frontal gyrus, part 6 (ventral area 44), right			✓	✓	0.78

Region of Interest	Control		ADHD		Correlation
	DMN	TPN	DMN	TPN	
orbital gyrus, part 1 (medial area 14), left	✓	✓			1.00
orbital gyrus, part 1 (medial area 14), right	✓	✓			1.00
orbital gyrus, part 2 (orbital area 12/47), left					0.99
orbital gyrus, part 2 (orbital area 12/47), right					0.99
orbital gyrus, part 3 (lateral area 11), left					0.97
orbital gyrus, part 3 (lateral area 11), right					0.99
orbital gyrus, part 4 (medial area 11), left	✓	✓			1.00
orbital gyrus, part 4 (medial area 11), right	✓	✓			1.00
orbital gyrus, part 5 (area 13), left	✓	✓			0.99
orbital gyrus, part 5 (area 13), right	✓	✓			0.99
orbital gyrus, part 6 (lateral area 12/47), left			✓	✓	-0.59
orbital gyrus, part 6 (lateral area 12/47), right			✓	✓	0.78
precentral gyrus, part 1 (area 4 head and face), left			✓	✓	0.99
precentral gyrus, part 1 (area 4 head and face), right			✓	✓	0.98
precentral gyrus, part 2 (caudal dorsolateral area 6), left			✓	✓	0.99
precentral gyrus, part 2 (caudal dorsolateral area 6), right			✓	✓	0.97
precentral gyrus, part 3 (area 4 upper limb), left					0.86

Region of Interest	Control		ADHD		Correlation
	DMN	TPN	DMN	TPN	
precentral gyrus, part 3 (area 4 upper limb), right			✓		0.99
precentral gyrus, part 4 (area 4 trunk), left					0.94
precentral gyrus, part 4 (area 4 trunk), right					0.96
precentral gyrus, part 5 (area 4 tongue and larynx), left			✓	✓	1.00
precentral gyrus, part 5 (area 4 tongue and larynx), right			✓	✓	0.99
precentral gyrus, part 6 (caudal ventrolateral area 6), left			✓	✓	0.99
precentral gyrus, part 6 (caudal ventrolateral area 6), right			✓	✓	0.95
paracentral lobule, part 1 (area 1/2/3 lower limb), left	✓	✓			0.87
paracentral lobule, part 1 (area 1/2/3 lower limb), right	✓	✓			0.77
paracentral lobule, part 2 (area 4 lower limb), left	✓	✓			0.91
paracentral lobule, part 2 (area 4 lower limb), right	✓	✓			0.99
superior temporal gyrus, part 1 (medial area 38), left					1.00
superior temporal gyrus, part 1 (medial area 38), right					0.98
superior temporal gyrus, part 2 (area 41/42), left			✓	✓	0.99
superior temporal gyrus, part 2 (area 41/42), right			✓	✓	1.00
superior temporal gyrus, part 3 (area TE), left			✓	✓	0.99
superior temporal gyrus, part 3 (area TE), right			✓	✓	1.00

Region of Interest	Control		ADHD		Correlation
	DMN	TPN	DMN	TPN	
superior temporal gyrus, part 4 (caudal area 22), left		✓	✓		0.89
superior temporal gyrus, part 4 (caudal area 22), right			✓	✓	0.99
superior temporal gyrus, part 5 (lateral area 38), left			✓	✓	-0.21
superior temporal gyrus, part 5 (lateral area 38), right			✓	✓	0.83
superior temporal gyrus, part 6 (rostral area 22), left			✓	✓	0.86
superior temporal gyrus, part 6 (rostral area 22), right			✓	✓	0.86
middle temporal gyrus, part 1 (caudal area 21), left	✓	✓			1.00
middle temporal gyrus, part 1 (caudal area 21), right	✓	✓			1.00
middle temporal gyrus, part 2 (rostral area 21), left	✓	✓			1.00
middle temporal gyrus, part 2 (rostral area 21), right	✓	✓			1.00
middle temporal gyrus, part 3 (dorsolateral area 37), left		✓		✓	0.75
middle temporal gyrus, part 3 (dorsolateral area 37), right				✓	0.83
middle temporal gyrus, part 4 (anterior superior temporal sulcus), left					0.97
middle temporal gyrus, part 4 (anterior superior temporal sulcus), right	✓				0.82
inferior temporal gyrus, part 1 intermediate ventral area 20), left					0.98
inferior temporal gyrus, part 1 (intermediate ventral area 20), right					0.99
inferior temporal gyrus, part 2 (extreme lateroventral area 37), left			✓	✓	0.98

Region of Interest	Control		ADHD		Correlation
	DMN	TPN	DMN	TPN	
inferior temporal gyrus, part 2 (extreme lateroventral area 37), right					0.58
inferior temporal gyrus, part 3 (rostral area 20), left					0.99
inferior temporal gyrus, part 3 (rostral area 20), right					0.99
inferior temporal gyrus, part 4 (intermediate lateral area 20), left	✓	✓			1.00
inferior temporal gyrus, part 4 (intermediate lateral area 20), right	✓	✓			1.00
inferior temporal gyrus, part 5 (ventrolateral area 37), left			✓	✓	0.99
inferior temporal gyrus, part 5 (ventrolateral area 37), right			✓	✓	-0.96
inferior temporal gyrus, part 6 (caudolateral of area 20), left					0.99
inferior temporal gyrus, part 6 (caudolateral of area 20), right	✓				0.99
inferior temporal gyrus, part 7 (caudoventral of area 20), left		✓			1.00
inferior temporal gyrus, part 7 (caudoventral of area 20), right	✓				0.97
fusiform gyrus, part 1 (rostroventral area 20), left				✓	0.83
fusiform gyrus, part 1 (rostroventral area 20), right					0.90
fusiform gyrus, part 2 (medioventral area 37), left			✓	✓	0.96
fusiform gyrus, part 2 (medioventral area 37), right			✓	✓	0.96
fusiform gyrus, part 3 (ventrolateral area 37), left			✓	✓	0.98
fusiform gyrus, part 3 (ventrolateral area 37), right			✓	✓	0.90

Region of Interest	Control		ADHD		Correlation
	DMN	TPN	DMN	TPN	
parahippocampal gyrus, part 1 (rostral area 35/36), left					0.90
parahippocampal gyrus, part 1 (rostral area 35/36), right					0.81
parahippocampal gyrus, part 2 (caudal area 35/36), left					0.80
parahippocampal gyrus, part 2 (caudal area 35/36), right					0.92
parahippocampal gyrus, part 3 (area TL), left					-0.05
parahippocampal gyrus, part 3 (area TL), right					0.83
parahippocampal gyrus, part 4 (area 28/34), left					0.73
parahippocampal gyrus, part 4 (area 28/34), right					0.94
parahippocampal gyrus, part 5 (area TI), left					0.38
parahippocampal gyrus, part 5 (area TI), right					0.81
parahippocampal gyrus, part 6 (area TH), left					0.64
parahippocampal gyrus, part 6 (area TH), right					-0.07
posterior superior temporal sulcus, part 1 (rostroposterior superior temporal sulcus), left					0.42
posterior superior temporal sulcus, part 1 (rostroposterior superior temporal sulcus), right					0.05
posterior superior temporal sulcus, part 2 (caudoposterior superior temporal sulcus), left		✓			0.97
posterior superior temporal sulcus, part 2 (caudoposterior superior temporal sulcus), right					0.98
superior parietal lobule, part 1 (rostral area 7), left				✓	0.96

Region of Interest	Control		ADHD		Correlation
	DMN	TPN	DMN	TPN	
superior parietal lobule, part 1 (rostral area 7), right				✓	0.98
superior parietal lobule, part 2 (caudal area 7), left		✓		✓	-0.35
superior parietal lobule, part 2 (caudal area 7), right				✓	-0.13
superior parietal lobule, part 3 (lateral area 5), left			✓	✓	0.90
superior parietal lobule, part 3 (lateral area 5), right					1.00
superior parietal lobule, part 4 (postcentral area 7), left				✓	0.96
superior parietal lobule, part 4 (postcentral area 7), right					0.94
superior parietal lobule, part 5 (intraparietal area 7), left			✓	✓	0.93
superior parietal lobule, part 5 (intraparietal area 7), right				✓	0.99
inferior parietal lobule, part 1 (caudal area 39), left					0.95
inferior parietal lobule, part 1 (caudal area 39), right	✓	✓			0.96
inferior parietal lobule, part 2 (rostr dors al area 39), left	✓	✓			0.95
inferior parietal lobule, part 2 (rostr dors al area 39), right	✓	✓			0.99
inferior parietal lobule, part 3 (rostr dors al area 40), left			✓	✓	0.99
inferior parietal lobule, part 3 (rostr dors al area 40), right			✓	✓	0.97
inferior parietal lobule, part 4 (caudal area 40), left	✓	✓			1.00
inferior parietal lobule, part 4 (caudal area 40), right				✓	-0.81

Region of Interest	Control		ADHD		Correlation
	DMN	TPN	DMN	TPN	
inferior parietal lobule, part 5 (rostroventral area 39), left	✓	✓			0.99
inferior parietal lobule, part 5 (rostroventral area 39), right	✓	✓			1.00
inferior parietal lobule, part 6 (rostroventral area 40), left			✓	✓	0.99
inferior parietal lobule, part 6 (rostroventral area 40), right			✓	✓	0.99
precuneus, part 1 (medial area 7), left	✓	✓			0.92
precuneus, part 1 (medial area 7), right	✓	✓			0.97
precuneus, part 2 (medial area 5), left	✓	✓			0.42
precuneus, part 2 (medial area 5), right	✓	✓			-0.29
precuneus, part 3 (dorsomedial parietooccipital sulcus), left	✓	✓			0.52
precuneus, part 3 (dorsomedial parietooccipital sulcus), right	✓	✓			0.75
precuneus, part 4 (area 31), left	✓	✓			0.97
precuneus, part 4 (area 31), right	✓	✓			0.99
postcentral gyrus, part 1 (area 1/2/3 upper limb), left			✓	✓	1.00
postcentral gyrus, part 1 (area 1/2/3 upper limb), right			✓	✓	0.99
postcentral gyrus, part 2 (area 1/2/3 tongue and larynx), left			✓	✓	0.99
postcentral gyrus, part 2 (area 1/2/3 tongue and larynx), right			✓	✓	0.99
postcentral gyrus, part 3 (area 2), left			✓	✓	1.00

Region of Interest	Control		ADHD		Correlation
	DMN	TPN	DMN	TPN	
postcentral gyrus, part 3 (area 2), right			✓	✓	1.00
postcentral gyrus, part 4 (area1/2/3 trunk), left					0.93
postcentral gyrus, part 4 (area1/2/3 trunk), right					0.91
insular, part 1 (hypergranular insula), left			✓		1.00
insular, part 1 (hypergranular insula), right			✓	✓	0.99
insular, part 2 (ventral agranular insula), left			✓		0.15
insular, part 2 ventral agranular insula), right				✓	0.15
insular, part 3 (dorsal agranular insula), left			✓	✓	0.99
insular, part 3 (dorsal agranular insula), right			✓	✓	1.00
insular, part 4 (ventral granular insula), left			✓	✓	0.99
insular, part 4 (ventral granular insula), right			✓	✓	0.99
insular, part 5 (dorsal granular insula), left			✓	✓	1.00
insular, part 5 (dorsal granular insula), right			✓	✓	1.00
insular, part 6 (dorsal dysgranular insula), left			✓	✓	1.00
insular, part 6 (dorsal dysgranular insula), right			✓	✓	1.00
cingulate gyrus, part 1 (dorsal area 23), left	✓	✓			0.98
cingulate gyrus, part 1 (dorsal area 23), right	✓	✓			0.98

Region of Interest	Control		ADHD		Correlation
	DMN	TPN	DMN	TPN	
cingulate gyrus, part 2 (rostroventral area 24), left	✓	✓			0.45
cingulate gyrus, part 2 (rostroventral area 24), right	✓	✓			0.93
cingulate gyrus, part 3 (pregenual area 32), left	✓	✓			0.98
cingulate gyrus, part 3 (pregenual area 32), right	✓	✓			-0.95
cingulate gyrus, part 4 (ventral area 23), left	✓	✓			0.89
cingulate gyrus, part 4 (ventral area 23), right	✓	✓			0.96
cingulate gyrus, part 5 (caudodorsal area 24), left			✓		0.98
cingulate gyrus, part 5 (caudodorsal area 24), right			✓		0.98
cingulate gyrus, part 6 (caudal area 24), left	✓	✓			0.02
cingulate gyrus, part 6 (caudal area 24), right	✓	✓			-0.68
cingulate gyrus, part 7 (subgenual area 32), left	✓	✓			1.00
cingulate gyrus, part 7 (subgenual area 32), right	✓	✓			1.00
cuneus, part 1 (caudal lingual gyrus), left			✓	✓	0.91
cuneus, part 1 (caudal lingual gyrus), right			✓	✓	0.94
cuneus, part 2 (rostral cuneus gyrus), left	✓	✓	✓		0.99
cuneus, part 2 (rostral cuneus gyrus), right	✓	✓	✓	✓	0.98
cuneus, part 3 (caudal cuneus gyrus), left					0.95

Region of Interest	Control		ADHD		Correlation
	DMN	TPN	DMN	TPN	
cuneus, part 3 (caudal cuneus gyrus), right			✓		0.99
cuneus, part 4 (rostral lingual gyrus), left			✓	✓	0.99
cuneus, part 4 (rostral lingual gyrus), right			✓	✓	0.95
cuneus, part 5 (ventomedial parietooccipital sulcus), left	✓	✓		✓	0.96
cuneus, part 5 (ventomedial parietooccipital sulcus), right	✓	✓		✓	0.23
occipital gyrus, part 1 (middle occipital gyrus), left			✓		0.96
occipital gyrus, part 1 (middle occipital gyrus), right			✓	✓	0.97
occipital gyrus, part 2 (area V5/MT), left			✓	✓	0.98
occipital gyrus, part 2 (area V5/MT), right			✓	✓	1.00
occipital gyrus, part 3 (occipital polar cortex), left					0.97
occipital gyrus, part 3 (occipital polar cortex), right			✓		0.95
occipital gyrus, part 4 (inferior occipital gyrus), left			✓	✓	0.89
occipital gyrus, part 4 (inferior occipital gyrus), right			✓	✓	0.93
superior occipital gyrus, part 1 (medial superior occipital gyrus), left	✓	✓			0.97
superior occipital gyrus, part 1 (medial superior occipital gyrus), right		✓			0.98
superior occipital gyrus, part 2 (lateral superior occipital gyrus), left	✓	✓			1.00
superior occipital gyrus, part 2 (lateral superior occipital gyrus), right	✓	✓			0.80

Region of Interest	Control		ADHD		Correlation
	DMN	TPN	DMN	TPN	
amygdala, part 1 (medial amyg), left					0.61
amygdala, part 1 (medial amyg), right					0.78
amygdala, part 2 (lateral amyg), left					-0.01
amygdala, part 2 (lateral amyg), right					0.34
hippocampus, part 1 (rostral hipp), left					0.97
hippocampus, part 1 (rostral hipp), right					0.91
hippocampus, part 2 (caudal hipp), left	✓	✓			0.14
hippocampus, part 2 (caudal hipp), right					0.07
striatum, part 1 (ventral caudate), left					0.76
striatum, part 1 (ventral caudate), right					0.46
striatum, part 2 (globus pallidus), left			✓		0.87
striatum, part 2 (globus pallidus), right			✓	✓	0.97
striatum, part 3 (nucleus accumbens), left					0.08
striatum, part 3 (nucleus accumbens), right		✓			0.71
striatum, part 4 (ventromedial putamen), left			✓		0.44
striatum, part 4 (ventromedial putamen), right			✓	✓	0.33
striatum, part 5 (dorsal caudate), left					-0.23

Region of Interest	Control		ADHD		Correlation
	DMN	TPN	DMN	TPN	
striatum, part 5 (dorsal caudate), right					0.30
striatum, part 6 (dorsolateral putamen), left			✓		0.97
striatum, part 6 (dorsolateral putamen), right			✓	✓	0.99
thalamus, part 1 (medial prefrontal thalamus), left					-0.56
thalamus, part 1 (medial prefrontal thalamus), right					0.20
thalamus, part 2 (medial premotor thalamus), left					0.25
thalamus, part 2 (medial premotor thalamus), right					-0.49
thalamus, part 3 (sensory thalamus), left					0.85
thalamus, part 3 (sensory thalamus), right					0.89
thalamus, part 4 (rostral temporal thalamus), left		✓			0.86
thalamus, part 4 (rostral temporal thalamus), right		✓			0.83
thalamus, part 5 (posterior parietal thalamus), left					0.88
thalamus, part 5 (posterior parietal thalamus), right					0.50
thalamus, part 6 (occipital thalamus), left		✓			0.54
thalamus, part 6 (occipital thalamus), right					0.98
thalamus, part 7 (caudal temporal thalamus), left		✓			0.77
thalamus, part 7 (caudal temporal thalamus), right		✓			0.57

Region of Interest	Control		ADHD		Correlation
	DMN	TPN	DMN	TPN	
thalamus, part 8 (lateral prefrontal thalamus), left					-0.59
thalamus, part 8 (lateral prefrontal thalamus), right					-0.80
Cerebellar lobule I-IV, left	✓				0.85
Cerebellar lobule I-IV, right	✓	✓		✓	0.60
Cerebellar lobule V, left			✓	✓	0.96
Cerebellar lobule V, right			✓	✓	0.91
Cerebellar lobule VI, left			✓	✓	0.97
Cerebellar lobule VI, vermis			✓	✓	0.94
Cerebellar lobule VI, right			✓	✓	0.98
Cerebellar Crus I, left			✓	✓	0.92
Cerebellar Crus I, right			✓	✓	0.73
Cerebellar Crus II, left					0.99
Cerebellar Crus II, vermis					0.52
Cerebellar Crus II, right					0.98
Cerebellar lobule VIIb, left				✓	-0.20
Cerebellar lobule VIIb, vermis					0.92
Cerebellar lobule VIIb, right					0.51
Cerebellar lobule VIIa, left				✓	0.59
Cerebellar lobule VIIa, vermis					0.45
Cerebellar lobule VIIa, right				✓	0.99
Cerebellar lobule VIIb, left					0.09
Cerebellar lobule VIIb, vermis					-0.65
Cerebellar lobule VIIb, right					0.82
Cerebellar lobule IX, left					0.97
Cerebellar lobule IX, vermis					0.94

Region of Interest	Control		ADHD		Correlation
	DMN	TPN	DMN	TPN	
Cerebellar lobule IX, right					0.95
Cerebellar lobule X, left					0.52
Cerebellar lobule X, vermis					0.40
Cerebellar lobule X, right					0.72

Further Acknowledgements

Chapter 2

This work was supported by National Science Foundation BCS INSPIRE 1533260, National Institutes of Health R01NS078095, National Institutes of Health 1R01MH111416-01, and the ISMRM Research Exchange Program. Data were provided by the Human Connectome Project, WU-Minn Consortium (Principal Investigators: David Van Essen and Kamil Ugurbil; 1U54MH091657) funded by the 16 NIH Institutes and Centers that support the NIH Blueprint for Neuroscience Research; and by the McDonnell Center for Systems Neuroscience at Washington University.

Chapter 3

Funding for this work was provided by NSF BCS INSPIRE 1533260, NIH R01MH111416, and NIH R01NS078095. The data used in this study in its entirety was acquired from the ADHD 200 Sample within the 1000 Functional Connectome Project. The authors would like to acknowledge the individuals involved in collection of all data and the various funding sources that supported the NeuroImage Sample, New York University dataset, and Peking University dataset, which are included but not limited to NIMH (R01MH083246), Autism Speaks, The Stavros Niarchos Foundation, Leon Levy Foundation, an endowment provided by Phyllis Green and Randolph Cōwen, Commonwealth Sciences Foundation, Ministry of Health, China (200802073), National Foundation, Ministry of Science and Technology, China (2007BAI17B03), National Natural Sciences Foundation, China (30970802), Funds for International Cooperation of the National Natural Science Foundation of China (81020108022), National Natural Science Foundation of

China (8100059), and the Open Research Fund of the State Key Laboratory of Cognitive Neuroscience and Learning.

Chapter 4

This work was supported by National Science Foundation BCS INSPIRE 1533260, National Institutes of Health R01NS078095, National Institutes of Health 1R01MH111416-01, and the ISMRM Research Exchange Program. Data were provided by the Human Connectome Project, WU-Minn Consortium (Principal Investigators: David Van Essen and Kamil Ugurbil; 1U54MH091657) funded by the 16 NIH Institutes and Centers that support the NIH Blueprint for Neuroscience Research; and by the McDonnell Center for Systems Neuroscience at Washington University.

References

Abbas, A., Belloy, M., Kashyap, A., Billings, J., Nezafati, M., Schumacher, E., & Keilholz, S. (2019a). Quasi-periodic patterns contribute to functional connectivity in the brain. *NeuroImage* 191:193-204. <https://doi.org/10.1016/j.neuroimage.2019.01.076>.

Abbas, A., Bassil, Y., & Keilholz, S. (2019b). Quasi-periodic patterns of brain activity in individuals with Attention-Deficit/Hyperactivity Disorder. *NeuroImage: Clinical* 21:101653.

Abbas, A., Langley, J., Howell, L., & Keilholz, S. (2016). Quasi-periodic patterns vary in frequency between anesthetized and awake monkeys. In: Resting State Brain Connectivity Biennial Conference, p. 141.

ADHD-200 Consortium. (2012). The ADHD-200 Consortium: A Model to Advance the Translational Potential of Neuroimaging in Clinical Neuroscience. *Frontiers in Systems Neuroscience*, 6, 62. <http://doi.org/10.3389/fnsys.2012.00062>

American Psychiatric Association. (2013). Diagnostic and statistical manual of mental disorders (5th ed.). Arlington, VA: American Psychiatric Publishing.

Andrews-Hanna, J. R., Snyder, A. Z., Vincent, J. L., Lustig, C., Head, D., Raichle, M. E., & Buckner, R. L. (2007). Disruption of Large-Scale Brain Systems in Advanced Aging. *Neuron*, 56(5), 924–935. <http://doi.org/10.1016/j.neuron.2007.10.038>

Arnold L. (1996) Sex differences in ADHD: conference summary. *J Abnorm Child Psychol* 1996; 24:555–569

Asemi, A., Ramaseshan, K., Burgess, A., Diwadkar, V. A., & Bressler, S. L. (2015). Dorsal anterior cingulate cortex modulates supplementary motor area in coordinated unimanual motor behavior. *Frontiers in Human Neuroscience*, 9, 309. <http://doi.org/10.3389/fnhum.2015.00309>

Aston-Jones, G., Chiang, C., & Alexinsky, T. (1991). Discharge of noradrenergic locus coeruleus neurons in behaving rats and monkeys suggests a role in vigilance. In *Progress in brain research* (Vol. 88, pp. 501-520). Elsevier.

Aston-Jones, G., Rajkowski, J., & Cohen, J. (1999). Role of locus coeruleus in attention and behavioral flexibility. *Biological psychiatry*, 46(9), 1309-1320.

Aston-Jones, G., Rajkowski, J., Kubiak, P., & Alexinsky, T. (1994). Locus coeruleus neurons in monkey are selectively activated by attended cues in a vigilance task. *Journal of Neuroscience*, 14(7), 4467-4480.

Aston-Jones, G., & Cohen, J. D. (2005). Adaptive gain and the role of the locus coeruleus–norepinephrine system in optimal performance. *Journal of Comparative Neurology*, 493(1), 99-110.

Bagwell C.L., Molina B.S., Pelham W.E.J., Hoza, B. (2001). Attention-deficit hyperactivity disorder and problems in peer relations: predictions from childhood to adolescence. *J Am Acad Child Adolesc Psychiatry*. 40:1285-1292.

Bär, K.-J., la Cruz, de, F., Schumann, A., Koehler, S., Sauer, H., Critchley, H., & Wagner, G. (2016). Functional connectivity and network analysis of midbrain and brainstem nuclei. *NeuroImage*, 134, 53–63. <http://doi.org/10.1016/j.neuroimage.2016.03.071>

Barch, D. M., Burgess, G. C., Harms, M. P., Petersen, S. E., Schlaggar, B. L., Corbetta, M., et al. (2013). Function in the human connectome: Task-fMRI and individual differences in behavior. *NeuroImage*, 80(C), 169–189. <http://doi.org/10.1016/j.neuroimage.2013.05.033>

Barkley RA, Anastopoulos AD, Guevremont DC, Fletcher KE: Adolescents with ADHD: patterns of behavioral adjustment, academic functioning, and treatment utilization. *J Am Acad Child Adolesc Psychiatry* 1991, 30:752-761.

Bassett, D. S., & Sporns, O. (2017). Network neuroscience. *Nature Neuroscience*, 20(3), 353–364. <http://doi.org/10.1038/nn.4502>

Belloy, M. E., Naeyaert, M., Abbas, A., Shah, D., Vanreusel, V., van Audekerke, J., et al. (2018). Dynamic resting state fMRI analysis in mice reveals a set of Quasi-Periodic Patterns and illustrates their relationship with the global signal. *NeuroImage*, 1–22. <http://doi.org/10.1016/j.neuroimage.2018.01.075>

Benjamini, Y., & Hochberg, Y. (1995). Controlling the False Discovery Rate: A Practical and Powerful Approach to Multiple Testing. *Journal of the Royal Statistical Society*, 57(1), 289–300.

Benjamini, Y., & Yekutieli, D. (2001). The Control of the False Discovery Rate in Multiple Testing Under Dependency. *The Annals of Statistics*, 29(4), 1165–1188.

Bickle, J. (2006). Reducing mind to molecular pathways: explicating the reductionism implicit in current cellular and molecular neuroscience. *Synthese*, 151(3), 411–434. <http://doi.org/10.1007/s11229-006-9015-2>

Biederman, J., Mick, E., Faraone, S., Braaten, E., Doyle, A., Spencer, T., et al. (2002). Influence of Gender on Attention Deficit Hyperactivity Disorder in Children Referred to a Psychiatric Clinic. *American Journal of Psychiatry*, 159, 36–42.

Biswal, B. B., Mennes, M., Zuo, X.-N., Gohel, S., Kelly, C., Smith, S. M., et al. (2010). Toward discovery science of human brain function. *Proceedings of the National Academy of Sciences of the United States of America*, 107(10), 4734–4739. <http://doi.org/10.1073/pnas.0911855107>

Biswal, B., Yetkin, F. Z., Haughton, V. M., & Hyde, J. S. (1995). Functional Connectivity in the Motor Cortex of Resting Human Brain Using Echo-Planar. *Magnetic Resonance in Medicine*, 34(4), 537–541.

Brown, M. R. G. (2012). ADHD-200 Global Competition: diagnosing ADHD using personal characteristic data can outperform resting state fMRI measurements. *Frontiers in Systems Neuroscience*, 1–22. <http://doi.org/10.3389/fnsys.2012.00069/abstract>

Buckner, R. L., Sepulcre, J., Talukdar, T., Krienen, F. M., Liu, H., Hedden, T., ... & Johnson, K. A. (2009). Cortical hubs revealed by intrinsic functional connectivity: mapping, assessment of stability, and relation to Alzheimer's disease. *Journal of neuroscience*, 29(6), 1860-1873.

Buzsáki, G. (2006). *Rhythms of the Brain* (pp. 1–465). Oxford University Press, Inc.

Bymaster, F. P., Katner, J. S., Nelson, D. L., Hemrick-Luecke, S. K., Threlkeld, P. G., Heiligenstein, J. H., ... & Perry, K. W. (2002). Atomoxetine increases extracellular levels of norepinephrine and dopamine in prefrontal cortex of rat: a potential mechanism for efficacy in attention deficit/hyperactivity disorder. *Neuropsychopharmacology*, 27(5), 699-711.

Calautti, C., & Baron, J. C. (2003). Functional neuroimaging studies of motor recovery after stroke in adults: a review. *Stroke*, 34(6), 1553-1566.

Canolty, R. T., & Knight, R. T. (2010). The functional role of cross-frequency coupling. *Trends in Cognitive Sciences*, 14(11), 506–515. <http://doi.org/10.1016/j.tics.2010.09.001>

Carrera, E., & Tononi, G. (2014). Diaschisis: past, present, future. *Brain*, 137(9), 2408-2422.

Carter, A. R., Astafiev, S. V., Lang, C. E., Connor, L. T., Rengachary, J., Strube, M. J., ... & Corbetta, M. (2010). Resting interhemispheric functional magnetic resonance imaging connectivity predicts performance after stroke. *Annals of neurology*, 67(3), 365-375.

Castellanos, F. X., Margulies, D. S., Kelly, C., Uddin, L. Q., Ghaffari, M., Kirsch, A., et al. (2008). Cingulate-Precuneus Interactions: A New Locus of Dysfunction in Adult Attention-Deficit/Hyperactivity Disorder. *Biological Psychiatry*, 63(3), 332–337. <http://doi.org/10.1016/j.biopsych.2007.06.025>

Chalermplanupap, T., Schroeder, J. P., Rorabaugh, J. M., Liles, L. C., Lah, J. J., Levey, A. I., & Weinshenker, D. (2018). Locus coeruleus ablation exacerbates cognitive deficits,

neuropathology, and lethality in P301S tau transgenic mice. *Journal of Neuroscience*, 38(1), 74-92.

Chang, C., & Glover, G. H. (2010). Time–frequency dynamics of resting-state brain connectivity measured with fMRI. *NeuroImage*, 50(1), 81–98. <http://doi.org/10.1016/j.neuroimage.2009.12.011>

Chang, C., Keilholz, S., Miller, R., & Woolrich, M. (2018). Mapping and interpreting the dynamic connectivity of the brain. *NeuroImage*, 180(Pt B), 335–336. <http://doi.org/10.1016/j.neuroimage.2018.07.018>

Chang, C., Leopold, D. A., Schölvinck, M. L., Mandelkow, H., Picchioni, D., Liu, X., ... & Duyn, J. H. (2016). Tracking brain arousal fluctuations with fMRI. *Proceedings of the National Academy of Sciences*, 201520613.

Chen, L., Vu, A. T., Xu, J., Moeller, S., Ugurbil, K., Yacoub, E., & Feinberg, D. A. (2015). Evaluation of highly accelerated simultaneous multi-slice EPI for fMRI. *NeuroImage*, 104(C), 452–459. <http://doi.org/10.1016/j.neuroimage.2014.10.027>

Cherkassky, V. L., Kana, R. K., Keller, T. A., & Just, M. A. (2006). Functional connectivity in a baseline resting-state network in autism. *Neuroreport*, 17(16), 1687-1690.

Choi, J., Jeong, B., Lee, S. W., & Go, H.-J. (2013). Aberrant Development of Functional Connectivity among Resting State-Related Functional Networks in Medication-Naïve ADHD Children. *Plos One*, 8(12), e83516–11. <http://doi.org/10.1371/journal.pone.0083516>

Cole, M. W., Ito, T., Bassett, D. S., & Schultz, D. H. (2016). Activity flow over resting-state networks shapes cognitive task activations. *Nature Neuroscience*, 19(12), 1718–1726. <http://doi.org/10.1038/nn.4406>

Cortese, S., Kelly, C., Chabernaud, C., Proal, E., Di Martino, A., Milham, M. P., & Castellanos, F. X. (2012). Toward Systems Neuroscience of ADHD: A Meta-Analysis of 55 fMRI Studies. *American Journal of Psychiatry*, (169), 1038–1055.

Daffertshofer, A., Ton, R., Kringelbach, M. L., Woolrich, M., & Deco, G. (2018a). Distinct criticality of phase and amplitude dynamics in the resting brain. *NeuroImage*.

Daffertshofer, A., Ton, R., Pietras, B., Kringelbach, M. L., & Deco, G. (2018b). Scale-freeness or partial synchronization in neural mass phase oscillator networks: Pick one of two? *NeuroImage*.

Damadian, R. (1971). Tumor detection by nuclear magnetic resonance. *Science*, 171(3976), 1151-1153.

Damadian, R., Zaner, K., Hor, D., & DiMaio, T. (1974). Human tumors detected by nuclear magnetic resonance. *Proceedings of the National Academy of Sciences*, 71(4), 1471-1473.

Damadian, R., Zaner, K., Hor, D., DiMaio, T., Minkoff, L., & Goldsmith, M. (1973). Nuclear magnetic resonance as a new tool in cancer research: human tumors by NMR. *Annals of the New York Academy of Sciences*, 222(1), 1048-1076.

Damaraju, E., Allen, E. A., Belger, A., Ford, J. M., McEwen, S., Mathalon, D. H., et al. (2014). Dynamic functional connectivity analysis reveals transient states of dysconnectivity in schizophrenia. *Neuroimage: Clinical*, 5(C), 298–308. <http://doi.org/10.1016/j.nicl.2014.07.003>

Damaraju, E., Turner, J., Preda, A., Van Erp, T., Mathalon, D., Ford, J. M., ... & Calhoun, V. D. (2012). Static and dynamic functional network connectivity during resting state in schizophrenia. In *American College of Neuropsychopharmacology*.

Das M., Oyarzabal E., Chen Y-W, Lee SH, Chen L, Zhang W, Jensen P, S. Y. Chemogenetic fMRI and 18F-FDG PET Reveal Functional Projections of Hoxb1-Derived Noradrenergic Neurons. in *Proc Int Soc Magn Reson Med* 1155 (2017).

David, O., & Friston, K. J. (2003). A neural mass model for MEG/EEG:: coupling and neuronal dynamics. *NeuroImage*, 20(3), 1743-1755.

Davidovitch, M., Koren, G., Fund, N., Shrem, M., & Porath, A. (2017). Challenges in defining the rates of ADHD diagnosis and treatment: trends over the last decade. *BMC Pediatrics*, 1–9. <http://doi.org/10.1186/s12887-017-0971-0>

Doyle, F. H., Pennock, J. M., Orr, J. S., Gore, J. C., Bydder, G. M., Steiner, R. E., Young, I. R., Clow, H., Bailes, D. R., Burl, M., Gilderdale, D. J., Walters, P. E. (1981). Imaging of the brain by nuclear magnetic resonance. *The Lancet*, 318(8237), 53-57.

Du, Y., Fu, Z., & Calhoun, V. D. (2018). Classification and Prediction of Brain Disorders Using Functional Connectivity: Promising but Challenging. *Frontiers in Neuroscience*, 12, 1248–29. <http://doi.org/10.3389/fnins.2018.00525>

Durston, S., Tottenham, N. T., Thomas, K. M., Davidson, M. C., Eigsti, I.-M., Yang, Y., et al. (2003). Differential patterns of striatal activation in young children with and without ADHD. *Biological Psychiatry*, 53(10), 871–878. [http://doi.org/10.1016/S0006-3223\(02\)01904-2](http://doi.org/10.1016/S0006-3223(02)01904-2)

Elton, A., & Gao, W. (2015). Task-related modulation of functional connectivity variability and its behavioral correlations. *Human Brain Mapping*, 36(8), 3260–3272. <http://doi.org/10.1002/hbm.22847>

Eyckmans, J., Boudou, T., Yu, X., & Chen, C. S. (2011). A Hitchhiker's Guide to Mechanobiology. *Developmental Cell*, 21(1), 35–47. <http://doi.org/10.1016/j.devcel.2011.06.015>

Fan, L., Li, H., Zhuo, J., Zhang, Y., Wang, J., Chen, L., et al. (2016). The Human Brainnetome Atlas: A New Brain Atlas Based on Connectional Architecture. *Cerebral Cortex*, 26(8), 3508–3526. <http://doi.org/10.1093/cercor/bhw157>

Feinberg, D. A., Moeller, S., Smith, S. M., Auerbach, E., Ramanna, S., Glasser, M. F., et al. (2010). Multiplexed Echo Planar Imaging for Sub-Second Whole Brain fMRI and Fast Diffusion Imaging. *Plos One*, 5(12), e15710–11. <http://doi.org/10.1371/journal.pone.0015710>

Foster, B. L., He, B. J., Honey, C. J., Jerbi, K., Maier, A., & Saalman, Y. B. (2016). Spontaneous Neural Dynamics and Multi-scale Network Organization. *Frontiers in Systems Neuroscience*, 10(309), 7. <http://doi.org/10.3389/fnsys.2016.00007>

Fox, M. D., Snyder, A. Z., Vincent, J. L., Corbetta, M., Van Essen, D. C., & Raichle, M. E. (2005). The human brain is intrinsically organized into dynamic, anticorrelated functional networks. *Proceedings of the National Academy of Sciences of the United States of America*, 102(27), 9673–9678. <http://doi.org/10.1073/pnas.0504136102>

Frahm, J., Merboldt, K. D., & Hänicke, W. (1993). Functional MRI of human brain activation at high spatial resolution. *Magnetic Resonance in Medicine*, 29(1), 139-144.

Gaub M, Carlson CL. (1997) Gender differences in ADHD: a meta-analysis and critical review. *J Am Acad Child Adolesc Psychiatry* 1997; 36:1036–1045

Gillebert, C. R., & Mantini, D. (2013). Functional connectivity in the normal and injured brain. *The Neuroscientist : a Review*. *The Neuroscientist*, 19(5), 509–522. <http://doi.org/10.1177/1073858412463168>

Gilzenrat, M. S., Nieuwenhuis, S., Jepma, M., & Cohen, J. D. (2010). Pupil diameter tracks changes in control state predicted by the adaptive gain theory of locus coeruleus function. *Cognitive, Affective, & Behavioral Neuroscience*, 10(2), 252-269.

Glasser, M. F., Coalson, T. S., Robinson, E. C., Hacker, C. D., Harwell, J., Yacoub, E., Ugurbil, K., Andersson, J., Beckman, C. F., Jenkinson, M., Smith, S. M., Van Essen, D. C. (2016). A multi-modal parcellation of human cerebral cortex. *Nature*, 536(7615), 171-178.

Goparaju, B., Rana, K. D., Calabro, F. J., & Vaina, L. M. (2014). A computational study of whole-brain connectivity in resting state and task fMRI. *Medical Science Monitor*, 20, 1024–1042. <http://doi.org/10.12659/MSM.891142>

Gratton, C., Laumann, T. O., Nielsen, A. N., Greene, D. J., Gordon, E. M., Gilmore, A. W., Nelson, S. M., Coalson, R. S., Snyder, A. Z., Schlagger, B. L., Dosenbach, N. U., Peterson, S. E. (2018). Functional brain networks are dominated by stable group and individual factors, not cognitive or daily variation. *Neuron*, 98(2), 439-452.

Grefkes, C., & Fink, G. R. (2014). Connectivity-based approaches in stroke and recovery of function. *The Lancet Neurology*, 13(2), 206-216.

Greicius, M. (2008). Resting-state functional connectivity in neuropsychiatric disorders. *Current opinions in neurology*, 21(4), 424-430.

Greicius, M. D., Flores, B. H., Menon, V., Glover, G. H., Solvason, H. B., Kenna, H., ... & Schlaggar, A. F. (2007). Resting-state functional connectivity in major depression: abnormally increased contributions from subgenual cingulate cortex and thalamus. *Biological psychiatry*, 62(5), 429-437.

Grimm, S., Boesiger, P., Beck, J., Schuepbach, D., Birmahler, F., Walter, M., et al. (2008). Altered Negative BOLD Responses in the Default-Mode Network during Emotion Processing in Depressed Subjects. *Neuropsychopharmacology*, 34(4), 932–943. <http://doi.org/10.1038/npp.2008.81>

Grooms, J. K., Thompson, G. J., Pan, W.-J., Billings, J., Schumacher, E. H., Epstein, C. M., & Keilholz, S. D. (2017). Infralow Electroencephalographic and Dynamic Resting State Network Activity. *Brain Connectivity*, 7(5), 265–280. <http://doi.org/10.1089/brain.2017.0492>

Hampson, M., Driesen, N., Roth, J. K., Gore, J. C., & Constable, R. T. (2010). Functional connectivity between task-positive and task-negative brain areas and its relation to working memory performance. *Magnetic Resonance Imaging*, 28(8), 1051–1057. <http://doi.org/10.1016/j.mri.2010.03.021>

Hart, H., Radua, J., Mataix-Cols, D., & Rubia, K. (2012). Meta-analysis of fMRI studies of timing in attention-deficit hyperactivity disorder (ADHD). *Neuroscience and Biobehavioral Reviews*, 36(10), 2248–2256. <http://doi.org/10.1016/j.neubiorev.2012.08.003>

He, B. J., Snyder, A. Z., Zempel, J. M., Smyth, M. D., & Raichle, M. E. (2008). Electrophysiological correlates of the brain's intrinsic large-scale functional architecture. *PNAS*, 105(41), 16039–16044.

Hebb, D. O. (1963). *The Organizations of Behavior: a Neuropsychological Theory*. Lawrence Erlbaum

Helps, S., Broyda, S., James, C., Karl, A., Chen, W., Sonuga-Barke, E. (2010) Altered spontaneous low frequency brain activity in Attention Deficit/Hyperactivity Disorder. *Brain Research*, 1322, 134-143. <https://doi.org/10.1016/j.brainres.2010.01.057>

Hiltunen, T., Kantola, J., Abou Elseoud, A., Lepola, P., Suominen, K., Starck, T., et al. (2014). Infra-Slow EEG Fluctuations Are Correlated with Resting-State Network Dynamics in fMRI. *Journal of Neuroscience*, 34(2), 356–362. <http://doi.org/10.1523/JNEUROSCI.0276-13.2014>

Hindriks, R., Adhikari, M. H., Murayama, Y., Ganzetti, M., Mantini, D., Logothetis, N. K., & Deco, G. (2016). Can sliding-window correlations reveal dynamic functional connectivity in resting-state fMRI?. *Neuroimage*, 127, 242-256.

Hodgkin, A. L., & Huxley, A. F. (1952). A quantitative description of membrane current and its application to conduction and excitation in nerve. *The Journal of physiology*, 117(4), 500-544.

Hoekzema, E., Carmona, S., Ramos-Quiroga, J. A., Richarte Fernández, V., Bosch, R., Soliva, J. C., et al. (2013). An independent components and functional connectivity analysis of resting state fMRI data points to neural network dysregulation in adult ADHD. *Human Brain Mapping*, 35(4), 1261–1272. <http://doi.org/10.1002/hbm.22250>

Hoekzema, E., Carmona, S., Ramos-Quiroga, J. A., Richarte Fernández, V., Bosch, R., Soliva, J. C., et al. (2013). An independent components and functional connectivity analysis of resting state fMRI data points to neural network dysregulation in adult ADHD. *Human Brain Mapping*, 35(4), 1261–1272. <http://doi.org/10.1002/hbm.22250>

Holt, D. J., Cassidy, B. S., Andrews-Hanna, J. R., Lee, S. M., Coombs, G., Goff, D. C., et al. (2011). An Anterior-to-Posterior Shift in Midline Cortical Activity in Schizophrenia During Self-Reflection. *Biol Psychiatry*, 69(5), 415–423. <http://doi.org/10.1016/j.biopsych.2010.10.003>

Holtzheimer, P. E., & Mayberg, H. S. (2011). Stuck in a rut: rethinking depression and its treatment. *Trends in Neurosciences*, 34(1), 1–9. <http://doi.org/10.1016/j.tins.2010.10.004>

Hutchison, R. M., Womelsdorf, T., Allen, E. A., Bandettini, P. A., Calhoun, V. D., Corbetta, M., et al. (2013). Dynamic functional connectivity: promise, issues, and interpretations. *NeuroImage*, 80, 360–378. <http://doi.org/10.1016/j.neuroimage.2013.05.079>

Jaim-Etcheverry, G., & Mari, L. (1980). DSP-4: a novel compound with neurotoxic effects on noradrenergic neurons of adult and developing rats. *Brain research*, 188(2), 513–523.

Jenkinson, M., & Smith, S. (2001). A global optimisation method for robust affine registration of brain images. *Medical Image Analysis*, 5(2), 143–156.

Jenkinson, M., Bannister, P., Brady, M., & Smith, S. (2002). Improved optimization for the robust and accurate linear registration and motion correction of brain images. *NeuroImage*, 17(2), 825–841.

Jenkinson, M., Beckmann, C. F., Behrens, T. E. J., Woolrich, M. W., & Smith, S. M. (2012). FSL. *NeuroImage*, 62(2), 782–790. <http://doi.org/10.1016/j.neuroimage.2011.09.015>

Jones, D. T., Vemuri, P., Murphy, M. C., Gunter, J. L., Senjem, M. L., Machulda, M. M., et al. (2012). Non-stationarity in the “resting brain's” modular architecture. *Plos One*, 7(6), e39731. <http://doi.org/10.1371/journal.pone.0039731>

Jonsson, G., Hallman, H., Ponzio, F., & Ross, S. (1981). DSP4 (N-(2-chloroethyl)-N-ethyl-2-bromobenzylamine)—a useful denervation tool for central and peripheral noradrenaline neurons. *European journal of pharmacology*, 72(2-3), 173-188.

Joshi, S., Li, Y., Kalwani, R. M., & Gold, J. I. (2016). Relationships between pupil diameter and neuronal activity in the locus coeruleus, colliculi, and cingulate cortex. *Neuron*, 89(1), 221-234.

Kelly, A. M. C., Uddin, L. Q., Biswal, B. B., Castellanos, F. X., & Milham, M. P. (2008). Competition between functional brain networks mediates behavioral variability. *NeuroImage*, 39(1), 527–537. <http://doi.org/10.1016/j.neuroimage.2007.08.008>

Kelly, C., de Zubicaray, G., Di Martino, A., Copland, D. A., Reiss, P. T., Klein, D. F., ... & McMahon, K. (2009). L-dopa modulates functional connectivity in striatal cognitive and motor networks: a double-blind placebo-controlled study. *Journal of Neuroscience*, 29(22), 7364-7378.

Khambhati, A. N., Medaglia, J. D., Karuza, E. A., Thompson-Schill, S. L., & Bassett, D. S. (2018). Subgraphs of functional brain networks identify dynamical constraints of cognitive control. *PLoS computational biology*, 14(7), e1006234.

Konrad, K., & Eickhoff, S. B. (2010). Is the ADHD brain wired differently? A review on structural and functional connectivity in attention deficit hyperactivity disorder. *Human brain mapping, 31*(6), 904-916.

Langhorne, P., Coupar, F., & Pollock, A. (2009). Motor recovery after stroke: a systematic review. *The Lancet Neurology, 8*(8), 741-754.

Lauterbur, P. C. (1973). Image formation by induced local interactions: examples employing nuclear magnetic resonance.

Liddle, E. B., Hollis, C., Batty, M. J., Groom, M. J., Totman, J. J., Liotti, M., et al. (2010). Task-related default mode network modulation and inhibitory control in ADHD: effects of motivation and methylphenidate. *Journal of Child Psychology and Psychiatry, 52*(7), 761–771. <http://doi.org/10.1111/j.1469-7610.2010.02333.x>

Lin, H.-Y., & Gau, S. S.-F. (2016). Atomoxetine Treatment Strengthens an Anti-Correlated Relationship between Functional Brain Networks in Medication-Naïve Adults with Attention-Deficit Hyperactivity Disorder: A Randomized Double-Blind Placebo-Controlled Clinical Trial. *International Journal of Neuropsychopharmacology, 19*(3), pyv094–15. <http://doi.org/10.1093/ijnp/pyv094>

Lindquist, M. A., Waugh, C., & Wager, T. D. (2007). Modeling state-related fMRI activity using change-point theory. *NeuroImage, 35*(3), 1125-1141.

Liu, X., & Duyn, J. H. (2013). Time-varying functional network information extracted from brief instances of spontaneous brain activity. *Proceedings of the National Academy of Sciences*, 201216856.

Liu, X., Zhang, N., Chang, C., & Duyn, J. H. (2018). Co-activation patterns in resting-state fMRI signals. *NeuroImage*.

Lu, H., Zuo, Y., Gu, H., Waltz, J. A., Zhan, W., Scholl, C. A., ... & Stein, E. A. (2007). Synchronized delta oscillations correlate with the resting-state functional MRI signal. *Proceedings of the National Academy of Sciences*, 104(46), 18265-18269.

Magnuson, M. E., Thompson, G. J., Pan, W. J., & Keilholz, S. D. (2014). Effects of severing the corpus callosum on electrical and BOLD functional connectivity and spontaneous dynamic activity in the rat brain. *Brain connectivity*, 4(1), 15-29.

Majeed, W., Magnuson, M., & Keilholz, S. D. (2009). Spatiotemporal dynamics of low frequency fluctuations in BOLD fMRI of the rat. *Journal of Magnetic Resonance Imaging: An Official Journal of the International Society for Magnetic Resonance in Medicine*, 30(2), 384-393.

Majeed, W., Magnuson, M., Hasenkamp, W., Schwarb, H., Schumacher, E. H., Barsalou, L., & Keilholz, S. D. (2011). Spatiotemporal dynamics of low frequency BOLD fluctuations in rats and humans. *Neuroimage*, 54(2), 1140-1150.

Mansfield, P. (1977). Multi-planar image formation using NMR spin echoes. *Journal of Physics C: Solid State Physics*, 10(3), L55–L58. <http://doi.org/10.1088/0022-3719/10/3/004>

Matsui, T., Murakami, T., & Ohki, K. (2016). Transient neuronal coactivations embedded in globally propagating waves underlie resting-state functional connectivity. *PNAS*, 113(23), 6556–6561. <http://doi.org/10.1073/pnas.1521299113>

Matza, L. S., Paramore, C., & Prasad, M. (2005). A review of the economic burden of ADHD. *Cost Effectiveness and Resource Allocation*, 3(5). <http://doi.org/10.1186/1478-7547-3-5>

Milchenko, M., & Marcus, D. (2012). Obscuring Surface Anatomy in Volumetric Imaging Data. *Neuroinformatics*, 11(1), 65–75. <http://doi.org/10.1007/s12021-012-9160-3>

Mitra, A., Snyder, A. Z., Hacker, C. D., & Raichle, M. E. (2014). Lag structure in resting-state fMRI. *Journal of Neurophysiology*, 111(11), 2374–2391. <http://doi.org/10.1152/jn.00804.2013>

Mohan, A., Roberto, A., Mohan, A., Lorenzo, A., Jones, K., Carney, M., et al. (2016). The Significance of the Default Mode Network (DMN) in Neurological and Neuropsychiatric Disorders: A Review. *Yale Journal of Biology and Medicine*, 89(1), 49–57.

Monto, S., Palva, S., Voipio, J., & Palva, J. M. (2008). Very slow EEG fluctuations predict the dynamics of stimulus detection and oscillation amplitudes in humans. *The Journal of Neuroscience*, 28(33), 8268–8272. <http://doi.org/10.1523/JNEUROSCI.1910-08.2008>

Müller, K., Lohmann, G., Neumann, J., Grigutsch, M., Mildner, T., & von Cramon, D. Y. (2004). Investigating the wavelet coherence phase of the BOLD signal. *Journal of Magnetic Resonance Imaging: An Official Journal of the International Society for Magnetic Resonance in Medicine*, 20(1), 145-152.

Murphy, K., & Fox, M. D. (2017). Towards a consensus regarding global signal regression for resting state functional connectivity MRI. *NeuroImage*, 154, 169–173. <http://doi.org/10.1016/j.neuroimage.2016.11.052>

Murphy, P. R., O'Connell, R. G., O'Sullivan, M., Robertson, I. H., & Balsters, J. H. (2014). Pupil diameter covaries with BOLD activity in human locus coeruleus. *Human brain mapping*, 35(8), 4140-4154.

Natterer, F. (1986). *The mathematics of computerized tomography* (Vol. 32). Siam.

Nir, Y., Mukamel, R., Dinstein, I., Privman, E., Harel, M., Fisch, L., et al. (2008). Interhemispheric correlations of slow spontaneous neuronal fluctuations revealed in human sensory cortex. *Nature Neuroscience*, 11(9), 1100–1108. <http://doi.org/10.1038/nn.2177>

Ogawa, S., Lee, T. M., Kay, A. R., & Tank, D. W. (1990a). Brain magnetic resonance imaging with contrast dependent on blood oxygenation. *Proceedings of the National Academy of Sciences*, 87(24), 9868-9872.

Ogawa, S., Lee, T. M., Nayak, A. S., & Glynn, P. (1990b). Oxygenation-sensitive contrast in magnetic resonance image of rodent brain at high magnetic fields. *Magnetic resonance in medicine*, 14(1), 68-78.

Owen, A. M., McMillan, K. M., Laird, A. R., & Bullmore, E. (2005). N-back working memory paradigm: A meta-analysis of normative functional neuroimaging studies. *Human brain mapping*, 25(1), 46-59.

Palva, J. M., & Palva, S. (2012). Infra-slow fluctuations in electrophysiological recordings, blood-oxygenation-level-dependent signals, and psychophysical time series. *NeuroImage*, 62(4), 2201–2211. <http://doi.org/10.1016/j.neuroimage.2012.02.060>

Pan, W. J., Thompson, G., Magnuson, M., Majeed, W., Jaeger, D., & Keilholz, S. (2011). Broadband local field potentials correlate with spontaneous fluctuations in functional magnetic resonance imaging signals in the rat somatosensory cortex under isoflurane anesthesia. *Brain connectivity*, 1(2), 119-131.

Pan, W.-J., Thompson, G. J., Magnuson, M. E., Jaeger, D., & Keilholz, S. (2013). Infralow LFP correlates to resting-state fMRI BOLD signals. *NeuroImage*, 74(C), 288–297. <http://doi.org/10.1016/j.neuroimage.2013.02.035>

Park, H. J., & Friston, K. (2013). Structural and Functional Brain Networks: From Connections to Cognition. *Science*, 342(6158), 1238411–1238411. <http://doi.org/10.1126/science.1238411>

Pievani, M., Filippini, N., van den Heuvel, M. P., Cappa, S. F., & Frisoni, G. B. (2014). Brain connectivity in neurodegenerative diseases—from phenotype to proteinopathy. *Nature Reviews Neurology*, 10(11), 620–633. <http://doi.org/10.1038/nrneurol.2014.178>

Posner, J., Park, C., & Wang, Z. (2014). Connecting the Dots: A Review of Resting Connectivity MRI Studies in Attention-Deficit/Hyperactivity Disorder. *Neuropsychology Review*, 24(1), 3–15. <http://doi.org/10.1007/s11065-014-9251-z>

Power, J. D., Cohen, A. L., Nelson, S. M., Wig, G. S., Barnes, K. A., Church, J. A., Vogel, A. C., Laumann, T. O., Miezin, F. M., Schlaggar, B. L., Petersen, S. E. (2011). Functional network organization of the human brain. *Neuron*, 72(4), 665-678.

Querne, L., Fall, S., Le Moing, A.-G., Bourel-Ponchel, E., Delignières, A., Simonnot, A., et al. (2014). Effects of Methylphenidate on Default-Mode Network/Task-Positive Network Synchronization in Children With ADHD. *Journal of Attention Disorders*, 21(14), 1208–1220. <http://doi.org/10.1177/1087054713517542>

Quinn, A. J., Vidaurre, D., Abeyesuriya, R., Becker, R., Nobre, A. C., & Woolrich, M. W. (2018). Task-Evoked Dynamic Network Analysis Through Hidden Markov Modeling. *Frontiers in neuroscience*, 12.

Radon, J. (1986). On the determination of functions from their integral values along certain manifolds. *IEEE transactions on medical imaging*, 5(4), 170-176.

Raichle, M. E. (2011). The restless brain. *Brain Connectivity*, 1(1), 3–12. <http://doi.org/10.1089/brain.2011.0019>

Raichle, M. E. (2015). The Brain's Default Mode Network. *Annual Review of Neuroscience*, 38(1), 433–447. <http://doi.org/10.1146/annurev-neuro-071013-014030>

Raj, A., & Powell, F. (2018). Models of Network Spread and Network Degeneration in Brain Disorders. *Biological Psychiatry: Cognitive Neuroscience and Neuroimaging*, 3(9), 788–797.

Rubia, K., Cubillo, A., Smith, A. B., Woolley, J., Heyman, I., & Brammer, M. J. (2009a). Disorder-specific dysfunction in right inferior prefrontal cortex during two inhibition tasks in boys with attention-deficit hyperactivity disorder compared to boys with obsessive-compulsive disorder. *Human Brain Mapping*, 13(4/5). <http://doi.org/10.1002/hbm.20864>

Rubia, K., Halari, R., Cubillo, A., Mohammad, A.-M., Brammer, M., & Taylor, E. (2009b). Methylphenidate normalises activation and functional connectivity deficits in attention and motivation networks in medication-naïve children with ADHD during a rewarded continuous performance task. *Neuropharmacology*, 57(7-8), 640–652. <http://doi.org/10.1016/j.neuropharm.2009.08.013>

Rubia, K., Smith, A. B., Brammer, M. J., & Taylor, E. (2007). Temporal Lobe Dysfunction in Medication-Naïve Boys With Attention-Deficit/Hyperactivity Disorder During Attention Allocation and Its Relation to Response Variability. *Biological Psychiatry*, 62(9), 999–1006. <http://doi.org/10.1016/j.biopsych.2007.02.024>

Safaai, H., Neves, R., Eschenko, O., Logothetis, N. K., & Panzeri, S. (2015). Modeling the effect of locus coeruleus firing on cortical state dynamics and single-trial sensory processing. *Proceedings of the National Academy of Sciences*, 112(41), 12834-12839.

Sakoğlu, Ü., Pearlson, G. D., Kiehl, K. A., Wang, Y. M., Michael, A. M., & Calhoun, V. D. (2010). A method for evaluating dynamic functional network connectivity and task-modulation: application to schizophrenia. *Magnetic Resonance Materials in Physics, Biology and Medicine*, 23(5-6), 351–366. <http://doi.org/10.1007/s10334-010-0197-8>

Schaechter, J. D. (2004). Motor rehabilitation and brain plasticity after hemiparetic stroke. *Progress in neurobiology*, 73(1), 61-72.

Schneider, M. F., Krick, C. M., Retz, W., Hengesch, G., Retz-Junginger, P., Reith, W., & Rösler, M. (2010). Impairment of fronto-striatal and parietal cerebral networks correlates with attention deficit hyperactivity disorder (ADHD) psychopathology in adults — A functional magnetic resonance imaging (fMRI) study. *Psychiatry Research: Neuroimaging*, 183(1), 75–84. <http://doi.org/10.1016/j.psychresns.2010.04.005>

Setsompop, K., Gagoski, B. A., Polimeni, J. R., Witzel, T., Wedeen, V. J., & Wald, L. L. (2011). Blipped-controlled aliasing in parallel imaging for simultaneous multislice echo planar imaging with reduced g-factor penalty. *Magnetic Resonance in Medicine*, 67(5), 1210–1224. <http://doi.org/10.1002/mrm.23097>

Sharp W, Walter J, Marsh W, Ritchie G, Hamburger S, Castellanos X. (1999) ADHD in girls: clinical comparability of a research sample. *J Am Acad Child Adolesc Psychiatry* 1999; 38:40–47

Sheline, Y. I., Price, J. L., Yan, Z., & Mintun, M. A. (2010b). Resting-state functional MRI in depression unmasks increased connectivity between networks via the dorsal nexus. *PNAS*, 107(24), 11020–11025. <http://doi.org/10.1073/pnas.1000446107>

Sheline, Y. I., Raichle, M. E., Snyder, A. Z., Morris, J. C., Head, D., WANG, S., & Mintun, M. A. (2010a). Amyloid Plaques Disrupt Resting State Default Mode Network Connectivity in Cognitively Normal Elderly. *Biol Psychiatry*, 67(6), 584–587. <http://doi.org/10.1016/j.biopsych.2009.08.024>

Sheline, Y., Barch, D. M., Price, J., Rundle, M., Vaishnavi, S. N., Snyder, A. Z., et al. (2009). The default mode network and self-referential processes in depression. *PNAS*, 106(6), 1942–1947.

Smith, S. M., Vidaurre, D., Beckmann, C. F., Glasser, M. F., Jenkinson, M., Miller, K. L., et al. (2013). Functional connectomics from resting-state fMRI. *Trends in Cognitive Sciences*, 17(12), 666–682. <http://doi.org/10.1016/j.tics.2013.09.016>

Sonuga-Barke, E. J. S., & Castellanos, F. X. (2007). Spontaneous attentional fluctuations in impaired states and pathological conditions: A neurobiological hypothesis. *Neuroscience and Biobehavioral Reviews*, 31(7), 977–986. <http://doi.org/10.1016/j.neubiorev.2007.02.005>

Sripada, C. S., Kessler, D., & Angstadt, M. (2014). Lag in maturation of the brain's intrinsic functional architecture in attention-deficit/hyperactivity disorder. *Proceedings of the National Academy of Sciences*, 111(39), 14259–14264. <http://doi.org/10.1073/pnas.1407787111>

Stam, C. J. (2014). Modern network science of neurological disorders. *Nature Publishing Group*, 15(10), 683–695. <http://doi.org/10.1038/nrn3801>

Subcommittee on Attention-Deficit/Hyperactivity Disorder, Steering Committee on Quality Improvement and Management (2011). ADHD: Clinical Practice Guideline for the Diagnosis, Evaluation, and Treatment of Attention-Deficit/Hyperactivity Disorder in Children and Adolescents. *Pediatrics*, 128(5), 1007–1022. <http://doi.org/10.1542/peds.2011-2654>

Thompson, G. J., Magnuson, M. E., Merritt, M. D., Schwarb, H., Pan, W.-J., McKinley, A., et al. (2013). Short-time windows of correlation between large-scale functional brain networks predict vigilance intraindividually and interindividually. *Human Brain Mapping*, 34(12), 3280–3298. <http://doi.org/10.1002/hbm.22140>

Thompson, G. J., Pan, W.-J., Magnuson, M. E., Jaeger, D., & Keilholz, S. D. (2014). Quasi-periodic patterns (QPP): large-scale dynamics in resting state fMRI that correlate with local infraslow electrical activity. *NeuroImage*, 84, 1018–1031. <http://doi.org/10.1016/j.neuroimage.2013.09.029>

Thompson, G. J., Pan, W.J., Billings, J. C. W., Grooms, J. K., Shakil, S., Jaeger, D., & Keilholz, S. D. (2014a). Phase-amplitude coupling and infraslow (<1 Hz) frequencies in the rat brain: relationship to resting state fMRI. *Frontiers in Integrative Neuroscience*, 8, 41. <http://doi.org/10.3389/fnint.2014.00041>

Tian, L., Jiang, T., Liang, M., Zang, Y., He, Y., Sui, M., & Wang, Y. (2008). Enhanced resting-state brain activities in ADHD patients: A fMRI study. *Brain and Development*, 30(5), 342–348. <http://doi.org/10.1016/j.braindev.2007.10.005>

Tian, L., Jiang, T., Wang, Y., Zang, Y., He, Y., Liang, M., et al. (2006). Altered resting-state functional connectivity patterns of anterior cingulate cortex in adolescents with attention deficit hyperactivity disorder. *Neuroscience Letters*, 400(1-2), 39–43. <http://doi.org/10.1016/j.neulet.2006.02.022>

Uddin, L. Q., Kelly, A. M. C., Biswal, B. B., Margulies, D. S., Shehzad, Z., Shaw, D., et al. (2008). Network homogeneity reveals decreased integrity of default-mode network in ADHD. *Journal of Neuroscience Methods*, 169(1), 249–254. <http://doi.org/10.1016/j.jneumeth.2007.11.031>

Van den Heuvel, M. P., & Hulshoff Pol, H. E. (2010). Specific somatotopic organization of functional connections of the primary motor network during resting state. *Human Brain Mapping*, 31(4), 631–644. <http://doi.org/10.1002/hbm.20893>

Van Den Heuvel, M. P., & Pol, H. E. H. (2010). Exploring the brain network: a review on resting-state fMRI functional connectivity. *European neuropsychopharmacology*, 20(8), 519-534.

Van Essen, D. C., Ugurbil, K., Auerbach, E., Barch, D., Behrens, T. E. J., Bucholz, R., et al. (2012). The Human Connectome Project: A data acquisition perspective. *NeuroImage*, 62(4), 2222–2231. <http://doi.org/10.1016/j.neuroimage.2012.02.018>

Van Meer, M. P., Van Der Marel, K., Wang, K., Otte, W. M., el Bouazati, S., Roeling, T. A., ... & Dijkhuizen, R. M. (2010). Recovery of sensorimotor function after experimental stroke correlates with restoration of resting-state interhemispheric functional connectivity. *Journal of Neuroscience*, 30(11), 3964-3972.

Varela, F., Lachaux, J.-P., Rodriguez, E., & Martinerie, J. (2001). The brainweb: Phase synchronization and large-scale integration. *Nature Reviews*, 2, 229–239.

Vincent, J. L., Kahn, I., Snyder, A. Z., Raichle, M. E., & Buckner, R. L. (2008). Evidence for a frontoparietal control system revealed by intrinsic functional connectivity. *Journal of Neurophysiology*, 100(6), 3328–3342. <http://doi.org/10.1152/jn.90355.2008>

Wang, L., Yu, C., Chen, H., Qin, W., He, Y., Fan, F., ... & Woodward, T. S. (2010). Dynamic functional reorganization of the motor execution network after stroke. *Brain*, 133(4), 1224-1238.

Wang, L., Zhu, C., He, Y., Zang, Y., Cao, Q., Zhang, H., et al. (2008). Altered small-world brain functional networks in children with attention-deficit/hyperactivity disorder. *Human Brain Mapping*, 30(2), 638–649. <http://doi.org/10.1002/hbm.20530>

Weyandt, L., Swentosky, A., & Gudmundsdottir, B. G. (2013). Neuroimaging and ADHD: fMRI, PET, DTI Findings, and Methodological Limitations. *Developmental Neuropsychology*, 38(4), 211–225. <http://doi.org/10.1080/87565641.2013.783833>

Whitfield-Gabrieli, S., & Ford, J. M. (2012). Default mode network activity and connectivity in psychopathology. *Annual review of clinical psychology*, 8, 49-76.

Wiggins, J. L., Bedoyan, J. K., Peltier, S. J., Ashinoff, S., Carrasco, M., Weng, S. J., ... & Monk, C. S. (2012). The impact of serotonin transporter (5-HTTLPR) genotype on the development of resting-state functional connectivity in children and adolescents: a preliminary report. *Neuroimage*, 59(3), 2760-2770.

Williams, D., Tijssen, M., Van Bruggen, G., Bosch, A., Insola, A., Lazzaro, V. D., ... & Brown, P. (2002). Dopamine-dependent changes in the functional connectivity between basal ganglia and cerebral cortex in humans. *Brain*, 125(7), 1558-1569.

Wilson, T. W., Franzen, J. D., Heinrichs-Graham, E., White, M. L., Knott, N. L., & Wetzel, M. W. (2011). Broadband neurophysiological abnormalities in the medial prefrontal region of the default-mode network in adults with ADHD. *Human Brain Mapping*, 63, n/a–n/a. <http://doi.org/10.1002/hbm.21459>

Wintermark, M., Colen, R., Whitlow, C. T., & Zaharchuk, G. (2018). The vast potential and bright future of neuroimaging. *The British Journal of Radiology*, 91(1087), 20170505. <http://doi.org/10.1259/bjr.20170505>

Wolf, R. C., Plichta, M. M., Sambataro, F., Fallgatter, A. J., Jacob, C., Lesch, K.-P., et al. (2009). Regional brain activation changes and abnormal functional connectivity of the ventrolateral prefrontal cortex during working memory processing in adults with attention-deficit/hyperactivity disorder. *Human Brain Mapping*, 30(7), 2252–2266. <http://doi.org/10.1002/hbm.20665>

y Cajal, S. R. (1972). *Histologie du système nerveux de l'homme et des vertébrés*: Ed. française revue et mise à jour par l'auteur. Trad. de l'espagnol par L. Azoulay. Inst. Ramon y Cajal.

Yang, H., Wu, Q.-Z., Guo, L.-T., Li, Q.-Q., Long, X.-Y., Huang, X.-Q., et al. (2011). Abnormal spontaneous brain activity in medication-naïve ADHD children: A resting state fMRI study. *Neuroscience Letters*, 502(2), 89–93. <http://doi.org/10.1016/j.neulet.2011.07.028>

Yousefi, B., Shin, J., Schumacher, E. H., & Keilholz, S. D. (2018). Quasi-periodic patterns of intrinsic brain activity in individuals and their relationship to global signal. *NeuroImage*, 167, 297–308. <http://doi.org/10.1016/j.neuroimage.2017.11.043>

Yu-Feng, Z., Yong, H., Chao-Zhe, Z., Qing-Jiu, C., Man-Qiu, S., Meng, L., et al. (2007). Altered baseline brain activity in children with ADHD revealed by resting-state functional MRI. *Brain and Development*, 29(2), 83–91. <http://doi.org/10.1016/j.braindev.2006.07.002>

Yuan, J., Li, X., Zhang, J., Luo, L., Dong, Q., Lv, J., ... & Liu, T. (2017). Spatio-temporal modeling of connectome-scale brain network interactions via time-evolving graphs. *Neuroimage*.

Zhang, D., Snyder, A. Z., Fox, M. D., Sansbury, M. W., Shimony, J. S., & Raichle, M. E. (2008). Intrinsic functional relations between human cerebral cortex and thalamus. *Journal of Neurophysiology*, 100(4), 1740–1748. <http://doi.org/10.1152/jn.90463.2008>

Zhang, H., Wang, S., Xing, J., Liu, B., Ma, Z., Yang, M., Zhang, Z., Teng G. (2009). Detection of PCC functional connectivity characteristics in resting-state fMRI in mild Alzheimer's disease. *Behavioural Brain Research*, 197(1), 103–108. <http://doi.org/10.1016/j.bbr.2008.08.012>

Zhang, Y., Brady, M., & Smith, S. (2001). Segmentation of brain MR images through a hidden Markov random field model and the expectation-maximization algorithm. *IEEE Transactions on Medical Imaging*, 20(1), 45–57. <http://doi.org/10.1109/42.906424>